An interpretative view of open-vent volcanoes

S. Vergniolle, N. Métrich

An interpretative view of open-vent volcanoes

Vergniolle S. and Métrich N.
Université de Paris Cité, Institut de Physique du Globe de Paris, CNRS, F-75005 Paris, France

Abstract

Open-vent volcanoes are special systems where the dynamics of sustained magmatic processes can be thoroughly investigated and where new monitoring tools can be tested and applied. However, various aspects remain puzzling at open-vent volcanoes for which forecasting their behaviour can be an important challenge. Recent papers highlight the very rapid improvements in spaceborn instruments, data acquisition techniques, data treatment and modelling over the last decade, and illustrate the fundamental contribution of long time-series data, either discontinuous or continuous, and the development of multi-parameter studies.

Here we provide an interpretative overview of the main characteristics of open-vent volcanoes on the basis of selected examples chosen to be representative of the diversity of their magma composition, their eruptive activity and their geodynamic context. We choose typical open-vent volcanoes (Stromboli, Yasur and Erebus), some of them hosting a lava lake (Erta 'Ale, Nyiragongo, Villarrica, Ambrym and Masaya), to those with vigourous activity, which are associated to a long-lasting eruption (Arenal, Fuego, Popocatépetl, Santiaguito). We briefly review their surface activity and report the values of SO_2 flux and the derived magma supply rate with emphasis on the key results found on their behaviour. We show the key role of the magma viscosity and its implication on the degassing. We present the current models used to explain how an open-vent volcano could be maintained, such as by the simultaneous rise and fall of a degassing and degassed magma (bi-directional flow models) and the few thermal models at lava lakes and in the conduit. Finally we discuss the sulphur evolution for three nearby volcanoes at the triple junction in Central America (Pacaya, Fuego, Santiaguito).

The diversity of geodynamic environments, geochemical compositions and physical properties of magmas

Open-vent volcanoes are built up in various geodynamic contexts (Tables 1a and 1b). Their erupted magmas span wide ranges of chemical composition from basalts to nephelinite or trachyandesite and phonolite (Fig. 1), temperature and viscosity (see reviews of Rose et al. 2013 and Edmonds et al. 2022). Low to moderate viscosity systems are characterized by permanent plumes and gas emissions, eventually explosive activity at the craters and/or emissions of lava flows, whereas high viscosity, silica-rich magmas able to retain gas bubbles promote lava dome growth and possibly vulcanian eruptions.

These systems may remain continuously active over time periods spanning decades to millennia, whereas changes in activity style and intensity occurs over the short (hours-days), medium (weeks-months) and long (years-decades) time scales. As an example Piton de la Fournaise (Réunion Island) experienced an activity of basaltic lava lake, high lava fountaining and lava flowing, during almost three centuries (1640-1848 CE; Michon et al. 2013). Arenal volcano in Costa Rica is not presently active but erupted during nearly 42 years between July 1968 and 2010 (Parat et al. 2014), with subplinian eruptions, pyroclastic flows and lava emissions (Cigolini et al. 1984; Wadge et al. 2006) and vulcanian and strombolian activity (Hagerty et al. 2000; Mora et al. 2022).

Short-lasting explosive and paroxysmal eruptions and hazardous fissure-type eruptions draining the persistent lava lake at the craters represent ones of the major hazards at open-vent volcanoes. Destructive fissure eruptions are known at Erta 'Ale (Barnie et al. 2016), Kilauea (Halema’uma’u crater; Patrick et al. 2019; Fig. 2a), Nyiragongo (Komorowski et al. 2004; Morrison et al. 2020; see Pouclet and Bram 2021 for a review; Fig. 2b), and Ambrym volcanoes (Németh and Cronin 2011; Shreve et al. 2019). Short-term explosive eruptions, interrupting the persistent activity of the crater (mild-strombolian activity, passive degassing, lava lake) occur repeatedly at Villarrica in Chile in 2015 CE (Aiuppa et al. 2017; Johnson and Palma 2015; Johnson et al. 2018), at Stromboli in Aeolian Islands in Italy (historic and present-day eruptions, Bertagnini et al. 2011; Rosi et al. 2013; Métrich et al. 2021; Aiuppa et al. 2021; Pichavant et al. 2022; Fig. 2c and 2d) or as recently observed at Fuego (Naismith et al. 2019; Liu et al. 2020) and Santiaguito (Wallace et al. 2020) in Guatemala. Erebus volcano (Antartica) also experienced an active explosive activity throughout the Pleistocene and Holocene as testified by tephra layers found up to ~180 km away (Harpel et al. 2004).

Popocatépetl, with cyclic construction and destruction of lava domes and a large gas flux at the surface may be considered part of the category of open-vent systems as do Arenal and Pacaya that produced homogeneous magma for decades. The cyclic eruptions of high-level magnitude at Fuego (Guatemala), as well as the long-term quasi-steady eruptive pattern at Santiaguito, and Pacaya are other examples of open-vent systems, which are discussed here.

The timescales of magma storage, ascent and eruption are now studied through the measurement of the chemical zoning and diffusion patterns in crystals (Costa 2020). Focussing on open-vent volcanoes we note a remarkably high decompression rate of magma and a short time of magma crustal transfer leading to explosive eruptions as retrieved from the modelling of the diffusion profiles of H_2O, CO_2, and S in glass embayments (open-pockets of magma) partly entrapped in crystals. The decompression rate of the magma body that sustained the subplinian eruption (VEI 4) on 17 October 1974 at Fuego reached 0.3–0.5 MPa/s, equivalent to 11–17 m/s ascent velocity (Lloyd et al. 2014), when considering a single-stage decompression. Hence the magma rose from~10 km depth - its storage region - within the extremely short span of time of 8 to 12 minutes. The total ascent time is between 10 and 35 minutes for a two-stage decompression modelling taking into account different depth ranges of CO_2 and H_2O degassing. At Kilauea, Fergusson et al. (2016) used the same method and report average decompression rates for the magmas that fed the Hawaiian lava fountains to basaltic subplinian eruptions of ~0.05–0.45 MPa per second (Fig. 2a). They calculate ascent timescales from ~5 to ~36 min for these magmas that are ascending from ~2 to ~4 km, respectively. The magma decompression rates of 0.1 to ~ 2 MPa/s during the 2017–2018 Plinian eruption of Aoba (Ambae; Vanuatu arc) suggest short travel time of less than 2 minutes from ~ 0.5 to 3 km depth (Moussallam et al. 2019).

Imbalance between the volume of magma that degassed and the volume of magma is the core of open-vent activity. First observed at basaltic volcanoes and named “endogenous growth” (Francis et al. 1993), it was widely used and debated in litterature (Shinohara 2008; Carn et al. 2017). The recent comparison between thermal and SO_2 fluxes suggests that the magma supply rate at Masaya and associated with SO_2 degassing may be 5.5 more than the amount of magma which reaches the surface from thermal fluxes estimated by satellites (Aiuppa et al. 2018).

Edmonds et al. (2022) provide a review of the degassing and volcanic activity at open-vent volcanoes producing a wide range of magma compositions from basalts to dacites and rhyolites. They propose that deep-derived volatile phase from magmas accumulating and degassing at crustal depths sustains the persistent degassing at these volcanic systems, which are gas-dominated. It implies the differential transfer of the deep-derived gas phase whereas a major part of the volume of degassing and crystallising magma would be accommodated at depth. As an example, at Masaya the calculated supply rate of tholeiitic magma of 0.19±0.06 km^3 per year is suggested to be totally accommodated at depth by extensional tectonic (Zureck et al. 2019). These features are also in agreement with the lack of seismicity other that associated with explosions at Erta 'Ale (Bouche et al. 2010).

Persistent degassing at open-vent volcanoes that may have an impact on the health of inhabitants and on agriculture in downwind communities is also a chronic volcanic hazard (see Edmonds et al. 2017 for a review). As an example, the two huge craters Benbow and Marum of Ambrym volcano in Vanuatu, each of them hosting a lava lake until December 2018 (Moussallam et al. 2021), deliver high fluxes of gas rich in trace elements, metals metalloids, halogens (Allard et al. 2016a, 2016b). Human and environmental impacts of halogens concentrate in the downwind western part of the island (Cronin and Sharp 2002; Bani et al. 2009; Allibone et al. 2012). Masaya is one of the strongest degassing sources of SO_2 in the Central America Volcanic Arc (Aiuppa et al. 2018), and possibly maintained its steady state behaviour for 30 ka (Zureck et al. 2019). Masaya is also recognised to emit such elements as Hg (Witt et al. 2008). Health and economic hazards associated to Masaya persistent degassing have been long time identified (Delmelle et al. 2002; Williams-Jones and Rymer 2015; Calkins and Delmelle 2021). The 2018 eruption along the lower East Rift Zone (LERZ) at Kilauea produced large quantities of gas and aerosols (i.e., 7.1–13.6 Mt SO_2 and 1.5–2.8 Mt CO_2) in 3 months with significant impacts on air quality (Kern et al. 2020). This aspect of the environmental impacts of the volcanic degassing will not be developed here.

In summary, the two main characteristics of open-vent volcanoes are the persistent and excess degassing on one side and on the other side their ability to prevent cooling either by reducing heat losses or by having additional sources of heat at a sufficient rate. We combine here geophysical modelling approach to magma geochemistry to pinpoint key aspects of a selection of well-known open-vent volcanoes. Our goal is to highlight the fundamental properties of these systems, and the rapid improvements of both techniques and modelling for better understanding of their volcanic activity and improvement of their eruption forecasting.

We focus on open-vent volcanoes, which cover a range of magma composition and rheology, and show a diversity of activity from persistent degassing to strombolian and vulcanian explosions, up to paroxysmal activity. These volcanoes are monitored and/or have been extensively or more poorly studied, such as Erebus (Antartica), Stromboli (Italy) and Yasur (Vanuatu), respectively. They can host a lava lake (Masaya in Nicaragua, Villarica in Chile, Ambrym in Vanuatu arc, Erta 'Ale and Nyiragongo-Nyamuragira system in Africa) or offer the top of the magma column to air (Stromboli, Yasur, Erebus). In complement Popocatépetl, a dome-forming volcano is considered as one of the largest emitter of SO_2 and Arenal (Costa-Rica), a mid-point in term of magma composition between basalt and dacite, for its long-lasting eruption and the number of studies triggered by its eruption (Mora et al. 2022). Finally three nearby volcanoes from Central American Volcanic Arc (Pacaya, Fuego and Santiaguito) are also selected to discuss the sulphur behaviour in arc-magmas. Kilauea volcano is mostly ignored, due to its enormous number of studies, which are synthetised in a recent special issue of this journal (see Patrick et al. 2020 for an introduction).

We first discuss the bulk chemical homogeneity of the magma, before presenting basic knowledge necessary to understand the eruptive patterns of our selected volcanoes. We further present the surface activity at lava lakes, including their degassing. We then focus on the strombolian activity of Erebus, Stromboli and Yasur, firstly based on their petrology and magma viscosity and secondly on their surface activity and degassing. We then turn to a summary on vulcanian explosions before reviewing the thermal models, applicable to both lava lakes and conduits. We present the various bi-directional flow models in the conduit and the key informations that can be obtained from sound waves studies. Lastly, we discuss the possible exsolution path of sulphur, firstly on the fate of the sulphur and secondly with the example of Popocatépetl and thirdly on the three nearby volcanoes in Central America, Pacaya, Fuego and Santiaguito.

A bulk chemical homogeneity of the magma on the long-term

A relatively homogenous bulk composition but a complex history of the crystal assemblage appear to be shared characteristics of steady-state open-vent volcanoes that may testify to magma recharge and mixing or convection motions without new magma injection.

Arenal volcano (Costa Rica) provides a good example of the long-term chemical homogeneity of the bulk lava samples but a complex history recorded by the crystals, involving magma injection, mixing, mineral dissolution and crystallisation (Mora et al. 2022). The distribution of SiO_2 contents of Arenal magma is unimodal and centered on the lavas at about 54 to 57 wt% SiO_2 (Bolge et al 2006; Fig. 1). Its mineralogy reveals a complex and diverse growth and mixing histories of the crystal assemblage, although the basaltic-andesitic composition of the extruded magma did not change since 1970 (Streck et al. 2002, Ryder et al. 2006; Parat et al. 2014). The basaltic andesites at Arenal are experimentally reproduced after a minimum of 15% fractional crystallisation at 200 MPa at 1000-1050°C from a basaltic melt (Parat et al. 2014). Streck et al. (2002) suggest, on the basis of mineral zoning and compositions, that recurrent basaltic magma recharges occur with sub-decadal frequency and may predate eruption by months or less. Stromboli is known for its persistent activity at the craters since the eighth century CE (Bertagnini et al. 2011; Rosi et al. 2013). Both the major and trace element of the magma vary in a very restricted range of basaltic-shoshonitic composition (Fig. 1) over the last centuries (Pompilio et al. 2011) while the plagioclase crystals record successive dissolution-crystallisation events (Landi et al. 2006; 2009). Erebus crater hosts a long-lived exposed magma column, often referred to as a “lava lake” fed by a nearly anhydrous phonolite (Giggenbach et al. 1973; Sims et al. 2021), while 1-cm-wide anorthoclase crystals register several (from 1 to 3) complete cycles between the reservoir and the exposed magma column via the conduit (Moussallam et al. 2015). These cycles also imply contrasting flow regimes in reservoir and conduit, with convection in the former (with 1 to 3 cycles of 150 days at a speed of 0.5 mms^{-1}) and more complex cycles of exchange flow and re-entrainment in the latter.

In summary, the petrological studies demonstrate the magma chemical homogeneity on several-years time scales, despite the heterogeneous but steady pattern of minerals at the spatial microscale scale.

Basic considerations on degassing and magma viscosity

Two main parameters, namely the degassing pattern and the magma viscosity, are playing a key role in understanding the eruptive regimes. To set the scene for open-vent volcanoes, we discuss here relevant basic informations that will be used later in the paper.

Degassing

Degassing at the surface can occur for rising bubbles with various geometries (small, spherical cap and Taylor bubbles (Fig. 3a, 3b and 3c). Laboratory experiments on bubble rise in inviscid to low viscosity fluids have shown that the geometry of rising bubbles depends only on a set of three dimensionless numbers (Clift et al. 1978). These are the Reynolds (*Re*), Eotvös (*Eo*) and Morton (*Mo*) numbers. The Reynolds number, *Re*, quantifies the respective role of viscous and inertia forces, the Eotvös number that of buoyancy versus surface tension forces and the Morton number (Mo) is the ratio between viscous and surface forces. They can be written as:

$Re = \rho dU/\mu$ (Eq.1)

$Eo = \rho gD^2/\sigma$ (Eq. 2)

$Mo = g\mu^4/\rho\sigma^3$ (Eq. 3)

where ρ and μ are the density (kg m^{-3}) and dynamical viscosity (Pa.s) of the magma, respectively; d is the bubble diameter (m); σ is the surface tension (kg s^{-2}) and U the bubble upwards velocity (m/s). The bubble velocity depends on the shape of the rising bubble for, small bubbles, i.e. called the Stokes velocity (Clift et al. 1978; Eq. 16 in Vergniolle and Jaupart 1986), spherical cap bubbles (Clift et al. 1978; Eq. 5 in Bouche et al. 2010) and Taylor bubbles (Clift et al. 1978; Eq. 12 and 17 in Vergniolle and Caplan-Auerbach 2006). Note that the Morton number only depends on the material properties of the magma and the gas, while Reynolds and Eotvös numbers depend on the bubble diameter. The regime diagram displaying the bubble shape during rise is classically used by presenting the Reynolds number as a function of Eotvös number (Clift et al. 1978; Fig. 11 in Vergniolle and Jaupart 1986).

Bubbles can also be stationary (Fig. 3d), as those accumulated below the crust of a lava lake, creating a foam. Local coalescence within this foam could lead to a long and thin bubble referred to as a flat bubble (Fig. 3d). These flat bubbles have been shown to exist at the Erta 'Ale lava lake (Bouche et al. 2010).

Key parameters on magma viscosity

The viscosity of a magma (μ), which is a three phase mixture of melt with dissolved water, crystals and bubbles (Le Losq et al. 2015), is calculated by summing terms as follows:

$$\log\mu_{magma} = \log\mu_{melt} + X_{water} + Y_{crystal} + Z_{bubble} \qquad \text{(Eq. 4)}$$

where X is the weight fraction of water, and Y and Z the volume fraction of crystals and bubbles, respectively.

The respective effects of the temperature (Fig. S1a), the water concentration of the melt (Fig. S1b), the fraction of crystals (Fig. S1c) and of the shape and size of bubbles (Fig. S1d) on the magma viscosity are displayed in the supplementary material.

The review paper of Mader et al. (2013) provides an excellent summary of the current models and of the physical processes, which play a role in estimating the magma viscosity at various volcanoes. The first parameter is the crystal volume fraction. The linear approximation of Einstein, who calculates magma viscosity by assuming that the crystal content is small (Mader et al. 2013), is not valid above a crystal volume fraction of 10%. The lowest valid estimate for the viscosity is obtained by Gluth and Gold, from the Taylor expansion of the linear Einstein's equation, made at the second order for the crystal volume fraction (Mader et al. 2013). Some models even predict an exponential increase above a volume fraction exceeding 0.65 (Mader et al. 2013), a case that is never met by our chosen open-vent volcanoes (Tables 1a and 1b).

The second parameter to consider is the crystal size and shape and their distributions (Cimarelli et al. 2011; Mueller et al. 2011). The crystal shape is important because it exerts a strong control on the value of the maximum packing fraction, the value for which the viscosity becomes infinite (Mader et al. 2013). This effect is complicated to quantify due to the range of aspect ratios (Mader et al. 2013). The only currently available analysis has to be restricted to that of the average value (Mader et al. 2013) giving a large uncertainty on the final result.

The third parameter is the amount of dissolved water in the magma in the conduit, which when large decreases significantly the magma viscosity (Giordano et al. 2008; Fig.S1b). The fraction of dissolved water in magma is drastically changing as the result of gas exsolution when approaching the surface. An accurate prediction of magma viscosity in the conduit requires a good knowledge of the close link between water degassing and crystallisation (Pichavant and MacDonald 2007), both parameters increasing the viscosity close to surface (Fig. S1b and S1c). The depth at which the viscosity starts to increase due to simultaneous loss of dissolved water and increase in the crystal volume fraction is a key ingredient to be known to have a correct view on the physical processes associated to the gas-liquid flow in the conduit, assuming that the crystals passively follow the magma global motion.

The fourth parameter is the gas volume fraction, which also increases due to gas exsolution when approaching the surface. The changing gas volume fraction from 0, i.e. small, to 30 and 60% increases the magma viscosity by a factor 2.5 and 10, respectively (Fig. S1c; Mader et al. 2013). The exact calculation of the gas volume fraction is also complex because it depends on whether the small bubbles present within the liquid can move in respect to the liquid, as for a separated gas flow, or are stagnant, as for a homogeneous gas flow (Vergniolle and Jaupart 1986). The consequence of having a separated gas flow is very important for the magma viscosity because the gas volume fraction is significantly reduced when compared to that of a homogeneous gas flow (Fig 5b and 6 in Vergniolle and Jaupart 1986). The first estimates of the gas volume fraction had assumed a homogeneous gas flow (Burton et al. 2007b; Allard et al. 2016b), whereas the framework to calculate the gas volume fraction for a separated gas flow had now been developed (Pioli et al. 2012; Pansino et al. 2019). Three mechanisms can lead to a separated gas flow. The first one is related to the existence of small bubbles sufficiently large, prior to the depth where the gas exsolution starts to be significant, to rise in respect to the melt. The second one is related to the existence of large bubbles and the third one to the existence of bubble clusters, i.e. an aggregate of small bubbles able to rise on its own. Bubble clusters may form in the underlying conduit below lava lakes, as shown to exist at Erta 'Ale (Bouche et al. 2010), and as discussed later in the lava lake section.

The fifth parameter is the bubble shape and its effect is displayed, in steady shear, by the Capillary number (*Ca*) (Mader et al. 2013). This dimensionless number is the ratio between the viscous stress ($\mu\dot{\gamma}$, where $\dot{\gamma}$ is the shear strain-rate) acting on a bubble of diameter d, and the restoring stress supplied by surface tension ($2\sigma/d$), giving:

$$Ca = \frac{\mu d \dot{\gamma}}{2\sigma} \qquad \text{(Eq. 5)}$$

The small and non-deformable bubbles increase the magma viscosity by adding some complexity and tortuosity into the path offered to the parcels of moving fluid, while the deformable bubbles decrease the magma viscosity by adding a free slip into the bubbly liquid (Mader et al 2013; Fig. S1d). In both cases, this effect starts to be noticeable for a gas volume fraction of 10 % and is more marked when the gas volume fraction increases. The viscosity of a bubbly magma containing a gas volume fraction of 35 % is either increased by a factor 1.4 for small bubbles or decreased by a factor 0.3 for deformable bubbles (Fig. S1d). The relevance of knowing the bubble shape in the conduit, such as schematically drawn at Santiaguito (Bluth and Rose 2004), might therefore be important. However, looking at the bubble shapes preserved in the ejecta might be misleading due to additional effects associated to expulsion.

Another challenging phenomemum arises when a separated gas flow exists in the conduit. Laboratory experiments show that a global liquid motion can result from the bubble motion (Pioli et al. 2012; Pansino et al. 2019). When these conditions are met the small crystals will passively follow the magma motion, thereby decreasing the local crystal volume fraction.

In summary, the spatial organisation of the degassing gas bubbles in the conduit is complicated for a magma relatively rich in water, because of the competitive effects of the water content of magma and the gas bubble on the viscosity. The question of the progressive degassing as water is exsolving and how thick an overlying plug can be an interesting question that is addressed further because it requires the knowledge of the dynamics of the magma motion and of its bubbles.

Magma supply rate

Two simultaneous pioneer studies, applied to Stromboli (Allard et al. 1994) and Izu-Oshima (Japon; Kazahaya et al. 1994), combined records of SO_2 fluxes with sulphur content prior (melt inclusions) and after (matrix glass) degassing at surface to assess the volume of the degassing magma. An average magma supply rate can be calculated for a given period. This chemical budget does not consider any specific physical process or depth. The only assumption is that the initial sulphur content is quasi-fully lost between depth and surface. This framework had been largely used to assess the magma supply rate at open-vent volcanoes (Tables 1a and 1b) using repetitive measurements of SO_2 fluxes (Tables 2a and 2b).

Long-term surface activity at lava lakes

Lava lakes: pressure gauges of the open-vent systems

Only a few open-vent volcanoes, although distributed all around the world in various geodynamic environments (subduction, rift, and hot spot), host long-lasting lava lakes (6-7 presently known) and/or intermittently active lave lakes (Table 1a). *Sensu stricto*, a lava lake is a natural magma body whose dimensions are large compared to the underlying conduit. In this respect, the so-called "lava lake" at Erebus has a roughly conical shape (Oppenheimer et al. 2009), 40 m across for 30 m depth with 4-10 m wide conduit opening at its base (Dibble 2008; Oppenheimer et al. 2009) and a thickness of a few tens of meters (Jones et al. 2015). Its small diameter and thickness, compared to that of the conduit, suggest it to be the top of a magma column rather than a proper lava lake. It offers a direct view of the underlying conduit when looking from above. For simplicity, we shall refer in the text of Erebus as an exposed magma column.

Now, the evidence emerges that most lava lakes have experienced sequences of draining-refilling along their life time that represents major hazards. At Ambrym volcano, several units derived from ponded lava lake bodies were recognised along the Marum crater rim that testifies repeated drainage, excavation or gentle subsidence (Németh and Cronin 2008). Pouclet and Bram (2021) give a detailed review of the activity of the Nyiragongo lava lake, observed since 1948, to have permanent to intermittent and episodic activity with long-term pauses. These authors discuss the mechanisms at the origin of the periodic oscillations of a few tens of minutes for meter-scale level variations. Short-term gas pistoning events and gas release for the rising and the falling phases respectively, modelled by Witham and Llewellin (2006), is discarded because of the absence of relationships between degassing process and oscillatory behaviour of the lava lake (Valade et al. 2018), as observed at Kilauea (Patrick et al. 2015). Sudden drops of several tens of meters with strong degassing are ascribed to temporary interruption of the magma convection in the conduit with the lack of fresh magma ascent according to Bobrowski et al. (2017). A draining-refilling model was proposed for Nyamuragira, which involved a gravity-driven drainage of a shallow magma body (or multiple interconnected magma pockets) induced by the eruption of deep undegassed magma along a lateral rift-parallel dike (Coppola et al. 2016).

The dynamics of the lava lakes has been intensively studied through the multiparametric measurements of gas and heat fluxes, surface lake motions and flow velocities (Pering et al. 2019, Lev et al. 2019). Measurements have been sporadic or inexistent in the past but they are becoming continuous at a few well-monitored volcanoes. The level of the lava lakes is measured directly at Kilauea (Tilling et al. 1987; Patrick et al. 2015; Fig. 4), Nyiragongo (Burgi et al. 2014; 2020; Barrière et al. 2018; Pouclet and Bram 2021; Fig. 5), Erebus (Jones et al. 2015; Peters et al. 2014a; 2018; Fig. 6) or estimated undirectly from satellites (MODIS) at Erta 'Ale (Vergniolle and Bouche 2016; Fig. 7) or by measuring the shadow length cast by the crater rim on satellites imagery (Oppenheimer and Francis 1997; Barrière et al. 2018). Unfortunately, the use of satellites is somehow restricted to lava lakes having a funnel shape, such as at Erta 'Ale (Vergniolle and Bouche 2016) and Nyiragongo (Burgi et al. 2014), a sufficient radiative surface and a reasonably unfrequent cloud cover.

Lava lakes, by being in direct connection with a shallow magma reservoir, offer a unique opportunity to decipher the physical processes at depth. Their level can act as a pressure gauge, making its measurement a key parameter to follow. At Ambrym (Fig. 8), the lava lakes were visually observed to be at a high-level prior the effusive activity of 21 February 2015 (Radebaugh et al. 2016; Hameling and Kilgour 2020; Shreve et al. 2021), as well as that of mid-December 2018 (Hameling et al. 2019; Shreve et al. 2019; Moussallam et al. 2021). This shows that the pressure was building up somewhere in the plumbing system prior to these major events. Similarly numerical simulations performed at Nyiragongo, and validated by 30 years of records, have also shown that (i) the level of lava lake rises prior to paroxysmal activity, but (ii) slows down in the preceding months/year (Burgi et al. 2020). Therefore, the fluctuations in the height of a lava lake can track changes in pressure and the dynamics of the magmatic systems.

At Masaya (Fig. 9), the lava lake has persisted with varying levels between 2015 to present (C. Wauthier personal communication). Occasionally, these vents have enlarged in dimension, most likely due to magma level increase in the conduit and crater floor collapse, ultimately leading to a lava lake (Aiuppa et al. 2018). Its surface activity had been explained qualitatively, but not quantitatively, by the behaviour of the stable foam accumulated at the top of the reservoir (Stix 2007). At Erta 'Ale, the lava lake level was also explained, and modelled, to be controlled by the thickness of the stable foam at the top of the shallow reservoir (Vergniolle and Bouche 2016). The lava lake rises when the underlying gas flux below the foam exceeded that associated to the foam spreading and it falls when the underlying gas flux had stopped (Fig. 10). The foam thickness was modelled with these two different boundary conditions and compared to the level of the lava lake, giving two independent constraints on the plumbing system, namely the area of the shallow magma reservoir and the underlying gas flux (Vergniolle and Bouche 2016). This analysis, done for several years, showed that the gas flux at the top of a magma reservoir could, at time, be oscillatory with a period of 10.8 days, continuous or nonexistent (Vergniolle and Bouche 2016).

The connection of the lava lake with a shallow plumbing system is in agreement with the good match observed between the pressure loss, the drop in lava lake level and the deformation pattern (Moore et al. 2019), as at Kilauea (Patrick et al. 2015; Poland and Carbone 2018), Ambrym (Németh and Cronin 2008), Nyiragongo (Pouclet and Bram 2021) and Erta 'Ale (Barnie et al. 2016) with a long-term influence of the regional tectonic activity.

Degassing and bubble regimes

We focus first on the present knowledge of lava lakes, which can often be seen from above, when they are not almost entirely covered by a solid crust and hidden as occurring, respectively in December 2004 at Erta 'Ale (Fig. 7c), and in January 2009 at Masaya (Fig. 9b).

At Erta 'Ale, the degassing occurs through the breaking of the spherical cap bubbles at a fixed location at the surface of the lava lake (insert in Fig. 7a) or through the flat bubbles (Fig. 3d) located on the incandescent zones, which sometimes separate the few cold plates of the crust

(Bouche et al. 2010; Fig. 7a). A spherical cap bubble rising in a conduit in such low viscosity magma can grow a bubbly wake, which periodically detaches from its base upon reaching a maximum volume proportional to that of the driving spherical cap bubble (Bouche et al. 2010). This bubble cluster can then rise in the conduit on its own at a relatively large velocity. The dismantling of these bubble clusters by the return flow of the lava lake is thought to be at the origin of the small bubbles. These small bubbles accumulate below the cooling crust where they can coalesce to produce the flat bubbles (Bouche et al. 2010). Spherical cap bubbles and flat bubbles co-exist and correspond to two different types of degassing. Both types of degassing at Erta 'Ale lead to a weak strombolian activity. However the driving gas overpressure leading to the breaking of spherical cap bubbles is significantly larger than that driving the breaking of the flat bubbles (Bouche et al. 2010). On some occasions, these bubbly clusters remain attached to their driving spherical cap bubbles until very close to the surface of the lava lake, and burst at the surface as small lava fountains (Bouche et al. 2010).

Is the rise of the large bubbles at other lava lakes sufficiently turbulent to grow a wake at the surface or in the conduit? Can this bubbly wake detach and incorporate small bubbles as proposed by Bouche et al. (2010)? The key point of such a mechanism is that some magma is rapidly brought to the surface, travelling at the velocity of the driving large bubble or that of a bubble cluster when within a detached bubbly wake. This depends on the value of the Reynolds number (Eq. 1). For a value above 30, a wake, a vortex zone initially attached to the driving large bubble, exists and can attract small bubbles in it (Fig. 15 in Vergniolle and Ripepe 2008; Fig. 27.11 in Taddeucci et al 2015). Above a value of 70-100, the wake becomes open, with strong interactions between the fluid around the bubble and the wake itself. This laminar wake is also unstable, hence can detach and rebuild. At Reynolds numbers exceeding 2000, the detachment of the wake, fully turbulent, occurs periodically upon reaching a critical volume, proportional to the volume of the driving bubble (Bouche et al. 2010). In this latter regime, the quantification of the volume of magma within the detached bubbly wake is possible, providing a knowledge of the volume of the driving bubble and the gas volume fraction within the bubbly wake. The magma might be sufficiently fluid at a depth where the amount of dissolved water is considered as partly or fully undegassed. This allows the large bubbles to rise at relatively high Reynolds number, despite their compression in gas volume with depth. In this case, the degassing is organised at depth with large driving bubbles and their detached bubbly wakes. Large bubbles and detached bubbly wakes can then rise towards the surface and potentially have their Reynolds number decreasing, despite their increase in gas volume, due to the rapid increase in the gas volume fraction existing in the magma containing stagnant bubbles. If the Reynolds number becomes below the critical value of 70-100, the values estimated for the large bubbles at the surface do not reflect anymore the fact that the detached bubbly wakes were previously formed in the conduit and had already led to a proper separated gas flow at depth. If a separated gas flow is organised at depth, the newly gas exsolved above this depth is likely to mainly diffuse into the small bubbles already present in the separated gas flow, enhancing their differential velocity in respect to the magma, hence the vigour of the separated gas flow.

One should then consider the Reynolds number (Eq. 1) to decide on the existence of the detached bubbly wakes somewhere in the conduit. For simplicity, we considered here the depth where the magma is still rich in dissolved water to be 500 m below the surface for all the selected lava lakes, based on the calculation of the gas volume fraction at Ambrym and its relatively high dissolved water content (Allard et al. 2016b). Assuming that the magma is fully degassed, the Reynolds number calculated a depth of 100 m, is reduced by a multiplicative factor of 0.19 (Table 3). It would be reduced by a factor of 0.087 at 500 m due to gas compression when assuming, for the sake of the argument, a fully degassed magma.

We are now going to discuss specific examples, using the Giordano's model (2008) unless specifically given elsewhere and the relevant parameters (Table 3). For each example, we discuss the final magma viscosity when adding crystals or small bubbles whenever possible.

The Reynolds number of the driving spherical caps at Erta 'Ale, is 1840 and 8000 at the surface when using an updated value of the magma viscosity of 22-27 Pa.s (Table 3). It is still well above the threshold value for which the detachment of the bubbly wake exists and is periodic. Again, this example illustrates the importance of the viscosity on the bubble regime as the value of 10 Pa.s used by Bouche et al. (2010) could have led to a different scenario. The formation of detached bubbly wakes (Fig. 11a), which is a mechanism at work even during a period of very low activity of the lava lake (Bouche et al. 2010; Vergniolle and Bouche 2016), is hence a persistent feature of its degassing (Fig. 11).

Similarly, the large bubbles observed at Nyiragongo, 10 m in diameter (Tazieff 1996), led to relatively high values of the Reynolds number at the surface, between 3152 and 822 (Table 3), for a magma viscosity from 56 Pa.s to 230 Pa.s (Burgi et al. 2014; 2018; 2020), respectively, a value also sufficient to produce detached bubbly wakes. The Reynolds number at a depth of 500 m is also sufficiently high, 306 and 71 for a magma viscosity of 56-230 Pa.s, respectively, (Table 3) to lead to a fully separated gas flow in the conduit, organised with driving spherical cap bubbles and their bubbly wakes (Fig. 11a).

The Reynolds number of the spherical cap bubbles observed at Villarica is between 65 and 232 at the surface (Table 3), with gas volumes between 200 m^3 and 2500 m^3 (Gurioli et al. 2008), respectively, and a magma viscosity of 1780 Pa.s, calculated by assuming a crystal volume fraction of 38 vol% obtained with stagnant crystals (Witter et al. 2004). Such a value of the Reynolds number is again mostly compatible with the formation of bubbly wakes and their detachment close to the surface. The very high Reynolds number at a depth of 500 m, 20000-71500 and 556-1990, when assuming a negligible crystal volume fraction and a magma viscosity of 0.5 Pa.s and 18 Pa.s, respectively, obtained for a dissolved water content of 4 wt% and 1 wt% (Witter et al. 2004; Table 3), clearly show that the driving spherical cap bubbles are organised at depth similarly to that of Erta 'Ale close to the surface (Fig. 11a), with a periodic detachment of the bubbly wake onto reaching a maximum wake volume of 4-6 that of the driving spherical cap (Bouche et al. 2010).

The bubbles observed at the surface of Ambrym lava lakes were very large, plurimetric (Allard et al. 2016b) with a diameter of 5-10 m at Benbow on 5 October 2008 (P. Allard, pers. com. on 25 October 2021) and even larger at Marum in May 2014, 12 to 16 m in diameter (Radebaugh et al. 2016). The Reynolds number of these bubbles at the surface is between 318 and 1820, for a bubble diameter of 5 and 16 m in diameter, respectively, and a magma viscosity between 170 and 250 Pa.s (Table 3). The conditions are therefore met to have the large bubbles rising in the lava lake and at the origin of detached bubbly wakes at the surface. However, the above calculation of the magma viscosity does not consider the gas volume fraction of small bubbles potentially suspended in the magma, a limit case for which most of the bubbles, even small, can move in respect to the liquid, hence in a separated gas flow. In contrast, the gas volume fraction has been estimated by combining records from open-path Fourier transform infrared spectroscopy of gas emissions at Ambrym, with the laws of the gas exsolution of H_2O, CO_2 and SO_2 from the melt at equilibrium, while all the newly produced gas is organised into small bubbles passively following the melt phase (Allard et al. 2016b). In these conditions, the magma viscosity is increased by a factor 10 (Fig. S1c; Mader et al. 2013) as soon as it reaches the threshold value, for which the small bubbles are touching one another, which occurs at a depth of 160 m (Allard et al. 2016b). In this case, the degassing at the surface of the lava lake at Ambrym does not present detached bubbly wakes for the smallest observed bubbles, 5 m in diameter (Fig. 11b). However the detached bubbly wakes can exist if the diameter of the driving large bubble exceeds 8.5 m (Fig. 11c), such as for the largest bubbles on 5 October 2008 (P. Allard, pers. com. 25 October 2021) and for the entire range of bubble diameters seen in May 2014 (Radebaugh et al. 2016).

The bubble diameters are relatively small at Masaya, with a median value of 2.6 m and a range of 0.6-8.5 m, even during a period of vigorous activity (Pering et al. 2019). The Reynolds number of a bubble, whose diameter is 2.6 m, is 156 and 30 at the surface and a depth of 100 m, respectively, (Table 3) for a magma viscosity between 140 and 180 Pa.s. The Reynolds number at the surface, calculated above with a negligible gas volume fraction, could be below the threshold of 70-100, if the magma viscosity is multiplied by 2.5, such as for a gas volume fraction exceeding a value of 30 % (Fig. S1c). The Reynolds number at a depth of 500 m, equal to 78 if we assume that the magma still contains 1.45 wt% of dissolved water (Table 3), is just above the lowest value for starting an open wake and initiating a separated gas flow. However, the magma at Masaya, being richer in dissolved water, 1.45 wt%, than that at Ambrym, 1.2 wt%, may have partially lost its initial dissolved water at a depth below than 500 m, up to a significant value. In this case, the magma viscosity at this depth increases, thereby decreasing the Reynolds number. It may then lead to a Reynolds number below the threshold value of 70-100, preventing both the formation of open wakes and that of a separated gas flow at this depth. If we consider that the depth at which the magma is still rich in dissolved water, 1.45 wt%, is 700 m rather than 500 m, the driving spherical cap bubble at Masaya cannot grow an unstable wake at the lowest possible value of the magma viscosity. This is even more the case if the depth, where part of the dissolved water is significantly lost, is larger than 700 m, invaliding the possibility to have a separated gas flow by this mechanism at any depth below 500 m.

Small lava fountains: detached bubble wakes

The existence of small lava fountains, which have been interpreted at Erta 'Ale as the surface expression of newly detached bubbly wakes, could be used as an independent constrain in favour of the existence of detached bubbly wakes at the surface (Bouche et al. 2010). Small lava fountains have also been observed at Nyiragongo (Burgi et al. 2014; 2018), Villarica (Palma et al. 2008) and Ambrym (Radebaugh et al. 2016). This suggests that a mechanism based on the existence of detached bubbly wakes is possible at the surface of these lava lakes, in agreement with relatively high values of the Reynolds number of their spherical cap bubbles close to the surface (Table 3). Furthermore, the results from the sulphur isotopes, which have shown that the degassing at Erta 'Ale occur in disequilibria (De Moor et al. 2013), also reinforce our proposed mechanism of spherical cap bubbles already existing at 500 m and sufficiently large to be able to produce detached bubbly wakes even when the activity at the lava lake is very low (Bouche et al. 2010).

Small lava fountains have been observed at Ambrym at a time where the bubbles were 12-16 m in diameter (Radebaugh et al. 2016). Their Reynolds numbers (Table 3) are either 1190-1820 or 119-182, when considering that the small bubbles suspended in the liquid phase move separately and at a low gas volume fraction or together with the liquid at a gas volume fraction of 60 %, respectively. These Reynolds numbers, well above the value of 70-100, cannot be used to give an indication on the gas volume fraction at the surface.

The lack of small lava fountains at Masaya during all periods of observations (P. Delmelle, pers. com., 2 November 2021) suggests that the Reynolds number at the surface is always below 70. The Reynolds number of the typical bubble observed during a vigorous period, 2.6 m in diameter (Pering et al. 2019), is equal to 156 when assuming a negligible gas volume fraction (Table 3). This suggests that the gas volume fraction at the surface must always exceed 30 %. Such a value can easily be explained by the richness in volatiles of the magma. The degassing at Masaya (Martin et al. 2010) has been shown to be at equilibrium, when using the sulphur isotopes during a period of very low activity (De Moor et al. 2013). The degassing at equilibrium is in agreement with the lack of open wakes below a depth of 700 m and a large gas volume fraction close to the surface. But we do not know whether the degassing at equilibrium is only occurring at periods of low activity or is persistent at the lava lake.

Homogeneous versus separated gas flow?

We now discuss Ambrym and Masaya as typical examples. The records from open-path Fourier transform infrared spectroscopy of gas emissions at Ambrym suggest that two types of degassing exist. The first one is associated to a separated gas flow, corresponding to the large bubbles observed at the surface and shown to exist already at depth (Allard et al. 2016b). This is in agreement with our proposed model of spherical cap bubbles and their detached bubbly wakes already existing at a depth of 500 m (Fig. 11b and 11c). The second type of degassing at Ambrym is due to a coupled magma-gas ascent, leading to a very shallow degassing of puffs, hence a separated gas flow, possibly occurring at depths above several tens of meters below the surface (Allard et al. 2016b), i.e. within the lava lake. The coupled degassing, and its resulting separated gas flow within puffs, can easily be produced if the gas volume fraction associated to the small bubbles is large, thereby favouring a local bubble coalescence or their simultaneous breaking at the surface. The relatively frequent multimetric CO_2-rich bubbles, 4 detected during 1h20min, on 5 October 2008 during a moderate period of activity (Allard et al. 2016b), suggests that the separated gas flow may play a significant role in the degassing pattern, thereby reducing the gas volume fraction in the conduit from that estimated by assuming gas exsolution within a fully homogenous gas flow.

The Reynolds number of the bubbles, with a diameter of 5-10m at a depth of 100 m, 61-172 is just slightly below the value of 70-100 (Table 3), suggesting that most of the time an open wake can also exist at 100 m depth during this period. The existence of detached bubble wakes at 100 m depth is even less questionable within the framework of the model proposed by Bouche et al. (2010) and the value used for the magma viscosity, when the bubbles are larger, 12-16 m in diameter (Radebaugh et al. 2016), due to their relatively large Reynolds number, 226-348, respectively (Table 3). We therefore propose that the degassing at Ambrym is mostly driven by a separated gas flow, induced below a depth of 500 m (Fig. 11b and 11c).

In the same line of reasoning, we could explore at other lava lakes the consequences of having large bubbles at a depth of 500 m on the degassing pattern in the conduit. The calculation of the Reynolds numbers is particularly revealing as it can show whether a wake can exist or no with a threshold value of 70-100 and whether a wake is closed and laminar or open and turbulent (Fan and Tsuchiya 1990). Among our choice of lava lakes, we note that the lava lake at Villarica presents the largest values of the Reynolds numbers associated to driving large bubbles, even for the largest value of the viscosity associated to the undegassed magma, 18 Pa.s (Table 3). The Reynolds numbers of 556-1990 are slightly below the transition for a fully turbulent rise for the large bubble, 2000 (Bouche et al. 2010). It only requires a decrease in viscosity by a factor 2 to place a typical driving large bubble, such as those observed (Gurioli et al. 2008), in the fully turbulent regime. This could perhaps be envisioned, as the maximum value of the initial dissolved water is very high, 4 wt% (Witter et al 2004).

In summary, the main restriction is related to the assumption of equilibrium degassing, shown to be appropriate at Masaya and incorrect at Erta 'Ale (De Moor et al. 2013). This is perhaps a possibility to consider or discard in the future, given the suggestion that the mixing of fluids between the degassing and degassed magma is turbulent at Villarica in contrast to Erebus and Kilauea (Moussallam et al. 2016).

The calculation of the Reynolds numbers, associated to a given period during which the measurements of the bubble volumes are performed, is dependent of the vigour of the lava lake, which can anywhere between quiet or vigorous. This variation in activity emphasises the need for continuous measurements. However, the technology to set continuous measurements even at low-danger lava lakes is complicated and/or costly, as for the records from open-path Fourier transform infrared spectroscopy, or the data analysis is very long to perform automatically and requires enormous amount of computer memory and storage, as for the video’s measurements in the visible, infra-red or ultra-violet range of recordings.

Strombolian activity at Erebus, Stromboli and Yasur

Petrology and magma viscosity

Erebus, Yasur and Stromboli are textbook examples of open-vent volcanoes that maintained long-term steady-state behaviour (centuries). As the magma is continuously degassing and losing temperature at the vents it crystallises and its viscosity significantly varies.

At Erebus, the mineral assemblage found in phonolitic lavas and tephra has not changed in composition for at least ~17 ka (Kelly et al. 2008). At 950 ±25°C, the anorthoclase bearing phonolite is almost dry (H_2O <0.2 wt% versus 1-2 wt% in the parental basanite) (Moussallam et al. 2013; 2015; Sims et al. 2021), its viscosity is calculated to be $10^{6.3}$ Pa.s (Le Losq et al. 2015) for 30 vol% anorthoclase, an amount of megacrystals that is kept constant through time (Kelly et al. 2008).

The temperature of the anorthoclase-bearing phonolite at Erebus is relatively high with respect to those of water-rich phonolites. Values of 760-780°C and 840-870°C are reported for the phonolitic magma of Laacher See (Rout and Wörner 2020) having 4.0-3.6 wt% H_2O (Harms and Schmincke 2000); 800-850°C for 3.0-2.5 wt% H_2O at Tenerife, 935°C for 3 wt% H_2O at Tambora; and 815±10°C for the 79AD phonolite having 6.2 wt% H_2O at Vesuvius and even lower (785-800°C) for the other Vesuvius phonolites for a range of H_2O content between 7.5 and 3.5 wt% H_2O (Andùjar and Scaillet 2012). Moussallam et al. (2015) propose that the CO_2 flux sustains the convective motion observed at Erebus with recycling of degassed magma in accordance with a bi-directional flow model in the conduit (see details in separated section). This is in agreement with the coexistence of two magma batches differing by their temperature and viscosity in a single conduit up to a depth of ~30 m, where the descending cold magma could be at least 100°C colder than the ascending flow of bubbly magma coming from 2-3 km (Molina et al. 2015). A temperature range from 950°C to 1000-1050°C would signify a change in viscosity of at least one order of magnitude ($10^{6.3}$-$10^{5.3}$ Pa.s and possibly as high as 10^7 Pa.s) (Le Losq et al. 2015.)

At Yasur, Firth et al. (2014) suggested that strombolian-style activity has persisted in its current form for the last 630–850 years from their study of recently exposed tephra sequences. They show that the emission rate is constant with ~5.7×10^5 kg per day expelled magma volume of basaltic tranchyandesitic magma. Neither the crystallisation temperatures nor the major and trace element composition of Yasur magma vary significantly over nearly 800 years activity (Firth et al. 2014). The magma supply rate, calculated on the basis of the SO_2 flux and the sulphur content of olivine hosted melt inclusions (Tables 1 and 2), achieves nearly 0.05 km^3 per year (Métrich et al. 2011; Woitischek et al. 2020). Woitischek et al. (2020) propose when assuming equilibrium conditions, that the degassed shallow conduit at Yasur consists of a crystal-rich region with a thickness of at least 0.6 and up to 2 km, if extensive crystallisation is driven by H_2O degassing at equilibrium following Métrich et al. (2011). In these conditions, the proportion of crystals increases from 10 to 32 vol% on degassing. Calculations, using a software called MELTS (Ghiorso and Gualda 2015), indicate that the bulk magma effective viscosity would vary from 5.8×10^2 Pa.s prior to degassing to 1.5×10^5 Pa.s after degassing and crystallisation, with H_2O from 1.1 wt% to 0 .2 wt% respectively (Woitischek et al. 2020). While the trachyandesitic magma at Yasur is degassing and crystallising, the SiO_2 concentration of the residual melt changes to reach 59 wt% (Métrich et al. 2011). Simultaneously, its viscosity becomes $10^{3.4}$ Pa.s for a water concentration of 0.3-0.2 wt% and using Giordano et al.'s model (2008). A volume fraction of crystals of ~ 30 % increases the viscosity by 0.5-1.0 log unit depending on their aspect ratio (Mader et al. 2013; Le Losq et al. 2015). It means that the Yasur conduits may be capped by a relatively viscous magma in agreement with equilibrium calculation of Woitischek et al. (2020).

At Stromboli, a magma supply rate of ~ 0.1 km^3 per year is needed to sustain the long-term average of SO_2 flux (220-260 tons per day (Allard et al. 2008) (Tables 1 and 2). The major element compositions of most degassed shoshonitic pyroclasts vary in a very restricted range (Pompilio et al. 2011) as do the percentage of crystals (Landi et al. 2004; 2006; 2009). In contrast, a complex zoning of phenocrysts, particularly of plagioclase, has been reported for a long time, supporting processes of magma mixing and up and down motion. As an example, the modal analysis of a series of 12 crystal-rich scoriae samples covering a period from 1986 to 2000 indicates 48 to 55 vol% crystals made of plagioclase (27-38 vol%), clinopyroxene (16-10 vol%) and olivine (2-5 vol%) (Landi et al. 2004). Modal analysis performed on 9 lava samples of the 2002-2003 lava flow provide similar results with 41 to 54 vol% (38 vol% in one sample) and similar proportions of plagioclase (23-34 vol%), clinopyroxene (5-19 vol%), olivine (2-8 vol%) (Landi et al. 2006). In the 2007 lava samples (9 samples analysed) the proportion of phenocrysts varies from 45 to 51 vol% (plaglioclase 29-33 vol%; clinopyroxene 11-14 vol%; 4-5 vol%) (Landi et al. 2009). The melt viscosity reaches $10^{2.7}$ Pa.s at 1100°C, when using Giordano et al.'s model (2008) and a water concentration of 0.3-0.2 wt%.

Erebus, Yasur and Stromboli conduits may be capped by degassed and relatively viscous magmas (10^4 Pa.s) when assuming equilibrium conditions. They contain a significant proportion of crystals from nearly 30 vol% (Yasur, Erebus) up to 55 vol% (Stromboli), for temperature range from 950°C (Erebus) to 1110-1120°C (Yasur, Stromboli). At Stromboli, a crystal content of 45 vol % corresponds to an increase in viscosity by a factor of 0.6-0.9 log unit, while a crystal content of 55 vol% leads to an increase by 1.2 to nearly 1.8 orders of magnitude (Fig. S1c). In these conditions, the magma existing during the classical strombolian activity has a viscosity of 500-820 Pa.s and 650-1000 Pa.s for 45 vol% and 55 vol% of crystals, respectively.

Input from surface measurements

Erebus, Stromboli and Yasur are well-studied strombolian volcanoes.

The description and quantification of the surface activity at Erebus, which can safely be observed from above (Fig. 6) are superbly done either using gas studies (Oppenheimer and Kyle 2008; Oppenheimer et al. 2009; 2011; Boichu et al. 2010; Ilanko et al. 2015a; 2015b) and/or geophysical studies, which include videos, infrasound, seismicity and radars (Rowe et al. 2000; Dibble et al. 2008; Johnson et al. 2008; Jones et al. 2008; Aster et al. 2003; 2008; Gerst et al. 2008; 2013). The degassing at Erebus (Dibble et al. 1988; Rowe et al. 2000; Dibble et al. 2008) is also mainly two-fold. It takes the form of rare explosions (Johnson et al. 2008; Peters et al. 2014b), whose gas is initially strongly overpressurised, here called active degassing, and of more frequent (each 11 min) and much smaller gas releases, associated to a very small gas overpressure (blue cloud on photo small bubble breaking on Fig. 6; Oppenheimer et al. 2009; Peters et al. 2014b; Ilanko et al. 2015a and 2015b), hence here called passive degassing, and similar gas puffing. Gas studies have been restricted to short continuous periods, the longest lasting 10 hours (Fig. 6d; Oppenheimer et al. 2009) and mostly mostly focused on the passive degassing (Oppenheimer and Kyle 2008; Peters et al. 2014b, 2018; Ilanko et al. 2015a) rather than on the explosions, which only occurred on average 3-6 times a day (Jones et al. 2008; Oppenheimer et al. 2009; Oppenheimer et al. 2011; Ilanko et al. 2015b). In contrast, infrasonic, seismic and radar measurements, which have been run continuously for several days, were able to constrain many physical parameters, such as velocities and gas volumes, and mechanisms occurring at the vent (Johnson et al. 2008; Jones et al. 2008; Aster et al. 2003; 2008; Gerst et al. 2008; 2013). Estimates of gas volume from explosions have been obtained from infrasonic measurements to vary between 10^3 and 3×10^4 m^3 (Johnson et al. 2008; Table 3). Gas puffing, although markedly smaller than explosions (Fig. 6d), could nevertheless significantly contribute to the gas fluxes due to their occurrence (Oppenheimer and Kyle 2008; Peters et al. 2014b, 2018; Ilanko et al. 2015a). Aster et al. (2003; 2008) showed that the Very Long Period of the seismic records (VLP) at Erebus could be very well explained by the response of the magma column to the ascent of a Taylor bubble (Fig. 3c) and its subsequent disequilibrium, in agreement with the laboratory experiments (Ripepe et al. 2001). The moment tensor inversion of the VLP events provided an estimate of the average displaced mass of magma, 8×10^7 kg for an acceleration of 1 m^2/s (Aster et al. 2008). This mass can be contained in a conduit radius of 5.6 m, when assuming a magma column height of 400 m (Aster et al. 2008), in perfect agreement with observations of the conduit radius at the surface, 5-10 m (Dibble et al. 2008; Oppenheimer et al. 2009). The oscillation in volume of the rising Taylor bubble (Fig. 3c), detected by using an array of 3 radars, showed that most of their gas overpressure in the conduit is released by these precursory oscillations rather than during their bursting (Gerst et al. 2013). They also show that the sound of the explosion is related to the bursting rather than by the bubble volume oscillation, in contrast to what had been proposed at Stromboli (Vergniolle and Brandeis 1994; 1996). The difference in the bursting mechanism of large bubbles between Erebus and Stromboli is likely to result from the large differences in magma viscosity, which are $10^{6.3}$ Pa.s (Le Losq et al. 2015) and $10^{2.7}$ Pa.s calculated using Giordano et al. (2008), respectively. The case of Erebus illustrates the importance of having an accurate estimate of the magma viscosity. The Taylor bubbles (Fig. 3c) associated to the explosions have been considered to be able to grow a wake at their bottom, when using the viscosity previously estimated to be ~1600 Pa.s (Kyle et al. 1992; Calkins et al. 2008), a value now considered as too low (Le Losq et al. 2015). However, this mechanism is now shown to be impossible when using the updated value of the magma viscosity of $10^{6.3}$ Pa.s (Le Losq et al. 2015), because their Reynolds number is very small (Table 3). This drastic change in the interpretation of the degassing pattern, at the surface and in the conduit, shows the key role of magma viscosity in understanding the eruptive behaviour. The result associated to this updated magma viscosity is in perfect agreement with the finding of Oppenheimer et al. (2009) and Moussallam et al. (2016), who have suggested that the degassing at Erebus is driven by a stable bi-directional flow, in which the new batch of magma regularly replaces the degassed sinking magma.

The degassing at Stromboli has been extensively described (Fig. 12) and quantified by gas and geophysical studies (Harris and Ripepe 2007; Ripepe et al. 2008; Ripepe et al. 2005; Del Donne and Ripepe 2012; Pering et al. 2020; Thivet et al. 2021). The main techniques, which have been used separately or simultaneously, consist into 1) videos in the visible and infrared range and rarely high-speed cameras (Patrick et al. 2007; Harris et al. 2012; Taddeucci et al. 2012a, b; Harris et al. 2013; Gaudin et al. 2014a; 2014b; Bombrun et al. 2015; Gaudin et al. 2017); 2) DOAS, multi-gas, open-path Fourier transform infrared spectroscopy, ultraviolet-cameras for gas studies (Burton et al. 2007; Aiuppa et al. 2010; Tamburello et al. 2012), 3) infrasound, seismicity and radar for geophysical studies (Weill et al. 1992; Vergniolle and Brandeis 1994; 1996; Chouet et al. 1999; 2003; Scharff et al. 2008; Genco and Ripepe 2010; Del Donne et al. 2016; Patanè et al. 2017) and 4) laboratory experiments and models (Lane et al. 2013; Del Bello et al. 2012; 2015). It is now well understood that the degassing at Stromboli is also mainly two-fold, with the weak puffs, which occurs quasi-permanently at the central vents but can also exist at times at the northeastern and southwestern vents (Harris and Ripepe 2007; Gaudin et al. 2017; Pering et al. 2020) and the explosions, whose physical parameters, such as ejecta and gas velocities or gas volumes, are now well known (Harris and Ripepe 2007; Patrick et al. 2007; Harris et al. 2012;

Taddeucci et al. 2012a, b; Gaudin et al. 2014a; 2014b; Bombrun et al. 2015; Thivet et al. 2021). Gas volumes from explosions have been estimated to be 2-100 m^3 (Vergniolle and Brandeis 1996), 20-35 m^3 (Ripepe and Marchetti 2002), 400 m^3 (Tamburello et al. 2012) whereas the gas volumes in the puffs only reach 19-211 m^3 (Harris and Ripepe 2007), 1.4-21.5 m^3 (Tamburello et al. 2012), 1-100 m^3 (Gaudin et al. 2017). The occurrence of puffs, each 1 to 2 seconds, is responsible for the major contribution of passive degassing to the total gas flux, > 95 %, (Ripepe and Marchetti 2002; Ripepe et al. 2008; Gaudin et al. 2017). Explosions and puffs at Stromboli differ significantly in their gas overpressure, large or small for explosions and puffs, respectively, and in a lesser extent on their gas volumes, large or small for explosions and puffs, respectively. They also differ in their depth of formation, 3 km for the deepest explosions and very shallow (11-150 m), for puffs (Burton et al. 2007). Hence explosions correspond to active degassing while puffs belong to the passive degassing.

To a lesser extent among the well-studied volcanoes, there is Yasur (Fig. 13a). Gas studies (Bani and Lardy 2007; Bani et al. 2012; Oppenheimer et al. 2006; Woitischek et al. 2020), visible, thermal and high speed videos (Bani et al. 2013; Gaudin et al. 2014a; 2014b; Gomez and Kennedy 2017) together with seismic, infrasonic and radar measurements (Nabyl et al. 1997; Battaglia et al. 2012; 2016a, b; Kremers et al. 2013; Marchetti et al. 2013; Spina et al. 2016; Meier et al. 2016; Jolly et al. 2017; Iezzi et al. 2019; Simmons et al. 2020; Perring et al. 2019; Fee et al. 2021) have in the past 20 years help to constrain the eruptive pattern. Some of these studies have also shown two classes of degassing (Oppenheimer et al. 2006; Bani et al. 2013; Meier et al. 2016; Kremers et al. 2013; Marchetti et al. 2013; Spina et al. 2016; Simmons et al. 2020; Fee et al. 2021), although in practice a continuum of degassing events may exist (Gaudin et al. 2017). The frequent and weakly overpressurised events on one side and the less frequent but strongly overpressurised events on the other side are also examples of passive and active degassing, referred by Spina et al. (2016) as minor and major events. Explosions at Yasur are very frequent, one per 1-2 min (Spina et al 2016; Woitischek et al. 2020), while the minor events occurs as frequently as one event each 1-5 min (Bani et al. 2013; Fee et al. 2021) to 40 per min (Spina et al. 2016). The gas volumes of the strong explosions have been estimated for at 5-80x10^3 m^3 from infrasound modelling during a vigourous period (Iezzi et al. 2019) and on average at 14.25x10^3 m^3 from open-path Fourier transform infrared spectroscopy combined with SO_2 flux measurements during an average period (Woitischek et al. 2020).

These three laboratory open-vent volcanoes clearly show that degassing consists in both a strong and a weak degassing, here referred to as active and passive degassing, respectively. In this respect, the active degassing at Erta 'Ale (spherical cap bubble; Fig. 3a) shares a similar origin than explosions at Stromboli and Erebus and to the major explosions at Yasur.

The strength of active degassing can be quantified by the maximum gas flux. Here we report values that can be compared together because they all derive from modelling the acoustic waves. The maximum gas fluxes reach 510 m^3/s at Erta 'Ale (Bouche et al. 2010), 680 m^3/s at Stromboli (Vergniolle and Brandeis 1996), $3x10^3$ - $6x10^4$ m^3/s at Yasur (Iezzi et al. 2019), and $7x10^3$ - $7x10^4$ m^3/s at Erebus (Johnson et al 2008). It is tempting to relate the difference in strength to the respective viscosities of undegassed and degassed magma that range from 22-27 Pa.s (Erta 'Ale), 500 - 10^3 Pa.s (Stromboli), 5.8 $\times 10^2$ - 1.5 $\times 10^5$ Pa.s (Yasur), up to $10^{6.3}$ Pa.s (Erebus). Similarly, the small gas release at Erebus (blue cloud; Fig. 6) should be compared to the puffs of Stromboli, to the minor events at Yasur or to the flat bubbles at Erta 'Ale, although at Erta 'Ale additional effects exist because of the cold crust.

This interpretation of the strombolian activity with a well identified two-fold degassing could be applied more broadly. Therefore time series need to be much larger than the typical return time of active degassing, if the goal is to assess its associated eruptive pattern. This may become a challenge at Erta 'Ale, from the relatively short time series possible in gas studies (Sawyer et al. 2008), as well as at Erebus, due to rarity of explosions, 4-6 per day (Rowe et al. 2000; Burgisser et al. 2012; Jones et al. 2015) and at Villarica (Sawyer et al. 2011; Moussallam et al. 2016).

Vulcanian activity at open-vent volcanoes

Our selection of open-vent volcanoes, associated to intermediate to high-silica magma compositions, may present short vulcanian explosions. It occurs at Arenal (Mora et al. 2022; Fig. 13b-d), Fuego (Morrissey et al. 2008; Marchetti et al. 2009; Diaz-Moreno et al. 2020), Popocatépetl (Schaaf et al. 2005; Fig. 14a-b) and Santiaguito (Fig. 14c; Rose 1972; Rose et al. 1987; Harris et al. 2002; 2003; Bluth and Rose 2004; Johnson et al. 2004b; Sahetapy-Engel et al. 2008; Sahetapy-Engel and Harris 2009a, 2009b; Marchetti et al. 2009; Johnson et al. 2011; Scott et al. 2013). A vulcanian explosion can be produced by the disruption of a solid cap suddenly failing under a significant underlying gas overpressure. The overpressurised gas is suddenly released and often leads to the formation of small eruptive columns of a few kilometers high or above and sometimes with pyroclastic dense flows (Clarke et al. 2013). The gas ejection at the vent is short compared to the rising time of the eruptive columns, making the initial injection of the gas in the atmosphere sustained by an initial pulse of overpressurised gas rather than by a continuous gas flow feeding the eruptive column.

The pre-eruption pressure and ejection velocity are relatively high, <1-10 MPa and 400 m/s (Morrissey and Chouet 1997; Arciniega-Ceballos et al. 1999, 2012; Chouet et al. 2005; Clarke et al. 2013). A shock wave, i.e. a pressure discontinuity, is produced in air upon disruption of the plug and travels into the atmosphere at a velocity exceeding that of the sound, while a decompression-induced fragmentation propagates down into the conduit (Kieffer 1981; Turcotte et al. 1990; Woods 1995). This fragmentation, inducing the formation of ejecta, only occurs in the shallowest portion of the conduit (Clarke et al. 2013). The magma left in the conduit cools until being sufficiently cold and rigid to seal the top of the magma column. Meanwhile, some vesiculation occurs below, inducing the building-up of pressure, ultimately responsible for the next vulcanian explosion (Clarke et al. 2013).

Several volcanoes, such as Arenal (Mora et al. 2022), sometimes Fuego (Martin and Rose 1981; Morrissey and Mastin 2000), and perhaps Santiaguito with the small and strong ash-and-gas explosions, are able to switch between periods of vulcanian explosions and periods of strombolian explosions. This implies that a drastic change of conditions, between a mechanically sealed vent and an open vent, can occur at the vent, although perhaps one vent can be sealed while another one is simultaneously unsealed, as recently proposed for Arenal (Mora et al. 2022). The conditions, which prevail at such transitions, have not yet been clearly identified. Alternatively, Clarke et al. (2013) had proposed that the difference between strombolian and vulcanian explosions results in the bubble motion, largely separated or stagnant in the magma, respectively.

Popocatépetl is also remarkably surprising because the dome prior to a vulcanian explosion is seen rising and growing into the conduit (R. Campion, pers. com., 7 July 2021; Fig. 14a and 14b), invalidating the conditions of a fully sealed vent. Furthermore the SO_2 flux is always quite high, (Table 2b; Campion et al. 2018). This high SO_2 flux exists not only during vulcanian explosions but also between 2 successive vulcanian explosions. This observation also appears to be incompatible with the condition of a fully mechanically sealed vent. The detection by a thermal camera of one or two circular hot zones, of 20-50 m in diameter, is likely to be associated to the gas percolation (R. Campion, pers. com., 7 July 2021).

In contrast, Santiaguito, which mostly display dacitic domes and sometimes, vulcanian explosions (Yamamoto et al. 2008; Scharff et al. 2012) as at Popocatépetl, has a surprisingly low SO_2 flux (Table 2b). The classification of explosions at Santiaguito is still a matter to debate, from a closed vent prior to explosions to a fully open vent. Explosions are considered as weak vulcanian explosions (Johnson et al. 2011), or referred to as small to moderate gas-and-ash explosions (De Angelis et al. 2019; Wallace et al. 2020), rather than strombolian explosions (Bluth and Rose 2008), while the vent is sometimes considered as fully open for degassing (Holland et al. 2011).

The level of the dome at the conduit varies at different periods (Lamb et al. 2019; Gottschammer et al. 2021). To our knowledge, no photographic evidence exists of a high-level dome being systematically emplaced prior to a vulcanian explosion. But the dome extrusion, often cyclic, is a frequent feature of its long-lasting eruption (Rose 1972; Rose et al. 1987; Harris et al. 2002; 2003). The initiation of a vulcanian explosion had been beautifully catched by a video taken from above, showing that an explosion starts with a very weakly overpressurised degassing on an annulus prior to the entire disruption of the solid cap in one unit from the center of this circle, as initially quantified by Bluth and Rose, (2008). This may be indicative that the eruptive pattern is similar at Popocatépetl and Santiaguito, although with two contrasting SO_2 fluxes (Table 2b) and perhaps different amplitudes in the variations of level of magma in the conduit. The strength in the explosions is also different at Popocatépetl and Santiaguito, typical and weak, respectively (Marchetti et al. 2009; Johnson et al. 2011; Scharff et al. 2012).

The differences between vulcanian and strombolian explosions have been tentatively quantified by looking at the simultaneous thermal and infrasonic records performed at Villarica, Stromboli, Fuego and Santiaguito (Marchetti et al. 2009). Strombolian explosions at Stromboli and Villarrica present relatively low values of thermal radiation energy, consistent with the short explosive events of these two volcanoes. In contrast, the longer-lasting thermal waveforms observed for explosions at Santiaguito and Fuego result in the longer ash plume dynamics, which corresponds to high values of thermal radiation energy. However, Santiaguito and Villarrica share similar infrasonic energies, both being lower than the values produced by explosions at Stromboli and Fuego (Marchetti et al. 2009). This may be associated to the very low level of activity both at Villarrica and Santiaguito during this period. The relationship between infrasonic energy, used as a proxy of gas thrust, and the difference between infrasonic and thermal energies, used as a proxy of buoyancy, shows that strombolian and vulcanian explosions are organised in two very different clusters of points, suggesting a method to fully quantified these types of activity (Marchetti et al. 2009). Furthermore, combining thermal and infrasonic records on open-vent volcanoes opens an avenue for a quantified description of surface activity. These joined records could be used for deciding whether the vent is properly sealed or open and also for understanding how the transitions between regimes can occur at a single volcano.

Thermal models

Open-vent volcanoes must release both gas and heat in order to maintain a persistent activity and one key ingredient to maintain an open-vent volcano active is to reduce the heat loss. We discuss below three mechanisms by which heat transfer can occur, mainly conduction, thermal convection and arrival of hot magma through bubbly wakes.

Thermal models of lava lakes

The radiated heat output had been measured at several volcanoes, mostly at the surface of lava lakes in relatively close proximity, such as at Erta 'Ale (Burgi et al. 2002; Harris et al. 2005; Spampinato et al. 2008), Erebus (Calkins et al. 2008), Nyiragongo (Spampinato et al. 2013) and Kilauea (Spampinato et al. 2012). But thermal measurements have also been done by satellites (Ramsey and Harris 2013), and routinely such as by MODIS (Harris et al. 1999; Copola et al. 2016; Vergniolle and Bouche 2016; Wright 2016; Aiuppa et al. 2018; Naismith et al. 2019) or by SEVERI (Field et al. 2012).

Thermal models of lava lakes, initially performed without considering the convection (Peck et al. 1977), aimed at modelling the cooling of lava lakes, thereby estimating the thickness of the crust as a function of time and quantifying the role of small bubbles in stopping of convection (Worster et al. 1993; Davaille 1993). The quantification of the heat budget of a lava lake or a magma reservoir requires the knowledge of the in and out heat fluxes. The heat transfer occurs by conduction for thin lava lakes as well as by thermal convection, if its thickness exceeds a critical value (Davaille 1993). The cooling is very slow for a sole thermal conduction, such as for the thinnest lava lakes at Kilauea (Davaille 1993) and at Erebus, whose magma depth in the crater area is only of a few tens of meters (Jones et al. 2015). Once the thermal convection sets in, the heat losses are drastically enhanced. Several additional factors can prevent thermal convection to exist, such as a gas volume fraction exceeding 0.6 vol% (Davaille 1993), as for the cooling of the Makaopuhi lava lake (Hawaii), or the settling of large crystals (Carrigan 1987) as for the Kilauea Iki lava lake (Helz, 1987; Davaille 1993; Jellinek and Kerr 2001). Additionally, the thickness of the solid crust growing at the surface has been modelled under the assumption of a strong thermal convection within the lava lake (Worster et al. 1993).

The temperature contrast between the magma within the lava lake and its surroundings rocks should lead to its cooling if given a sufficient time. This occurs briefly at the lava lake of Erta 'Ale for several months around December 2004 (Fig. 7c). At this time, the degassing occurred at the site of the 3 hornitos, located above the underlying conduits (Fig. 7c; Vergniolle and Bouche 2016). Furthermore, the existence of hornitos, which could result from the local accumulation of ejecta able to reach the surface of the partially encrusted lava lake rather than falling back within the lava lake, showed that the Strombolian explosions were still ongoing at this time. Therefore, lava lakes never cooled entirely, hence could restart as a hot lava lake when the solid crust disappeared.

The lava lake at Villarrica, when encrusted, has small openings by which the degassing can occur (Gurioli et al. 2008; Goto and Johnson 2011; Johnson et al. 2018). The comparison between Villarrica and Erta 'Ale lava lakes suggests that the openings at Villarrica may be located above the underlying conduits. However the lack of a small structure around the openings at Villarrica suggests that the level of the underlying lava lake is further away from its solid crust than that at Erta 'Ale, as also suggested from acoustic records (Johnson et al. 2018).

The observed lack of cooling of lava lakes has been first explained by the arrival of hot magma brought to the surface by convective processes, driven by a density difference between a volatile-rich magma and a degassed magma. This model, here referred to as a bi-directional flow model (Fig. 15) considers that the hot and gas-rich magma rises while the degassed and cold magma falls back in the conduit (Francis et al. 1993; Kazahaya et al. 1994; Stevenson and Blake 1998; Oppenheimer and Francis 1998; Harris et al. 1999; Oppenheimer et al. 2004; Witter et al. 2004; Harris et al. 2005; Jones et al. 2006; Huppert and Hallworth 2007; Harris 2008; Palma et al. 2011; Beckett et al. 2011; 2014). The bi-directional flow models of Stevenson and Blake, (1998; Fig. 15a) and Huppert and Hallworth, (2007; Fig. 15c) were used at Nyiragongo to estimate both the conduit diameter and the net magma flux necessary to maintain its giant lava lake (> 15×10^6 m^3) in a molten state (Burgi et al. 2014; 2020).

Alternatively the heat could be transferred from depth to the lava lake by the arrival of bubble clusters, initially formed in the wake produced at the bottom of the driving spherical cap bubbles during their rise in the conduit (Bouche et al. 2010; Fig. 11). The heat brought to the lava lake is provided by the interstitial magma initially present in the bubbly wake prior to its fragmentation in the lava lake (Bouche et al. 2010) rather than that solely brought by the series of small hot bubbles, as incorrectly deduced for Villarrica and Kilauea (Moussallam et al. 2016). The key point of the qualitative thermal model of Bouche et al. (2010) is that the hot magma added to the lava lake had been kept hot because it had travelled from depth to the surface at a relatively large velocity, that of the driving spherical cap bubble. The second point is that this mechanism for heat transfer is only possible if the rise of the large bubbles is sufficiently vigorous to grow an instable wake, laminar or a turbulent for Reynolds number of 70(100) - 2000 and >2000, respectively (Bouche et al. 2010). At Erebus, the large bubbles responsible for explosions cannot grow a wake when using the updated value of the viscosity $10^{6.3}$ Pa.s (Le Losq et al. 2015), in agreement with the findings that the behaviour of the lava lake is governed by a magma exchange rather than by an underlying gas flux from the reservoir (Peters et al. 2014b). The heat at Erebus is therefore provided either by magma upwards motion in a bi-directional flow in the conduit (Oppenheimer et al. 2009, 2011; Moussallam et al. 2015) or by the enthalpy of the shallow reservoir (Aster et al.

2003), located either at 400 m (Aster et al. 2008) or between 80 m and 1300 m, when assuming that the volatile species are at equilibrium (Burgisser et al. 2012), or by a combination of the two. A source of heat, which combined the enthalpy of the shallow reservoir with a bi-directional flow in the conduit, is our preferred interpretation, given the comparatively large conduit diameter at Erebus, 4-10 m (Dibble et al. 2008; Oppenheimer et al. 2009), which exceeds the value of 1 m proposed to balance the heat loss from the conduit walls with the assumed magma supply rate in the conduit at Stromboli (Giberti et al. 1992).

It is particularly important to realise that lava lakes, which expose large hot areas to the surface, have a sole or an additional source of heat, which is provided by the existence of the detached bubbly wakes (Fig. 11), when compared to open-vent volcanoes only presenting tops of magma columns. The thermal effect at lava lakes, associated to the possible existence of detached bubbly wakes, is complicated to calculate in detail because it requires to know both the occurrence of the driving large bubbles on a long time scale, due to fluctuations in the level of activity, and the local gas volume fraction in the conduit.

Several main types of degassing at lava lakes can exist. On one side, the existence of detached bubbly wakes at depths of > 1 km and > 500 m-1 km at Erta 'Ale and Nyiragongo, respectively (Table 3; Fig. 11a), suggests that their heat could be a significant source over the entire length of the conduit up to 1 km. Hence it would promote efficient exchange of heat between this depth and the surface during the rise of the driving large bubbles. On the other side, the detached bubbly wakes may mostly exist at depths and be partially or fully suppressed in the conduit, such as at Villarrica and Ambrym at times (Table 3; Fig. 11b and 11c), respectively, but still play a key role in providing heat or in decreasing the gas volume fraction by favouring the separated gas flow.

Thermal models in conduit

The first model considered that the magma undergoes thermal convection in the conduit (Carrigan 1983). In this case, ascending hot (possibly gas-rich) magma mixes with the magma residing in the conduit and the cooling occurs at the expense of the reservoir enthalpy (Carrigan 1983). The second model that was applied to Stromboli suggested that thermal convection could be ignored due to both the small diameter of the conduit and the constant rise of large bubbles in the conduit (Giberti et al. 1992). They suggested that the only communication between magma reservoir and conduit occurs after an explosion when the magma level in the conduit had returned to its equilibrium value, an interpretation fully validated by laboratory experiments (Ripepe et al. 2001) and by the location of the tremor and Very Long Period events (Chouet et al. 1999; 2003). The numerical model of Giberti et al. (1992), which considers a large reservoir located below a small conduit, showed that the persistent state of Stromboli could be very well be explained by a shallow reservoir at a few hundreds of meters below the vent, a result entirely validated by further independent studies (Chouet et al. 1999; 2003; Harris and Ripepe 2007). The same model could be partly applicable to Erebus, which presents a shallow reservoir at a depth of 400 m (Aster et al. 2003; 2008), and a conduit slightly larger than twice that at Stromboli (Dibble et al. 2008; Oppenheimer et al. 2009).

Bi-directional flow models in conduit

Another potential convective mechanism, that may occur in the conduit, is driven by the density difference between a hot and volatile-rich magma, light and rising, and a cold and volatile-poor magma, hence dense, flowing in opposite direction (Fig. 15a). This mechanism is based on an exchange flow in the conduit (Kazahaya et al. 1994; Harris and Stevenson 1997; Stevenson and Blake 1998). The excess degassing observed at the surface of Stromboli, estimated when comparing the volumes expelled by gas and magma during strombolian explosions (Chouet et al 1974; Ripepe et al. 1993; Patrick et al. 2007; Ripepe et al. 2008; Delle Donne and Ripepe 2012; Harris et al. 2012; Harris et al. 2013; Gaudin et al. 2014b), had been explained by the existence of such a flow loop. This bi-directional flow is a potential mechanism for explaining both the persistent outgassing and providing heat for the thermal budget of conduits and lave lakes.

Existing models

Several models, now referred as bi-directional flow models (Fig. 15), were developed with various assumptions detailed below. Several studies use this model to explain the behaviour of several open-vent volcanoes, without any clear indication on how such a flow loop could be initiated in the conduit and maintained for very long periods. The rising magma is degassing on its way towards the surface due to gas exsolution, thereby increasing its positive buoyancy. Laboratory experiments of exchange flows in vertical pipes, performed in conditions for which the net volume flux of ascending magma is matched by the volume flux of the descending magma, have shown the key role of the ratio of viscosities, between that of the more viscous fluid divided by that of the less viscous fluid (Stevenson and Blake 1998; Huppert and Hallworth 2007; Beckett et al. 2011; Palma et al. 2011). Models describing the spatial organisation of the upwards and downwards magma flows in the conduit had been called bi-directional flow models (Fig. 15).

The pioneer quantitative work of Stevenson and Blake (1998) used laboratory experiments to show that the bi-directional flow is a core-annular flow, in which the less viscous fluid flows in the center and the more viscous flows in an annulus close to conduit walls (Fig. 15a). They present a theoretical model for the core-annular flow, which is used to give a reasonable estimate of conduit radius at Stromboli (Stevenson and Blake 1998) and Villarrica (Witter et al. 2004). Burton et al. (2007b) added to the core-annular flow (Fig. 15b) the degassing path at each depth along the conduit, constrained by petrology data and SO_2 flux at Stromboli but ignore the crystallisation path. The rising magma is modelled to be degassing at equilibrium due to the gas exsolution. The area available for the rise of the degassing magma is calculated by assuming that its velocity is maximum (Burton et al. 2007b), an assumption later shown to be incorrect (Beckett et al. 2011; Suckale et al. 2018). Nevertheless, this early model gave an estimate of the radius and the velocity of the rising degassing magma at each depth, as well as those of the falling degassed magma (Burton et al. 2007b). They also provide an estimate of the conduit radius, in agreement with radius observed at the surface.

This model was later refined by laboratory experiments (Fig. 15c), performed for both vertical and inclined conduits, and a dimensionless analysis, which included lateral gradients in magma viscosity and density (Palma et al. 2011). But the properties of the rising and degassed magma were taken to be constant during transport (Palma et al. 2011). This model was used to constrain the degassing and ascent rates of volatile-rich magma, which, when combined with petrologic data on magmatic volatile content at Villarrica, led to an estimate of the conduit radius (Palma et al. 2011). Palma et al. (2011) only consider the flow in the lowest conduit, in which the degassing occurs with stagnant CO_2-bubbles and ignore the shallowest conduit for which the bubbles become sufficiently large to have a separated gas flow in respect to the magma, on which a significant exsolution of water is added.

The model of Huppert and Hallworth, (2007), carefully and extensively performed to assess the effects of each physical parameter, showed that the core-annular flow is the most frequent regime (Fig. 15d). They also noted that the fluid may be highly irregular and may present a varicose instability, sometimes leading to the fragmentation of the degassing hot magma in many discrete blobs (Huppert and Hallworth 2007). When this situation occurs, the flow of the degassing magma is not organised in the conduit as a continuous stream but as a discontinuous series of vertically spaced blobs of degassing magma. A coefficient flux, defined by a ratio of two dimensionless numbers, is used to analyse the flux of the exchange flow (Huppert and Hallworth 2007; Palma et al. 2011). This coefficient was experimentally estimated for vertical and inclined flows (Palma et al. 2011). Note that these laboratory experiments were performed with fluid reservoirs at the end of the pipes to ensure a longer duration for the bi-directional flow in the conduit (Huppert and Hallworth 2007; Beckett et al. 2011; Palma et al. 2011).

When the ratio of viscosities exceeds 75, the bi-directional flow is organised with an axisymmetric core-annular flow (Fig. 15d), in which the less viscous fluid occupies a cylindrical core and the denser and more viscous fluid flows downwards in an annulus (Huppert and Hallworth 2007; Beckett et al. 2011). The bi-directional flow is a side-by-side flow, for which both fluids are in contact with the conduit walls and there is a single interface between them (Fig. 15 d), for a ratio of viscosities less than 117 (Beckett et al. 2011). The side-by-side flow is transitional (Fig. 15d) for a ratio of viscosities between 5 and 59 and presents simultaneously both a core-annular flow and a side-by-side flow at different depths (Beckett et al. 2011). In this case, the flow of the degassing magma is not a continuous stream from depth to the surface (Fig. 15d).

Huppert and Hallworth (2007) use a dimensionless analysis for quantifying the flux of the dense fluid, referred with index u for upper fluid in equations, as a function of the ratio of the two viscosities, γ, and the Reynolds number of the upper fluid, Re_U. The dimensionless number, called the transport number for exchange flow, *Te*, is defined by:

$Te=\mu_U Q / (g\Delta\rho R^4)$ (Eq. 6)

where Q, Δρ and g are the volume flux in either fluid in the tube of radius R, the difference in density between the denser and the lighter fluids and the acceleration of gravity, respectively. For low Reynolds number, two equations allow the calculation of the transport number *Te* as a function of the viscosity ratio γ

(□□□□□□□□□□□□□□□□□□□□□□□□□□□□o□□□□□□□□□□□□□□□□□□□□□□□□□ fluid divided by that of the less viscous fluid). The coefficient is estimated from laboratory experiment scaled by a dimensionless analysis.

$Te=0.01\gamma \ (\gamma << 1)$ (Eq. 7a)

$Te=0.125 \ (\gamma >> 1),$ (Eq. 7b)

whereas for large Reynolds number, the transport number, *Te*, depends on is the value of the Reynolds number of the upper fluid, Re_U as :

$Te=0.556\ \Re_U^{-1} \quad (Re_U >> 1)$ (Eq. 8)

where Re_U is the Reynolds number of the upper fluid.

Beckett et al. (2014) showed a similar relationship, for an axisymmetric core-annular flow, between the net magma flux of the ascending magma, Q, and the viscosity ratio between the degassed and the volatile-rich buoyant magma components, β:

$Q = 0.059\beta^{-0.74}(g\Delta\rho R^4/2\mu_b)$ (Eq. 9) where $\Delta\rho$ is their difference in density, μ_b is the dynamic viscosity of the buoyant component, g is gravitational acceleration and R is the effective conduit radius.

This model had been applied to Stromboli and combined to the degassing and crystallisation paths of the ascending and descending magmas, constrained by gas flux and melt inclusion data (Beckett et al. 2014). They propose, based on their choice of viscosity ratio, that the bi-directional flow below a depth of 3 km is a core-annular flow, in which the degassing magma rises in the center while the degassed magma flows around it (Beckett et al. 2014). Above a depth of 3 km, they suggest that the bi-directional flow is a side-by-side flow, with both ascending and descending magma adjacent to a portion of the conduit walls (Beckett et al. 2014). In this model, the degassing due to gas exsolution is assumed to occur at equilibrium and with an implicit assumption that the small bubbles embodied in the magma are stagnant (Beckett et al. 2014). The implications of such a hypothesis, also used previously at Stromboli (Burton et al. 2007b) and later at Ambrym (Allard et al. 2016b), are strong, as previously discussed. No theoretical relationship between the exchange flux and the pressure gradient so far exists (Beckett et al. 2014), limiting volcanological applications to the use of empirical laws, such as the coefficient flux (Huppert and Hallworth 2007; Palma et al. 2011) or that of Beckett et al. (2014) used at Ambrym (Allard et al. 2016b). The core-annular flow, the most common flow configuration, is also shown to be inherently bistable, i.e. able to switch between two steady states, and the regime at work cannot be predicted solely from the material properties of the fluids and the tube geometry alone (Suckale et al. 2018).

The spatial configuration of a bi-directional flow can only be organised as discussed above if no large bubble rises in the conduit and perturb the flow field. The existence of large bubbles rising in the conduit as spherical cap bubbles or Taylor bubbles (Fig. 3b and 3c), and the potential formation of detached bubbly wakes (Bouche et al. 2010; section lava lakes; Fig. 11) at several lava lakes, can erase and replace the above bi-directional flow models when the driving large bubbles are very frequent in the conduit. The above bi-directional flow models can be solely at work in between the rise of two successive large bubbles, 1 hr at lava lake of Erta 'Ale (Bouche et al. 2010).

Implications and examples of bi-directional flows

By definition, a bi-directional flow involves a rising degassing magma and the descending degassed magma, hence is a form of convection. Their relative velocity in the conduit cannot be estimated directly. In the past, it has been derived from the direct measurements of surface velocity at lava lakes, as summarised in Lev et al. (2019). A notable exception is the case of Kilauea, where ejecta were directly sampled during the enhanced activity of 9 April 2008 (Carey et al. 2013). They allowed the first quantification of the convective velocity and the height of the convective cell in the conduit (Fig. 15e) to be, 0.02-0.8 m/s and 100-300 m, respectively, from the dimensions of the halo of re-dissolving bubbles within the downward flow of magma (Carey et al. 2013).

Modelling the bi-directional flow in a conduit implies to know the relative areas of the rising degassing magma and the descending degassed magma. They vary with depth as a consequence of increasing the gas volume fraction within the degassing magma due to gas exsolution. The velocities of the rising and degassed magma were estimated at each depth based on the magma supply rate when assuming equilibrium conditions and full gas exsolution (Burton et al. 2007). The calculation of the gas volume fraction in the conduit, as estimated for Stromboli (Burton et al. 2007b) and Ambrym (Allard et al. 2016b) is based on two implicit assumptions, one is that the bubbles are small, hence cannot move in respect to the liquid, and the second is that gas and its surrounding magma are in chemical equilibrium for degassing.

A certain amount of small bubbles may be produced in the rising magma mainly due to gas exsolution when approaching to the surface. Alternatively the excess in volatiles can migrate with gas diffusion towards pre-existing bubbles. These bubbles, if small, can either be moving with the rising magma, such as in a homogeneous gas flow, or have their own differential velocity in respect to the liquid, as in a separated gas flow. In the first case, the calculation of the magma viscosity, used by Beckett et al (2014), should consider the gas volume fraction in the magma as part of single phase while in the second case, the magma viscosity should only consider the magma without the small bubbles, which are flowing on their own. The first consequence of a separated gas flow is to reduce the gas volume fraction (Vergniolle and Jaupart 1986), by allowing a larger gas flux in the conduit. The second consequence is that a separated gas flow can enhance the disequilibrium between dissolved and exsolved gas, due to the relatively fast transport of exsolved gas towards the surface. In this respect, the sulphur isotopes could be used to assess the amount of chemical disequilibrium in volatiles, shown to exist at Erta 'Ale in contrast to Masaya (De Moor et al. 2013).

The bubbles present in the rising degassing magma may be sufficiently large to behave as a separated gas flow, or drift flow, in regards to that of the liquid (Vergniolle and Jaupart 1986). In this case, the gas volume fraction should be calculated from the superficial velocity of the gas phase and the drift velocity of a bubble, which depends on both the bubble diameter and the liquid viscosity (Vergniolle and Jaupart 1986; Pioli et al. 2012; Pansino et al. 2019). These calculations rely on a good knowledge of the magma viscosity, estimated without the bubbles present in the separated gas flow, and of the conduit radius, a second key parameter (Pansino et al. 2019). Quantifying the gas volume fraction at the surface also requires the independent determination of the flux of the rising magma and the total gas flux. The magma supply rate derives from the SO_2

flux and the melt sulphur content, which implies full magma degassing from depth to surface. The total gas flux used by Pansino et al. (2019) combines the ratios of di-atomic gases such as CO_2/SO_2 and H_2O/ SO_2, with the SO_2 flux at several volcanoes. However, the total gas flux, i.e. obtained by adding CO_2, H_2O, SO_2 fluxes, and the magma supply rate are not independent, invalidating the use of the estimates of gas volume fractions obtained by Pansino et al. (2019). Nevertheless, a proper estimate of the gas volume fraction should consider whether the small bubbles are flowing in a homogenous flow, i.e. moving together with the liquid, or in a separated gas flow. Because of the key role of the viscosity in understanding the physical process at work in a given volcano, these two limit cases must be considered, unless being able to measure independently whether the gas flow of the small suspended bubbles, induced by gas exsolution, is homogeneous or separated.

The key informations derived from sound waves studies

Studies on infrasonic (<20 Hz) and acoustic (>20 Hz) sound waves, applied for the first time to volcanoes in the 1990's (Vergniolle and Brandeis 1994; 1996; Vergniolle et al. 1996; Garcès et al. 1996; Johnson et al.,1998), can also provide constraints on eruptive patterns. The use of broad-band sensors such as microbarographs (a few tenths of Hz to 200 Hz) have been developed to run continuously, in contrast to microphones (0.1 and 4 kHz) more complicated to protect outdoor. This technique is now expanding significantly for monitoring the volcanic activity, particularly at open-vent volcanoes with an "easy" access. The main interest of acoustic measurements is to provide a remote way to monitor the surface of the magma column and to locate the source of sound when using an array. The location of the source of the sound, often due to degassing at the vent (e.g., Johnson 2005; Johnson et al. 2011; Colo et al. 2010; Marchetti et al. 2013; Kondo et al. 2019), can also be produced by the front of a lahar, such as at Santiaguito (Johnson et al. 2011) or at Villarica, thereby providing an estimate of the flow front in time (Johnson and Palma 2015; Johnson et al. 2015). The frequency of the infrasound had been used at Villarica as a mean of following the level of the lava lake (Goto and Johnson 2011; Richardson et al. 2014), which rises 2 days before the paroxysmal phase of 2015 (Johnson et al. 2018). However, this analysis was only possible because of a very specific geometry of the lava lake, mostly encrusted with a small opening in the crust (Johnson et al. 2018). The satellite SAR imagery at Nyiragongo, which can constrain the lava lake by measuring the length of the shadow cast by the rim of the pit crater hosting the lava lake, can be joined to the analysis of a seismic and infrasonic records to deduce the lava lake level in the future from a single seismic and infrasonic station (Barrière et al. 2018). Combining infrasonic and thermal measurements allows the recognition of vulcanian and strombolian explosions (Marchetti et al. 2009), whereas it can be difficult from acoustic records alone (Mora et al. 2022). This approach could be particularly relevant in the future for open-vent volcanoes with a high-silica magma composition, if run continuously. These volcanoes can either produce vulcanian explosions when the vent is mechanically sealed, strombolian explosions when the vent is mechanically open, and small to moderate gas-and-ash explosions as shown at Santiaguito (De Angelis et al. 2019; Wallace et al. 2020). But transitions exist at times between vulcanian and strombolian explosions, as at Arenal (Mora et al. 2022) and Fuego (Diaz-Moreno et al. 2020; Brill et al. 2022). This requires continuous measurements for a better modelling of this transition.

Various models exist to explain the sound produced by strombolian explosions, each being driven at the vent by the breaking of a Taylor bubble (Fig. 3c). These models are based on the: 1) oscillations in volume of a large bubble prior to its bursting (Vergniolle and Brandeis 1994; 1996); 2) resonances of a rigid cavity opened by a small hole as for Helmholtz resonators (Vergniolle and Caplan-Auerbach 2004); 3) formation of a hole piercing the magma layer overlying a small bubble, either with an extremely thin and inviscid liquid film, as for soap bubbles in water (Vidal et al. 2010; Sanchez et al. 2014) or in a viscous fluid (Koyabashi et al. 2010). The observations that the source of the sound is mostly monopolar had led Johnson et al. (2008) and Gerst et al. (2013), to estimate the gas volume and the gas flux under this assumption for some strombolian explosions at Erebus, with further validation from comparison with video records, at least for the beginning of the explosion (Witsil and Johnson 2018). The robust assumption of a monopole source is valid for any type of explosion (strombolian and vulcanian) providing that the sound propagation is linear, hence not associated to shock waves. The effect of the topography had also been included on the inversion of acoustic waveforms recorded with an array, giving estimates of gas flux and gas volume at Yasur (Iezzi et al. 2019, Fee et al. 2021). The use of a single acoustic sensor, set at a proximal distance from the vent and with an unobstructed line-of sight, provides reasonable estimates of gas fluxes and gas volumes when using the geometrical spreading of a monopole source and ignoring the topography (Johnson and Miller 2014). Furthermore, the use of a monopole approximation to recover the source parameters, such as maximum gas flux and gas volume, is more useful for monitoring purposes than just using the maximum radiated acoustic pressure, sometimes seen to be poorly correlated with the height of the eruptive column (Johnson and Miller 2014). Topography effects can sometimes affect the infrasonic waveforms, such as at Fuego (De Angelis 2019), but the perturbation can be much reduced by the use of an infrasonic array and inversions of waveforms (Iezzi et al. 2019; Diaz-Moreno et al. 2020). However, the use of a single sensor, located at a proximal distance and with unobstructed line-of-sight to the vent, had been proven to give a reasonable estimate of the source parameters also for vulcanian explosions when using a simple monopole source (Johnson and Miller 2014). Inversions of infrasonic waveforms done for small and moderate gas-and-ash explosions at Santiaguito provides the time history of mass eruption rates in good agreement with thermal or visible imagery, validating the use of acoustic measurements for estimates of gas volumes and gas fluxes (Johnson et al. 2010; De Angelis et al. 2016). The radiation pattern of the strombolian explosions at Yasur was also measured by using infrasound sensors aboard a tethered aerostat above the crater area, showing that both path effects from crater walls and source directionality could play a role in the infrasonic waveforms (Jolly et al. 2017).

Non-linear effects in the sound propagation, such as existing during blast waves and shock waves, have been reported for the most vigourous strombolian explosions, with a velocity just slightly above the sound wave at Yasur (Marchetti et al. 2013; Taddeucci et al. 2014; Maher et al. 2022) or well-marked during vulcanian explosions and during the 2018 paroxysm at Fuego (Morrissey et al. 2008; Diaz-Moreno et al. 2020). The modelling using strong shock waves could be applicable to weak shock waves produced by volcanoes (Medici, et al. 2014). Blast waves can often be distinguished from linear sources of sound based on their specific shape and amplitudes exceeding several hundreds of Pa within a few hundred metres from the source and also by their characteristic N-shape acoustic waveforms at a far distance (De Angelis et al. 2019). However, specific acoustic waveforms, asymmetrical with the larger compressive peak in comparison with its following rarefaction peak, are sometimes associated to shock waves and supersonic fluid flow, can be easily obtained for subsonic flows (Brogi et al. 2018), for which the monopole approximation holds. Futhermore, a recent study, also discussing supersonic jet flows, had shown that the sound associated to volcanic vortices and jet noise could be used to retrieve vent size and eruption parameters at open-vent volcanoes (Taddeucci et al. 2021).

In addition, gas velocity and gas volume were also estimated by using the infrasonic power on a subplinian basaltic eruptive column at Shishaldin (USA; Vergniolle and Caplan-Auerbach 2006) and during the 2006 eruption of Augustine (USA; Caplan-Auerbach et al. 2010). However care should be used due to the multiphase nature (solid particles and liquid droplets carried by a hot gas) of the volcanic eruptive cloud when simplifying the acoustic source produced by a sustained eruptive column to a simple dipole or quadrupole (Matoza et al. 2009; 2013). The temporal evolution of the infrasonic power was also used to locate the depth of the reservoir at Shishaldin (Vergniolle and Caplan-Auerbach 2006), at 3.9 km in agreement with melt inclusions (> 3km) (Rasmussen et al., 2018), and the rise in the lava lake prior to the paroxysm at Villarica (Johnson et al. 2018).

The sole use of infrasonic records to estimate the gas volumes at strombolian volcanoes often leads to an underestimate on the total gas volume, as infrasonic records can only record the unsteady gas flow (Johnson 2003) or that of the overpressurised gas expanding at the surface (Vergniolle and Brandeis 1994, 1996). The difference in total gas volumes deduced from infrasonic records with that obtained from records of videos in the visible or infrared or ultra-violet range, open-path Fourier transform infrared spectroscopy and radar is noticeable (see discussion in Vergniolle and Gaudemer 2015). The cause of this discrepancy is mainly a consequence of the significant amount of passive degassing associated to each explosion, keeping in mind that any technique, which cannot measure directly at the vent but above the vent, is also measuring air entrained within the volcanic cloud, such often the case with video, open-path Fourier transform infrared spectroscopy and radar techniques. The existence of passive degassing associated to explosions at Erebus is very clear from the comparison between videos and infrasonic records, in full agreement in the early part of explosion (gas decompression at the vent) but not later (Witsil and Johnson 2018). Although passive degassing could sometimes be associated to a bubbly wake attached to the bursting of the large bubble driving the explosion, the large viscosity of Erebus magma, $10^{6.3}$ Pa.s (Le Losq et al. 2015), prevents such a mechanism to be called for. It is then likely that the passive degassing expelled during an explosion at Erebus is induced by the bursting of numerous small bubbles present in the shallowest part of the magma column and made to burst by the rarefaction wave induced by the explosion and propagating down in the conduit. The active degassing, even if not major in term of gas volume at the vent in comparison with passive degassing, needs to be estimated because is a key to unravel the eruptive pattern, and in particular estimate the gas flux at depth. The comparison between videos and infrasonic records also shows the strong potential of combining various techniques at open-vent volcanoes to assess the extent of both passive and active degassing, hence to obtain a refined estimate of the gas flux.

Sulphur evolution path

The fate of the suphur

New inventory and detection of new and unquantified sources of SO_2 passive emissions in volcanic arcs (Aleutian, Papouasie New Guinea, Indonesia) (Carn et al. 2017), and a better evaluation of the budgets of global volcanic SO_2 and CO_2 emissions (Fisher et al. 2019) have benefited from the advances in space-borne instruments, data treatments, and the combination of satellite-derived measurements with ground-based techniques and networks. It is recognised that the Nyiragongo –

Nyamuragira system significantly contributes to the CO_2 volcanic flux of continental rift (Fisher et al. 2019), and to the global emissions of SO_2 (Carn et al. 2017), after Ambrym (Allard et al. 2016a, b). Since 2012, Nyamuragira strongly contributes to the global budgets of bromine (18–35% Br_{total}) and iodine (8–18% I_{total}) (Bobrowski et al. 2017). It is characterised by an “excess” of sulphur degassing during effusive activity (Bluth and Carn 2008). A comparison between the SO_2 emissions inferred from the melt inclusion data for the 1986 and 2006 eruptions with satellite based records is compatible with pre eruption gas loss and gas accumulation together with degassing of unerupted shallow magma (Head et al. 2011). However, such an excess degassing is questioned and could not be the rule at Nyamuragira (Coppola et al. 2013). Hence the sulphur-degassing budget remained difficult to be constrained because of its multi-valence states and dependence on such parameters as fO_2, fS_2, pressure and magma composition (e.g., Wallace and Edmonds 2011; Métrich 2021).

Erebus is another case where the sulphur evolution path can be tricky. The phonolitic magma that fills the magma at the top of the column is derived from the extensive differentiation of a parental basanite, after the removal of 75 % of crystals (Kyle et al. 1992). The parental melt may contain up 0.25 wt% S versus 0.03-0.06 wt% S in the phonolite as measured in melt inclusions of olivine and anorthoclase, respectively (Moussallam et al. 2014). A part of this sulphur is locked in the sulphide globules described in melt inclusions of their host crystals (Moussallam et al. 2016) as well as in the lava mineralogy (Kelly et al. 2008). A very rough estimation of the magma volume that is sustaining the low SO_2 flux at Erebus during passive degassing could be tentatively derived from the dissolved S content (610 ppm the highest S content in anorthoclase) and the SO_2 flux (on average 52t/d; Oppenheimer et al. 2004; Sawyer et al. 2008; de Moor et al. 2013). The volume of magma that sustained the passive SO_2 emissions at Erebus would be 0.25 m^3/s (7.6 10^{-3} km^3/yr, Tables 1 and 2).

New strategies now involve Unmanned Aerial Aircraft Systems (drone), in complement to satellite based-SO_2 flux measurements (Tropospheric Ozone Monitoring Instrument (TROPOMI); Ozone Mapping and Profiler Suite (OMPS)), to provide large scale and repeated measurements of volcanic gas emissions, and they have been proved to be efficient for almost inaccessible volcanoes (Lui et al. 2020). Manam in Papua New Guinea whose vents have been active for several decades is an example of a newly identified contributor to the global volcanic fluxes of CO_2 and SO_2 (Lui et al. 2020; Edmonds et al. 2021). Observed correlations between the molar CO_2/SO_2 ratios of surface gas emissions and incompatible trace element ratios in bulk rocks (i.e., Ba/La; Sr/Nd) of bulk rocks (Aiuppa et al. 2019) represent a major step forward towards a better quantification of the volcanic gas fluxes. Such an approach has been tested at Pacaya, regarded as the strongest degassing source in Central America (Battaglia et al. 2018), and used to predict the CO_2/SO_2 emissions of so called "unmeasured" volcanoes, as Fuego and Santiaguito in Guatemala (Aiuppa et al. 2019). In Japan six persistently active volcanoes (Miyakejima, Sakurajima, Satsuma-Iwojima, Asama, Aso, Suwanosejima) dominate the annual SO_2 flux (Shinohara 2013) and produce CO_2-poor gas emissions that mirror to the low amount of carbon in subducted sediments (Aiuppa et al. 2019).

The example of Popocatépetl volcano in Mexico

Popocatépetl volcano provides a good example of passive degassing (Delgado-Granados et al. 2001) as a large part of the magma that supports the surface SO_2 emissions is not erupting and continued to degas at depth while crystallising (Witter et al. 2005; Roberge et al. 2009). Popocatépetl is observed to be in a state of permanent open-vent activity since 1994 with cycles of building and destruction (associated to vulcanian explosions) of dacitic lava domes (Gómez-Vazquez et al. 2016; Taquet et al. 2019) and strong gas emissions (5000 tons/d SO_2 as measured on 28/2/2019) from the central part of the dome (Campion et al. 2018). The activity renewed after ~70 years of repose time, the last eruption occurred in 1920 and lasted 7 years (Delgado-Granados 2001). Campion et al (2018) report a 4-year average SO_2 flux of 45 kg/s (3888 t/d against an average value of 1658±893 tons per day (1σ) given by Carn (2017) from SO_2 camera measurements between 2013 and 2016, during which degassing dominates (>95% of the time). They place Popocatépetl as one of the strongest permanent emitters of volcanic SO_2 over this period together with Ambrym (100 kg/s; Allard et al. 2016a, b), Kilauea (10–60 kg/s; Nadeau et al. 2015), and Nyamuragira (20–60 kg/s; Coppola et al. 2016).

From March 1996 to 1st January 1998, the total SO_2 emissions achieved 9 Mt (9-13 kt/d) that is 4 times higher than the SO_2 flux during the inter-eruption period (2-3 kt/d; Delgado-Granado et al. 2001). Roberge et al (2009) conclude to a recharge of a minimum of 0.8 km^3 (equivalent of a magma supply rate of 0.285 kg per year over this period) of mafic magma (for a magma containing 2000 ppm S) for sustaining this high discharge amount of SO_2, rather than convection of magma in the uppermost part of the system. It would imply an initial CO_2 content of 1 wt% (Roberge et al. 2009). They propose a model of decompression and degassing of magma (with up to 5 wt% H_2O) at 150-350 MPa, with only a small portion of this magma reaching the surface, while being mixed with the silicic shallow magma. The effect of H_2O loss promotes crystallisation and increases the mixture viscosity that may slow down the convection. They thus suggest a mechanism based on the intrusion and degassing of a mafic magma batch at the origin of these emissions rather than one based of convection in the shallowest part of the subvolcanic conduits. On the basis of the presence of Mg-rich olivine together with textural and compositional evidence for mixing, Schaaf et al.

(2005) propose dominant recharge of olivine-bearing basaltic andesite magma with relatively high volatile content.

Long-time series of the gas composition at Popocatépetl between 2012 and 2016, after the 2011 magma reinjection, indicate variation of the SO_2 flux between 1990 to 3680 tons per day (Table 2b) with the highest value corresponding active activity with magma extrusion and the lowest quiet period, and an average for the whole period of 2790 tons per day (Taquet et al. 2019). Following the approach developed by Roberge et al. (2009), we have tentatively calculated the magma supply rate for the 2012-2016 period using Taquet et al. (2019) SO_2 flux of 2790 tons per day. The magma supply rate could achieve 0.1 km^3 per year while Campion et al. (2018) obtained a value of 0.16 km^3 (Table 1b) from a compilation of the SO_2 flux since 1995, including periods of high and low activity.

Persistent degassing and sulphur behaviour at open-vent volcanoes in Central American Volcanic Arc

Pacaya, Fuego and Santiaguito are three open-vent volcanoes in Guatemala and are located at the triple junction of the North American, Cocos, and Caribbean tectonic plates that have sustained persistent degassing activity during several decades (Battaglia et al. 2018).

The case of these three volcanoes provide the opportunity of discussing the sulphur behaviour in arc related basalts able to ascent before extensive crystal fractionation at Pacaya, to basalt and basaltic andesites at Fuego and dacitic magmas that are the final products of differentiation of such basaltic melts. Their magmas share comparable Ba/La ratios (on average 44-52) and CO_2/S_{total} ratio of 1-1.5 at Pacaya; 1.5±0.75 at Fuego, and 1.4±0.75 at Santiaguito (Aiuppa et al. 2017; Battaglia et al. 2019). According to these authors they thus share similar nature of slab component with dominant aqueous fluids derived from the slab dehydration, and small amount of carbonate in subducted sediments.

Pacaya volcano, resumed Strombolian activity in 1961, after 200 years of rest and produced lava flow and pyroclastic explosive eruptions over nearly 50 years of activity, with flank eruptions that possibly emptying the upper most parts within the cone (Rose et al. 2013b). Violent explosive eruptions and lava fountains are reported in January and February 2000, and in 2010 (Rose et al. 2013b). Pacaya produced homogeneous crystal-rich high-Al basalt having between nearly 30 to 50 vol% phenocrysts with an average eruption rate for Pacaya of 0.17 ± 0.04 m^3/s (78 kg/s) from 1961 to 2001 (Rose et al. 2013b). The rapid ascent and crustal transfer of magma could have been facilitated by local extensional regime (Cameron et al. 2002; et al. 2018).

Time series of in-situ (Multi-GAS) and remote (ultra-violet camera) plume measurements carried out in January 2016, during a period of relatively mild-strombolian activity at Pacaya, provide a SO_2 flux of 885±550 t/d (Battaglia et al. 2019). In contrast, it has fluctuated since the onset of the ongoing eruptive period in 1965, from 260-290 tons/day in the period of 1972-1992 (Andres et al. 1993). It peaked at 1350 t/d within the 1999–2002 time period of higher level of explosive activity and reached 1570 tons per day while a lava lake is observed at the crater from August 2000 until May 2002 (Rodriguez et al. 2004). These observations led Rodríguez et al. (2004) to propose that Pacaya has a substantial convecting and circulating magma body near the surface that is degassing high-Al basalt, only partially extruded.

A magma production rate of 0.17 ± 0.04 m^3/s (equivalent to 5×10^{-3} km^3 per year) would imply an initial concentration of sulphur >> 1 wt% for a flux of varying from 260 to 1350 t/d that is unrealistic. The initial concentration of sulphur in parental basalt is not accurately known since only a few values are available (≤0.17 wt% S; Walker et al. 2003). Considering the highest value of 0.17 wt% S measured by Walker et al. (2003), that could be underestimated, would imply a volume ratio between the degassed and extruded magma of the order of 7, for an intermediate SO_2 flux of 885 t/d (Table 2b), with thus excess of sulphur degassing as concluded by Rose et al. (2013).

Fuego is regarded as the most dangerous volcano in Central America known, since 1524, for its Subplinian eruptions (volcanic explosivity index 4), as occurred in October 1974 (Rose et al 1978; Chesner and Rose 1984) after periods of repose times that lasted years or decades as reviewed by Naismith et al. (2019). The October 1974 Subplinian eruption produced hybrid magma from basaltic (crystal-poor) to basaltic andesite (crystal-rich) magmas (Rose et al. 1978). It was sustained by an influx of ~0.1 km^3 H_2O-rich high-alumina basaltic magma (Rose et al. 1978; 2008). Low-level Strombolian activity persisted until 1979 (Martin and Rose 1981) and from 1980 to 1999 Fuego had irregularly spaced subplinian (volcanic explosivity index 1-2) events with periods of repose (Lyons et al. 2010). The magma erupted in 1999 and 2003, after two decades of quiescence (Lyons et al. 2010), is partly residual from 1974 (Berlo et al. 2012). During 2 years of continuous observations (2005–2007) Fuego was persistently active, with a repeating cycle of activity: 1) passive lava effusion and minor strombolian explosion, followed by 2) paroxysmal eruptions, and finally 3) degassing explosions without lava effusion (Lyons et al. (2010). One of Fuego's largest eruptions in the period 1999–present occurred on 13th September 2012 whereas the most destructive eruption occurred on 3 June 2018 (Naismith et al. 2019; Liu et al. 2020). This explosive eruption was preceded by 5-month hiatus in activity that was proposed to be sufficient a time for crystallisation of a shallow low permeability plug and by the flowing of hot and high-speed lava flows (Liu et al. 2020).

It is found to be part of a 45-year cycle of high-energy eruption that produced a magma volume of 0.04 ±0.01 km^3 (dense rock equivallent) and 130 ktons of SO_2 (IASI satellite data) that could have involved the influx of basaltic magma (Pardini et al. 2019). This SO_2 flux would imply a concentration of sulphur of nearly 500 ppm a value by far lower than the S dissolved amount in the 1974 olivine-hosted melt inclusions up to 2250 ppm (Lloyd et al. 2014) and ~2500 ppm (Berlo et al. 2012).

The hybrid magma body erupted in between 14 and 23 October 1974 was proposed to reflect the contribution of several magma rather than a single magma composition, the basaltic magma (0.60 wt% K_2O) standing at >10 km depth and a second basaltic andesite magma (0.90 wt% K_2O) at 3–8 km depth (Roggensack 2001). Accordingly, the observed variability is a reflection of magma hybridization immediately before the eruption and that the pre-mixing water contents of basaltic magma were likely 4–5 wt%. Lloyd et al. (2014) measured in the 1974 melt inclusions 4.5 wt% H_2O. Most data of 1974 olivine-hosted melt inclusions of Fuego can be reproduced by decompression-crystallisation trend between 1010°C and 1100°C in a vertically extended reservoir (Cashman and Edmonds 2019). According to these authors, the high Al_2O_3 content recorded in MIs (4.5 wt% H_2O; Lloyd et al. 2014) prior to late-stage plagioclase crystallisation supports a high proportion (50%) of crystal fractionation (olivine and clinopyroxene) from a parental melt possibly having up to 7.6-9.6 wt%. Ion-probe analysis of S, H_2O and CO_2 diffusion profile in open glassy gulfs (embayments) in olivine crystals still connected to the carrier magma indicate a decompression rate 0.24 to 0.60 MPa/s (~8–21 m/s) of the magma erupted on 17 October 1974 (Lloyd et al. 2014).

Liu et al. (2020) proposed a top-down decompression of magma in the conduit as the triggering mechanism of the eruption of 3 June 2018, shallow crystallised magma acting as a plug. Liu et al. (2020) also showed that the frequency of paroxysms at Fuego is broadly proportional to the gas supply rate.

Low sulphur concentration (~500 ppm) corresponds to the sulphide saturated melt, which has lost H_2O (Wade et al. 2006). Pyrrhotite is actually observed in association with titanomagnetite (Rose et al 1978, Berlo et al. 2012). Comparatively basaltic-andesite magma at Arenal contains similar S concentrations (2500 ppm), and becomes sulphide saturated as it is degassing and crystallising (Wade et al. 2006). Hence, low SO_2 flux reflects the degassing of crustal magma that is losing water and crystallising, a part of sulphur being locked in segregated sulphide globules.

Santiaguito complex consists of four domes, along an East-West trending fracture. The activity of dome-building began in 1922 within the crater formed during the cataclysmic 1902 eruption of Santa María (Rose 1972, 1987, 2013; Scott et al. 2012, 2013) and continues today. The longevity and continuous activity of Santiaguito are unusual among historic dome eruptions (Scott et al. 2013). Magma extrusion rates have shown a cyclicity with 3–6-year-long periods of higher extrusion (0.6–2.1 $m^3 s^{-1}$), which are separated by 4- to 11-year-long periods of lower (~0.2 $m^3 s^{-1}$) extrusion rate (Rose 1987; Harris et al. 2003, 2004). The activity at Santiaguito since 1975 is characterised by effusion of blocky lava flows and small-to-moderate gas-rich explosions (Harris et al. 2003) reaching up to 1.5 km above the vent with explosions occurring at different intervals, from a few minutes up to ~6 days (Carter et al. 2020). Santiaguito dacitic rocks are typically porphyritic, with a phase assemblage dominated by plagioclase (~20 to ~30 modal%) (Scott et al. 2013). Dacitic magma is found to be derived from the andesite via ~20 to 25% fractional crystallisation (Scott et al. 2013). Singer et al. (2011) propose that the dacite erupted in 1902 and during the early dome-forming cycles of Santiaguito lavas resulted from ~25 ka of fractional crystallisation in a closed system. The erupted magma has become progressively less evolved over time, with a decrease in whole rock SiO_2 from ~66 to ~62 wt% from 1922 to 2002 (Scott et al. 2013) with magma being extracted progressively from a chemically-stratified lower crustal (~12 to ~25 km) storage zone thought to have formed during the ~25 ka of quiescence that preceded the 1902 eruption. Santiaguito is by some aspect comparable to Colima for its cyclic emissions of SO_2, with low background and high emissions of gas (1/3 of the emissions) leading to a range of SO_2 flux and explosion phenomenology (Lamb et al. 2019).

Battaglia et al. (2018) report time-averaged SO_2 fluxes of 127±58 tons/day at Santiaguito (Table 2b), which reflects a very shallow magma degassing. Santiaguito parental melt have most likely similar parental basaltic magma, rich in water and sulphur as shown for Pacaya and Fuego. Whereas at Pacaya the SO_2 flux is sustained by high-alumina basalt degassing, dacitic magma evolution requires long-term fractional crystallisation (Singer et al. 2011), it thus implies titanomagnetite crystallisation, magma degassing and thus change in the redox conditions promoting melt sulphide saturation.

In summary, these examples highlight the great need to combine time-series data, geochemical and petrological approaches as the necessity of having good geochemical modeling of depth-dependent magma redox.

Concluding points

Combining time series infrasonic data and measurements of gas fluxes on well monitored open-vent volcanoes on the field is essential for the interpretation and modelling of the degassing pattern at the surface and in the conduit and understanding the eruptive activity. However, it cannot be dissociated from the good knowledge of the texture of the erupted products, the depth-evolution of the dissolved amount of water in the melt and thus its crystallinity owing to the key role of magma viscosity in modelling the bubbles and magma motions. Key advances could be made by any techniques constraining the in-situ bubble diameters and the gas volume fraction of the small bubbles, as one way to view the different eruptive regimes at basaltic and explosive volcanoes is a consequence of the ability of their largest bubbles to rise with a differential velocity in respect to the liquid or be stagnant, respectively. An accurate modelling of the magma viscosity itself combining physical and thermodynamic parameters is thus a challenge.

A better modelling of the processes at the vent could be obtained by the joined and systematic use of thermal and infrasonic records. The inputs, which could be offered by imagery of the surface activity, possibly at high-speed, such as in the visible, infra-red or UV range, are enormous for our understanding, as these open-vent volcanoes remain an open window onto a deeper plumbing system, in which the future activity at the surface is being prepared. Similarly, be able to measure systematically and continuously the level of the magma column in the conduit or in the lava lake could be used as a key to detect pressure changes at depth and/or be used as a precursory signal of an enhanced activity. The case of Masaya shed lights on the interest to record simultaneous thermal and SO_2 fluxes to quantify the magma supply rate.

Another interesting avenue to explore is that provided by the analysis of long-time series as open-vent volcanoes show sudden or progressive changes in behaviour. Several observatories across the world obtain these data but so far continuous long-time series are mainly restricted to geophysical methods.

Additionally, a key parameter to know for a better quantification of the SO_2 flux in term of volume of degassed magma is the magma redox evolution during its crustal evolution and crystallisation. The fate of the degassed magma is also important, as it may remain at depth, be forcefully intruded into the edifice or be partly recycled by a convective loop in the conduit, i.e. the bi-directional flow at work at the less viscous open-vent volcanoes.

Acknowledgements: Many beautiful photographs had been given by colleagues, who we would like to thank warmely for making our paper visually captivating (P. Allard, O. Aragon, J-M Bardintzeff, T. Boyer, R. Campion, S. Carn, P. Delmelle, A. Finizola, Y Moussallam, C Oppenheimer, M. Patrick, T. Ricci, G. Sartoris, B. Smets, T. Staudacher). We would also like to thank authors, who had provided original figures for us to redraw (F Beckett, M. Burton, R. Carey, DJ Ferguson, C. Le Losq, J Palma, D. Patanè, A. Pouclet, H. Mader). We also would like to thank Y. Gaudemer, the reviewers (unknown and M. Patrick) and the associated editor, J. Taddeucci, who help us to improve significantly the clarity of the text.

References

Aiuppa A, Bertagnini A, Métrich N, Moretti R, Di Muro A, Liuzzo M, Tamburello G (2010) A model of degassing for Stromboli volcano. Earth Planet Sci Lett 295: 195–204

Aiuppa A, Bitetto M, Delle Donne D, Paolo La Monica F, Tamburello G, Coppola D, Della Schiava M, Innocenti L, Lacanna G, Laiolo M, Massimetti F, Pistolesi M, Silengo M C, Ripepe M (2021) Volcanic CO_2 tracks the incubation period of basaltic paroxysms. Sci Adv 7:38 https://doi.org/eabh0191

Aiuppa A, Bitetto M, Francofonte V, Velasquez, G, Parra, CB, Giudice G, Liuzzo M, Moretti R, Moussallam Y, Nials P, Tamburello G, Valderrama OA, Curtis A (2017) A CO_2-gas precursor to the March 2015 Villarrica volcano eruption. Geochem Geophys Geosyst 18:2120–2132. https://doi.org/10.1002/2017GC006892

Aiuppa A, Fisher TP, Plank T, Bani P (2019) CO_2 flux emissions from Earth's most actively degassing volcanoes 2005-2015. Sci Rep 9:5442. https://doi.org/10.1038/s41598-019-41901-y

Allard P, Aiuppa A, Burton M, Caltabiano T, Federico C, Salerno G, La Spina A (2008) Crater gas emissions and the magma feeding system of Stromboli volcano. In: Calvari S, Inguaggiato S, Puglisi G, Ripepe M and Rosi M (eds), Learning from Stromboli. Amer Geophys Union Geophys Monograph 182:65-80

Allard P, Aiuppa A, Bani P, Métrich, N, Bertagnini A, Gauthier, P-J, Shinohara H, Sawyer G, Parello F, Bagnato E, Pelletier B, Garaebiti E (2016a) Prodigious emission rates and magma degassing budget of major, trace and radioactive volatile species from Ambrym basaltic volcano, Vanuatu island Arc. J Volcanol Geotherm Res 322:119-143, in Special issue Understanding volcanoes in Vanuatu arc (Eds. S. Vergniolle and N. Métrich). https://doi.org/10.1016/j.jvolgeores.2015.08.022

Allard P, Burton M, Sawyer G, Bani P (2016b) Degassing dynamics of basaltic lava lake at a top-ranking volatile emitter: Ambrym volcano, Vanuatu arc. Earth Planet Sci Lett 448:69-80. http://dx.doi.org/10.1016/j.epsl.2016.05.014

Allibone R, Cronin SJ, Charley DT, Neall VE, Stewart RB, Oppenheimer C (2012) Dental fluorosis linked to degassing of Ambrym volcano, Vanuatu: a novel exposure pathway. Environ Geochem Health 34 (2):155–170. https://doi.org/10.1007/s10653-010-9338-2.

Andres RJ, Rose WI, Stoiber R., Williams SN, Matı´as O, Morales R, (1993) A summary of sulfur dioxide emission rate measurements from Guatemalan volcanoes. Bull Volcanol 55:379-388

Andújar J, Scaillet B (2012) Relationships between pre-eruptive conditions and eruptive styles of phonolite–trachyte magmas. Lithos 152:122-131. https://doi.org/10.1016/j.lithos.2012.05.009

Arciniega-Ceballos A, Chouet B, Dawson P (1999) Very long-period signals associated with vulcanian explosions at Popocatepetl volcano, Mexico. Geophys Res Lett 26: 3013-3016

Arciniega-Ceballos A, Dawson P, Chouet BA (2012) Long period seismic source characterization at Popocatépetl volcano, Mexico. Geophys Res Lett 39:L20307. https://doi.org/10.1029/2012GL053494

Aster R, Mah S, Kyle P, McIntosh W, Dunbar N, Johnson J, Ruiz M, McNamara S (2003) Very long period oscillation of Mount Erebus volcano. J Geophys Res 108/(11). https://doi.org/10.1029/2002JB002101

Bani P, Oppenheimer C, Tsanev VI, Carn SA, Cronin SJ, Crimp R, Calkins JA, Charley D, Lardy M, Roberts TR (2009) Surge in sulphur and halogen degassing from Ambrym volcano, Vanuatu. Bull Volcanol 71(10):1159–1168

Bani P, Harris AJL, Shinohara H, Donnadieu F (2013) Magma dynamics feeding Yasur's explosive activity observed using thermal infrared remote sensing. Geophys Res Lett 40:3830–3835

Bani P, Oppenheimer C, Allard P, Shinohara H, Tsanev V, Carn S, Lardy M, Garaebiti E (2012) First estimate of volcanic SO_2 budget for Vanuatu island arc. J Volcanol Geotherm Res 211-212:36-46. https://doi.org/10.1016/j.jvolgeores.2011.10.005

Barnie TD, Oppenheimer C, Pagli C (2016) Does the lava lake of Erta 'Ale volcano respond to regional magmatic and tectonic events? An investigation using Earth Observation data. From: Wright TJ, Ayele, A, Ferguson DJ, Kidane T, Vye-Brown C (eds) 2016. Magmatic Rifting and Active Volcanism. Geol Soc London Spec Pub 420:181–208. https://doi.org/10.1144/SP420.15

Barrière J, d'Oreye N, Oth A, Geirsson H, Mashagiro N, Johnson JB, Smets B, Samsonov S, Kervyn F (2018) Single-Station Seismo-Acoustic Monitoring of Nyiragongo's Lava Lake Activity (D.R. Congo). Front Earth Sci 6:82

Battaglia, J, Métaxian, JP, Garaebiti, E (2012) Earthquake-volcano interaction imaged by coda wave interferometry. Geophys Res Lett 39:11

Battaglia J, Métaxian, J-P, Garaebiti E (2016a) Short term precursors of Strombolian explosions at Yasur volcano (Vanuatu). Geophys Res Lett 43:1-6, doi:10.1002/2016GL067823

Battaglia J, Métaxian, J-P, Garaebiti E (2016b) Families of similar events and modes of oscillation of the conduit at Yasur volcano (Vanuatu). J Volcanol Geotherm Res, Special issue on Understanding volcanoes in the Vanuatu arc, 322:196--211

Battaglia A, Bitetto M, Aiuppa A, Rizzo AL, Chigna G, Watson IM, D'Aleo R, Juárez Cacao FJ, de Moor M (2018) The magmatic gas signature of Pacaya Volcano, with implications for the volcanic CO_2 flux from Guatemala. Geochem Geophys Geosyst. 19:667-692. https://doi.org/10.1002/2017GC007238

Beckett FM, Mader HM, Phillips JC, Rust AC, Witham F (2011) An experimental study of low-Reynolds-number exchange flow of two Newtonian fluids in a vertical pipe. J Fluid Mech 682:652-670

Beckett FM, Burton M, Mader HM, Phillips JC, Polacci M, Rust AC, Witham F (2014) Conduit convection driving persistent degassing at basaltic volcanoes. J Volcanol Geotherm Res 283:19-35

Berlo K, Stix J, Roggensack K, Ghaleb B (2012) A tale of two magmas, Fuego, Guatemala. Bull Volcanol 74(2):377–390. https://doi.org/10.1007/s00445-011-0530-8

Bertagnini A, Di Roberto A, Pompilio M (2011) Paroxysmal activity at Stromboli: lessons from the past. Bull Volcanol 73:1229-1243. https://doi.org/ 10.1007/s00445-011-0470-3

Bluth GJS, Carn SA (2008) Exceptional sulphur degassing from Nyamuragira volcano, 1979–2005. Int J Remote Sens 29:6667–6685. https://doi.org/10.1080/01431160802168434

Bobrowski N, Giuffrida GB, Arellano S, Yalire M, Liotta M, Brusca L, Calabrese S, Scaglione S, Rüdiger J, Castro JM, Galle B, Tedesco D (2017) Plume composition and volatile flux of Nyamulagira volcano, Democratic Republic of Congo, during birth and evolution of the lava lake, 2014–2015. Bull Volcanol 79-90. https://doi.org/10.1007/s00445-017-1174-0

Bolge LL, Carr MJ, Feigenson MD, Alvarado GE (2006) Geochemical stratigraphy and magmatic evolution at Arenal Volcano, Costa Rica. J Volcanol Geotherm Res 34-48. https://doi.org/10.1016/j.jvolgeores.2006.03.036

Bouche E, Vergniolle S, Staudacher T, Nercessian A, Delmont JC, Frogneux M, Cartault F, Le Pichon A (2010) The role of large bubbles detected from acoustic measurements on the dynamics of Erta'Ale lava lake (Ethiopia). Earth Planet Sci Lett 295:37-48

Brill KA, Waite GP, Carn S, Chigna G, Palma R (2022) Long term stability of conduit dynamics at Fuego volcano, Guatemala, 2008-2015 84:37 this issue

Brogi F, Ripepe M, Bonadonna C (2018) Lattice Boltzmann modeling to explain volcano acoustic source. Sci Rep 8:9537. https://doi.org/10.1038/s41598-018-27387-0

Buckingham MJ, Garcès MA (1996) A canonical model of volcano acoustics. J Geophys Res 101:8129-8151

Burgi P-Y, Caillet M, Haefeli S (2002) Field temperature measurements at Erta' Ale lava lake, Ethiopia. Bull Volcanol 64(7):472-485

Burgi P-Y, Caillet M, Haefeli S (2002) Field temperature measurements at Erta' Ale lava lake, Ethiopia. Bull Volcanol 64(7):472-485

Burton MR, Oppenheimer C, Horrocks LA, Francis PW (2000) Remote sensing of CO_2 and H_2O emission rates from Masaya volcano, Nicaragua. Geology 28(10):915-918

Burton M, Allard P, Muré F, La Spina A (2007) Magmatic gas composition reveals the source depth of slug-driven strombolian explosive activity. Science 317:227-230

Burton M, Sawyer G, Bani P (2016) Degassing dynamics of basaltic lava lake at a top-ranking volatile emitter: Ambrym volcano, Vanuatu arc. Earth Planet Sci Lett 448:69-80. https://doi.org/10.1016/j.epsl.2016.05.014

Calkins J, Oppenheimer C, Kyle PR (2008) Ground-based thermal imaging at Erebus volcano, Antartica. J Volcanol Geotherm Res 177:695-704

Calkins JA, Delmelle P (2021) Quantitative analysis of persistent volcanic fluoride risk reveals differential exposure pathways for adults and children downwind of Masaya Volcano, Nicaragua. Bull Volcanol 83:83 https://doi.org/10.1007/s00445-021-01504-w this issue

Cameron BI, Walker JA, Carr MJ, Patino LC, Mat O, Feigenson MD (2002) Flux versus decompression melting at stratovolcanoes in southeastern Guatemala. J Volcanol Geotherm Res 119:21-50

Campion R (2014) New lava lake at Nyiamuragira volcano revealed by combined ASTER and OMI SO_2 measurements. Geophys Res Lett 41:7485-7492. https://doi.org/10.1012/2014GL061808

Campion R, Delgado-Granados H, Legrand D, Taquet N., Boulesteix T, Pedraza-Espitía S Lecocq T (2018) Breathing and Coughing: The Extraordinarily High Degassing of Popocatépetl Volcano Investigated With an SO_2 Camera. Front Earth Sci 6:163. https://doi.org/ 10.3389/feart.2018.00163

Caplan-Auerbach J. Bellesiles A, Fernandes JK (2010) Estimates of eruption velocity and plume height from infrasonic recordings of the 2006 eruption of Augustine Volcano, Alaska. J Volcanol Geotherm Res 189:12–18

Carrigan, CR (1983) A heat pipe model for vertical, magma-filled conduits. J Volcanol Geotherm Res 16, 279-298

Carrigan C R (1987) The magmatic Rayleigh number and time dependent convection in cooling magma. Geophys Res Lett 14 9:915-918

Carn SA, Fioletov VE, McLinden CA, Li C, Krotkov NA (2017) A decade of global volcanic SO_2 emissions measured from space. Sci Rep 7:44095. https://doi.org/10.1038/srep44095.

Cashman KV, Edmonds M (2019) Mafic compositions: a record of magma storage conditions, mixing and ascent. Phil Trans R Soc A377:20180004. https://doi.org/10.1098/rsta.2018.0004

Chesner CA, Rose WI (1984) Geochemistry and evolution of the Fuego volcanic complex, Guatemala. J Volcanol Geotherm Res 21:25–44

Chouet B, Dawson P, Arciniega-Ceballos A (2005) Source mechanism of Vulcanian degassing at Popocatépetl Volcano, Mexico, determined from waveform inversions of very long period signals. J Geophys Res 110:B07301. https://doi.org/10.1029/2004JB003524

Cigolini C, Borgia A, Casertano L (1984) Intra-crater activity, AA-block lava, viscosity and flow dynamics: Arenal volcano, Costa Rica. J Volcanol Geotherm Res 20:155-176

Cimarelli C, Costa A, Mueller S, Mader HM (2011), Rheology of magmas with bimodal crystal size and shape distributions: Insights from analog experiments. Geochem Geophys Geosyst, 12:Q07024. https://doi.org/10.1029/2011GC003606

Clarke AB (2013) Unsteady vulcanian explosions. Modeling Volcanic Processes: The Physics and Mathematics of Volcanism, eds. SA Fagents, TKP Gregg, and RMC Lopes. 27:129-152 Cambridge University Press

Clarke AB, TE Ongaro, A Belousov (2015) Vulcanian explosions. The Encyclopedia of Volcanoes, 2nd edition, 28:505-518 Academic Press

Clift R., JR Grace, ME Weber (1978) Bubbles, drops and particles. Academic press, London, 1-380

Coppola D, Campion R, Laiolo M, Cuoco E, Balagizi C, Ripepe M, Cigolini C, Tedesco D (2016) Birth of a lava lake: Nyamulagira volcano 2011-2015. Bull Volcanol 78:20. https://doi.org/10.1007/s00445-016-1014-7

Coppola D, Laiolo M, Massimetti F, Cigolini C (2019) Monitoring endogenous growth of open-vent volcanoes by balancing thermal and SO_2 emissions data derived from space. Sci Rep 9:9394. https://doi.org/10.1038/s41598-019-45753-4

Costa F, Shea T, Ubide T (2020) Diffusion chronometry and the timescales of magmatic processes Nature Reviews Earth and Environment 1:201-214

Cronin SJ, Sharp DS (2002) Environmental impacts on health from continuous volcanic activity at Yasur (Tanna) and Ambrym, Vanuatu. Int J Environ Health Res 12:109-123

De Angelis S, A Diaz-Moreno, L Zuccarello (2019) Recent Developments and Applications of Acoustic Infrasound to Monitor Volcanic Emissions. Remote Sens 11:1302. https://doi.org/10.3390/rs11111302

Delgado-Granados H, Cárdenas-Gonzáles L, Piedad-Sánchez N (2001) Sulphur dioxide emissions from Popocate´petl volcano (Mexico): case study of a high-emission rate, passively degassing erupting volcano. J Volcanol Geotherm Res 108:107-120

Delmelle P, Stix J, Baxter P, Garcia-Alvarez, J, Barquero J (2002) Atmospheric dispersion, environmental effects and potential health hazard associated with the low-altitude gas plume of Masaya volcano, Nicaragua. Bull Volcanol 64(6):423–434

De Moor JM, Fischer TP, Sharp ZD, King PL, Wilke M, Botcharnikov RE, Cottrell E, Wilke Zelenski M, Marty B, Klimm K, Rivard C, Ayalew D, Ramirez C, Kelley KA (2013) Sulfur degassing at Erta Ale (Ethiopia) and Masaya (Nicaragua) volcanoes: Implications for the degassing processes and oxygen fugacities of basaltic systems. Geochem Geophys Geosyst 14:4076-4108. https://doi.org/10.1002/ggge.20255

Diaz-Moreno A, Roca A, Lamur A, Munkli BH, Ilanko T, Pering TD, Pineda A, De Angelis S (2020) Characterization of Acoustic Infrasound Signals at Volcán de Fuego, Guatemala: A baseline for volcano monitoring. Front Earth Sci 8:54977. https://doi.org/10.3389/feart.2020.549774

Edmonds M, Wallace P (2017) Volatiles and exsolved vapor in volcanic systems. Elements 13:29-34. https://doi.org/10.2113/gselements.13.1.29

Edmonds M, Liu EJ, Cashman KV (2022) Open-vent volcanoes fuelled by depth-integrated magma degassing. Bull Volcanol 84:28. https://doi.org/10.1007/s00445-021-01522-8 this issue

Fan L-S, Tsuchiya K (1990) Bubble wake dynamics in liquids and liquid-solid suspensions. Butterworth-Heinemann series in chemical engineering, Boston, 1-363

Fee D, Izbekov P, Kim K, Yokoo A, Lopez T, Prata, F, Kazahaya R, Nakamichi H, Iguchi M (2017) Eruption mass estimation using infrasound waveform inversion and ash and gas measurements: evaluation at Sakurajima Volcano, Japan. Earth Planet Sci Lett 480:42–52. https://doi.org/10.1016/j.epsl.2017.09.043

Fee D, Toney L, Kim K, Sanderson RW, Iezzi AM, Matoza RS, De Angelis S, Jolly AD, Lyons JJ, Haney MM (2021) Local Explosion Detection and Infrasound Localization by Reverse Time

Migration Using 3-D Finite-Difference Wave Propagation. Front Earth Sci 9:620813. https://doi.org/10.3389/feart.2021.620813

Ferguson DJ, Gonnermann HM, Ruprecht P, Plank T, Hauri EH, Houghton BF, Swanson DA (2016) Magma decompression rates during explosive eruptions of Kīlauea volcano, Hawaii, recorded by melt embayments. Bull Volcanol (2016) 78:71

Field L, Barnie T, Blundy J, Brooker RA, Keir D, Lewi E, Saunders K (2012) Integrated field, satellite and petrological observations of the November 2010 eruption of Erta Ale. Bull Volcanol. https://doi.org/10.1007/s00445-012-0660-7

Firth CW, Handley HK, Cronin SJ, Turner SP (2014) The eruptive history and chemical stratigraphy of a post-caldera, steady-state volcano: Yasur, Vanuatu. Bull Volcanol 76:837 https://doi.org/10.1007/s00445-014-0837-3

Fischer TP, Arellano S, Carn S, Aiuppa A, Galle B, Allard P, Lopez T, Shinohara H, Kelly P, Werner C, Cardellini C, Chiodini G (2019) The emissions of CO_2 and other volatiles from the world's subaerial volcanoes. Sci Rep 9:8716. https://doi.org/10.1038/s41598-019-54682-1

Francis P, Oppenheimer C, Stevenson D (1993) Endogenous growth of persistently active volcanoes. Nature 366:554–557. https://doi.org/10.1038/366554a0

Gaudin, D, Moroni, M, Taddeucci, J, Scarlato, P, Shindler, L (2014a) Pyroclast Tracking Velocimetry: A particle tracking velocimetry-based tool for the study of Strombolian explosive eruptions. J. Geophys. Res. 119, 5369-5383. https://doi.org/10.1002/2014JB011095

Gaudin, D, Taddeucci, J, Scarlato, P, Moroni, M, Freda, C, Gaeta M, Palladino DM (2014b) Pyroclast Tracking Velocimetry illuminates bomb ejection and explosion dynamics at Stromboli (Italy) and Yasur (Vanuatu) volcanoes. J Geophys Res 119:5384-5397. https://doi.org/10.1002/2014JB01109

Gaudin D, Taddeucci J, Scarlato P, Harris A, Bombrun M, Del Bello E, Ricci T (2017) Characteristics of puffing activity revealed by ground-based, thermal infrared imaging: the example of Stromboli Volcano (Italy). Bull Volcanol 79: 24. https://doi.org/10.1007/s00445-017-1108-x

Genco R, Ripepe M (2010) Inflation-deflation cycles revealed by tilt and seismic records at Stromboli volcano. Geophys. Res. Lett. 37, L12302. https://doi.org/10.1029/2010GL04292

Gerst A, Hort M, Aster RC, Johnson JB (2013) The first second of volcanic eruptions from the Erebus Volcano lava lake, Antarctica - Energies, pressures, seismology, and infrasound. J Geophys Res 118:1–23

Ghiorso MS, Gualda GA (2015) An H_2O–CO_2 mixed fluid saturation model compatible with rhyolite-MELTS. Contrib Mineral Petrol 169:5

Giberti G, Jaupart C, Sartoris G (1992) Steady-state operation of Stromboli Volcano, Italy: Constraints on the feeding system. Bull Volcanol 54:535-541. https://doi.org/doi:10.1007/BF00569938

Giggenbach WF, Kyle PR, Lyon GL (1973) Present volcanic activity on Mount Erebus, Ross Island, Antarctica. Geology 1(3):135-136

Giordano D, Russell J, Dingwell D (2008) Viscosity of magmatic liquids: a model. Earth Planet Sci Lett 271:123–134

Global Volcanism Program. Report on Pacaya (Guatemala) (2021) In Sennert SK (ed) Weekly volcanic activity Report 31 March-6 April 2021. Smithsonian Institution and US Geol Survey

Guth E, Gold O (1938) On the hydrodynamical theory of the viscosity of suspensions. Phys Review 53:322.

Gomez C, B Kennedy (2017) Capturing volcanic plumes in 3D with UAV-based photogrammetry at Yasur Volcano – Vanuatu. J Volcanol Geotherm Res 350:84-88

Gómez-Vazquez A, De la Cruz-Reyna S, Mendoza-Rosas AT (2016) The ongoing dome emplacement and destruction cyclic process at Popocatépetl volcano, central Mexico. Bull Volcanol 78:2–15

Goto A, Johnson JB (2011) Monotonic infrasound and Helmholtz resonance at Volcan Villarrica (Chile), Geophys Res Lett 38:L06301. https://doi.org/10.1029/2011GL046858.

Goto A, Ripepe M, Lacanna G (2014) Wideband acoustic records of explosive volcanic eruptions at Stromboli: New insights on the explosive process and the acoustic source. Geophys Res Lett 41:3851–3857. https://doi.org/10.1002/ 2014GL060143

Hagerty MT, Schwartz SY, Garcés MA, Protti M (2000) Analysis of seismic and acoustic observations at Arenal volcano, Costa Rica, 1995-1997. J Volcanol Geotherm Res 101:27-65

Harms E, Schmincke H-U (2000) Volatile composition of the phonolitic Laacher See magma (12,900 yr BP): implications for syn-eruptive degassing of S, F, Cl and H_2O. Contrib Mineral Petrol 138:84-98

Harpel CJ, Kyle PR, Caldwell DA, McIntoshWC, Esser RP (2004) $^{40}Ar/^{39}Ar$ dating of the eruptive history of Mount Erebus, Antarctica: summit flows and caldera collapse. Bull Volcanol 66:687-702

Harris AJL, DS Stevenson (1997) Magma budget and steady-state at Stromboli and Vulcano. Geophys Res Lett 24 9:1043-1046

Harris AJL, Flynn LP, Rothery DA, Oppenheimer C, Sherman SB (1999) Mass flux measurements at active lava lakes: implication for magma recycling. J Geophys Res 104:B4:7117-7136

Harris AJL, Flynn LP, Matias O, Rose WI (2002) The thermal stealth flows of Santiaguito: implications for the cooling and emplacement of dacitic block lava flows. Geol Soc Am Bull 114:533-546

Harris AJL, Rose WI, Flynn LP (2003) Temporal trends in lava dome extrusion at Santiaguito 1922–2000. Bull Volcanol 65:77-89

Harris AJL, Flynn LP, Matias O, Rose WI, Julio Cornejo J (2004) The evolution of an active silicic lava flow field: an ETM+ perspective. J Volcanol Geotherm Res 135:147-168

Harris AJL, Carniel R, Jones J (2005) Identification of variable convective regime at Erta 'Ale lava lake. J Volcanol Geotherm Res 142:207-223

Harris AJL, Ripepe M (2007) Temperature and dynamics of degassing at Stromboli, J Geophys Res 112:B03205. https://doi.org/doi:10.1029/2006JB00439

Harris AJL, Ripepe M, Hughes EA (2012) Detailed analysis of particle launch velocities, size distributions and gas densities during normal explosions at Stromboli. J Volcanol Geothermal Res 231-232:109-131

Harris AJL, Delle Donne D, Dehn J, Ripepe M, Worden AK (2013) Volcanic plume and bomb field masses from thermal infrared camera imagery, Earth Planet Sci Lett 365:77-85

Head EM, Shaw AM, Wallace PJ, Sims KWW, Carn SA (2011) Insight into volatile behavior at Nyamuragira volcano (D.R. Congo, Africa) through olivine hosted melt inclusions. Geochem Geophys Geosyst 12:Q0AB11. https://doi.org/10.1029/2011GC003699

Helz RT (1987) Diverse olivine types in lava of the 1959 eruption of Kilauea volcano and their bearing on eruption dynamics. In Volcanism in Hawaii, US. Geol Surv Prof Pap 1350:691-722

Holland PAS, Watson MI, Phillips JC, Caricchi L, Dalton MP (2011) Degassing processes during lava dome growth: Insights from Santiaguito lava dome, Guatemala, J Volc Geotherm Res 202:153–166. https://doi.org/10.1016/j.jvolgeores.2011.02.004

Huppert HE, Hallworth M (2007) Bi-directional flows in constrained systems. J Fluid Mech 578:95-112

Iezzi AM, Fee D, Kim K, Jolly AD, Matoza RS (2019) Three-Dimensional Acoustic Multipole Waveform Inversion at Yasur Volcano, Vanuatu. J Geophys Res Solid Earth 124:8679–8703. https://doi.org/10.1029/2018JB017073

Ilanko T, Oppenheimer C, Burgisser A, Kyle PR (2015a) Cyclic degassing of Erebus volcano, Antarctica. Bull Volcanol 77:56. https://doi.org/10.1007/s00445-015-0941-z

Ilanko T, Oppenheimer C, Burgisser A, Kyle P (2015b) Transient degassing events at the lava lake of Erebus volcano, Antarctica: Chemistry and mechanisms. Geo Res J 7:43–58

Jellinek MA, Kerr RC (2001) Magma dynamics, crystallization, and chemical differentiation of the 1959 Kilauea Iki lava lake, Hawaii, revisited. J Volc Geotherm Res 110:235-263

Johnson JB (2003) Generation and propagation of infrasonic airwaves from volcanic explosions J Volcanol Geotherm Res 121:1-14

Johnson JB, Lees JM, Gordeev EI (1998) Degassing explosions at Karymsky Volcano, Kamchatka. Geophys Res Lett 25:3999-4002

Johnson JB (2004a) Volcanic eruptions observed with infrasound. Geophys Res Lett 31:L14604

Johnson JB, Harris AJL, Sahetapy-Engel S, Wolf RE, Rose WI (2004b) Explosion dynamics of pyroclastic eruptions at Santiaguito, Guatemala. Geophys. Res. Lett. 31 (L06610)

Johnson JB (2005) Source location variability and volcanic vent mapping with a small-aperture infrasound array at Stromboli Volcano, Italy. Bull Volcanol 67:1-14. https://doi.org/10.1007/s00445-004-0356-8

Johnson JB, Sanderson R, Lyons J, Escobar-Wolf R, Waite G, Lees JM (2009) Dissection of a composite volcanic earthquake at Santiaguito, Guatemala. Geophys Res Lett 36:L16308

Johnson JB, Lees JM, Varley N (2010) Characterizing complex eruptive activity at Santiaguito Volcano, Guatemala using infrasound semblance in networked arrays. J Volc Geotherm Res 199:1-14

Johnson JB, Lees J, Varley N (2011) Characterizing complex eruptive activity at Santiaguito, Guatemala using infrasound semblance in networked arrays. J Volcanol Geotherm Res 199:1–14

Johnson JB, Miller AJC (2014) Application of the Monopole Source to Quantify Explosive Flux during Vulcanian Explosions at Sakurajima Volcano (Japan). Seismol Res Lett 85:1163-1176

Johnson JB, Palma JL (2015), Lahar infrasound associated with Volcán Villarrica's 3 March 2015 eruption. Geophys Res Lett 42:6324–6331. https://doi.org/10.1002/2015GL065024

Johnson JB, Watson, LM, Palma JL, Dunham EM, Anderson JF (2018) Forecasting the Eruption of an Open-Vent Volcano Using Resonant Infrasound Tones. Geophys Res Lett 45:2213-2018

Jolly AD, Matoza RS, Fee D, Kennedy BM, Iezzi AM, Fitzgerald,RH, Austin A, Johnson R (2017) Capturing the acoustic radiation pattern of strombolian eruptions using infrasound sensors aboard a tethered aerostat, Yasur volcano, Vanuatu. Geophys Res Lett 44:9672–9680. https://doi.org/10.1002/2017GL074971

Jones LK, Kyle PR, Oppenheimer C, Frechette JD, Okal MH (2015) Terrestrial laser scanning observations of geomorphic changes and varying lava lake levels at Erebus volcano, Antarctica. J Volcanol Geotherm Res 295:43–54. https://doi.org/10.1016/j.jvolgeores.2015.02.011

Kazahaya K, Shinohara H, Sato G. (1994) Excessive degassing of Izu-Oshima volcano: magma convection in a conduit. Bull Volcanol 56:207-216

Kelly PJ, Kyle PR, Dunbar NW, Sims KWW (2008) Geochemistry and mineralogy of the phonolite lava lake, Erebus volcano, Antarctica: 1972-2004 and comparison with older lavas. J Volcanol Geotherm Res 177:589-605

Kern C, Lerner AH, Elias T, Nadeau PA Holland L, Kelly PJ, Werner CA, Clor LE, Cappos M (2020) Quantifying gas emissions associated with the 2018 rift eruption of Kīlauea volcano using ground-based DOAS measurements. Bull Volcanol 82:55. https://doi.org/10.1007/s00445-020-01390-8

Kieffer SW (1981) Fluid dynamics of the May 18 blast at Mount St. Helens. US Geol Surv Prof Pap 1250:379

Kim K, Fee D, Yokoo A, Lees JM (2015) Acoustic source inversion to estimate volume flux from volcanic explosions. Geophys Res Lett 42:5243–5249. https://doi.org/10.1002/2015GL064466

Komorowski J-C, Tedesco D, Kasereka M, Allard P, Papale P, Vaselli O, Durieux J, Baxter P, Halbwachs M, Akumbe M, Baluku B, Briole P, Ciraba M, Dupin J-C, Etoy O, Garcin D, Hamaguchi H, Houlié N, Kavotha KS, Lemarchand A, Lockwood J, Luckaya N, Mavonga G, De Michele M, Mpore S, Mukambilwa K, Munyololo F, Newhall C, Ruch J, Yalire M, Wafula M (2004) The January 2002 flank eruption of Nyiragongo volcano (Democratic Republic of Congo): chronology, evidence for a tectonic rift trigger, and impact of lava flows on the city of Goma. Acta Vulcanol 14-15:27–62. https://doi.org/ 10.1400/19077

Kondo G, Aoyama H, Nishimura T, Ripepe M, Lacanna G, Genco R, Kawaguchi R, Yamada T, Miwa T, Fujita E (2019) Gas flux cyclic regime at an open vent magmatic column inferred from seismic and acoustic records. Sci. Rep. Nature 9:5678. https://doi.org/10.1038/s41598-019-42033-z

Kremers S, Wassermann J, Meier K, Pelties C, van Driel M, Vasseur J, Hort M (2013) Inverting the Source Mechanism of Strombolian Explosions at Mt. Yasur, Vanuatu, using a Multi-Parameter Dataset. J Volcanol Geotherm Res 262:104-122

Kyle PR, Moore JA, Thirlwall MF (1992) Petrologic evolution of anorthoclase phonolite lavas at Mount Erebus, Ross Island, Antarctica. J Petrol 33:849–875. http://dx.doi. org/10.1093/petrology/33.4.849

Lamb OD, Lamur A, Díaz-Moreno A, De Angelis S, Hornby AJ, von Aulock FW, Kendrick JE, Wallace PA, Gottschämmer E, Rietbrock A, Alvarez I, Chigna G, Lavallée Y (2019) Disruption of Long-Term Effusive-Explosive Activity at Santiaguito, Guatemala. Front Earth Sci 6:253. http://dx.doi. org/10.3389/feart.2018.00253

Landi P, Corsaro RA, Francalanci L, Civetta L, Miraglia L Pompilio M, Tesoro R (2009) Magma dynamics during the 2007 Stromboli eruption (Aeolian Islands, Italy): Mineralogical, geochemical and isotopic data. J Volcanol Geotherm Res 182:255–268 https://doi.org/10.1016/j.jvolgeores.2008.11.010

Landi P, Francalanci L, Pompilio M, Rosi M, Corsaro RA, Petrone CM, Nardini I, Miraglia L (2006) The December 2002–July 2003 effusive event at Stromboli volcano, Italy: an insight into the shallow plumbing system by petrochemical studies. J Volcanol Geotherm Res 155:263–284

Landi P, Métrich N, Bertagnini A, Rosi, M (2004) Dynamics of magma mixing and degassing recorded in plagioclase at Stromboli (Aeolian Archipelago, Italy). Contrib Mineral Petrol 147:213–227

Le Losq C, Neuville DR, Moretti R, Kyle PR, Oppenheimer C (2015) Rheology of phonolite magmas: the case of the Erebus lava lake. Earth Planet Sci Lett 411:53–61. http://dx.doi.org/10.1016/j.epsl.2014.11.042

Liu EJ, Cashman KV, Miller E, Moore H, Edmonds M, Kunz KE, Jenner F, G Chigna (2020) Petrologic monitoring at Volcán de Fuego, Guatemala. J Volcanol Geotherm Res 405:107044. https://doi.org/10.1016/j.jvolgeores.2020.107044

Lui EJ, Aiuppa A, Alan A, Arellano S, Bitetto M, Bobrowski N, Carn S, Clarke R, Corrales E, de Moor JM, Diaz JA, Edmonds M, Fischer TP, Freer J, Fricke GM, Galle B, Gerdes G, Giudice G, Gutmann A, Hayer C, Itikarai I, Jones J, Mason E, McCormick Kilbride BT, Mulina K, Nowicki S, Rahilly K, Richardson T, Rüdiger J, Schipper CI, Watson IM, Wood K 2020 Aerial strategies advance in volcanic gas measurements at inaccessible, strongly degassing volcanoes. Sci Adv 6:eabb9103

Lyons JJ, Waite GP, Rose WI, Chigna G (2010) Patterns in open vent, strombolian behaviour at Fuego volcano, Guatemala, 2005-2007. Bull Volcanol 72:1-15. http://dx.doi.org/10.1007/s00445-009-0305-7

Mader HM, Llewellin EW, Mueller SP (2013) The rheology of two-phase magmas: A review and analysis. J Volcanol Geotherm Res 257:135-158

Maher SP, RS Matoza, C de Groot-Hedlin, KL Gee, Fee D (2022) Evidence for near-source nonlinear propagation of volcano infrasound from strombolian explosions at Yasur volcano, Vanuatu (2022). Bull Volc 84:41 this issue

Marchetti E, Ripepe M, Delle Donne D, Genco R, Finizola A, Garaebiti E (2013) Blast waves from violent explosive activity at Yasur Volcano, Vanuatu. Geophys Res Lett 40:5838-5843. https://doi.org/10.1002/2013GL057900

Martin DP, Rose WI (1981) Behavioral patterns of Fuego volcano, Guatemala. J Volcanol Geotherm Res 10:67–81

Martin RS, Sawyer GM, Spampinato G, Salerno GG, Ramirez C, Ilyinskaya I, Witt MLI, Mather TA, Watson IM, Phillips JC, Oppenheimer C (2010) A volatile inventory for Masaya Volcano, Nicaragua. J Geophys Res 115, B09215

Matoza RS, Fee D, Neilsen K, Gee L, Ogden DE (2013) Aeroacoustics of volcanic jets: Acoustic power estimation and jet velocity dependence. J Geophys Res Solid Earth 118:6269–6284. https://doi.org/10.1002/2013JB010303.

Matoza RS, Fee D, Garcès MA, Seiner JM, Ramón PA, Hedlin MAH (2009) Infrasonic jet noise from volcanic eruptions, Geophys Res Lett 3: L08303. https://doi.org/10.1029/2008GL036486

Medici EF, Allen JS, Waite GP (2014) Modeling shock waves generated by explosive volcanic eruptions. Geophys Res Lett 41:414–421. https://doi.org/10.1002/2013GL058340

Meier K, Hort M, Wassermann J, Garaebiti E (2016) Strombolian surface activity regimes at Yasur volcano, Vanuatu, as observed by Doppler radar, infrared camera and infrasound. J Volcanol Geotherm Res, Special issue, on Understanding volcanoes in the Vanuatu arc 322:184-195

Métrich N, Allard P, Aiuppa A, Bani P, Bertagnini A, Shinohara H, Parello F, Di Muro A, Garaebiti E, Belhadj O, Massare D (2011) Magma and volatile supply to post-collapse volcanism and block resurgence in Siwi caldera (Tanna island, Vanuatu arc). J Petrol 51:603-626. https://doi.org/10.1093/petrology/egr019

Métrich N, Bertagnini A, Pistolesi M (2021) Paroxysms at Stromboli volcano (Italy): source, genesis and dynamics. Front Earth Sci 9:593339. https://doi.org/10.3389/feart.2021.593339

Métrich N. (2021) Redox state of volatiles and their relationships with iron in silicate melts: Implications for magma degassing. In Magma redox geochemistry (Moretti R and Neuville D eds). Monograph, Amer Geophys Union 266:215-230. https://doi.org/10.1002/9781119473206.ch11

Michon L, Di Muro A, Villeneuve N, Saint-Marc C, Fadda P, Manta F (2013) Explosive activity of the summit cone of Piton de la Fournaise volcano (La Réunion island): A historical and geological review. J Volcanol Geotherm Res 264:117-133. https://doi.org/10.1016/j.jvolgeores.2013.06.012

Molina I, Burgisser A, Oppenheimer C (2015) A model of the geochemical and physical fluctuations of the lava lake at Erebus volcano, Antarctica. J Volcanol Geotherm Res 308:142-157. http://dx.doi.org/10.1016/j.jvolgeores.2015.10.027

Mora MM, Lesage P, Taylor-Castillo W, Vergniolle S, Fourel L, Soto GJ (2022) Retrospective of an open-vent eruption at Arenal volcano (Costa Rica, 1968-2010): evolution, dynamics, what we learned, and future perspectives. Bull Volc 84:66 this issue. https://doi.org/10.1007/s00445-022-01570-8

Morrissey M, Garcés M, Ishihara K, Iguchi M (2008) Analysis of infrasonic and seismic events related to the 1998 Vulcanian eruption at Sakurajima. J Volcanol Geotherm Res 175:315-324

Morrissey MM, Chouet B (1997) A numerical investigation of choked flow dynamics and its application to the triggering mechanism of long-period events at Redoubt Volcano, Alaska. J Geophys Res 102(B4):7965-7983

Morrissey MM, Mastin LG (2000) Vulcanian eruptions. Encyclopedia of volcanoes, first eddition, Academic Press, 463-475

Morrison AA, Whittington A, Smets B, Kervyn M, Sehlke A (2020) The Rheology of Crystallizing basaltic lavas from Nyiragongo and Nyamuragira volcanoes, D.R.C. Volcanica 3(1):1-28. http://dx.doi.org/10.30909/vol.03.01.0128

Moussallam Y, Oppenheimer C, Scaillet B, Kyle P (2013) Experimental Phase-equilibrium Constraints on the Phonolite Magmatic System of Erebus Volcano, Antarctica. J Petrol 54:1285-1307. https://doi.org/10.1093/petrology/egt012

Moussallam Y, Bani P, Curtis A, Barnie T, Moussallam M, Peters N, Schipper CI, Aiuppa A, Giudice G, Amigo A, Velasquez G, Cardona C (2016) Sustaining persistent lava lakes: Observations from high-resolution gas measurements at Villarrica Volcano, Chile. Earth Planet Sci Lett 454:237–247

Moussallam Y, Rose-Koga EF, Koga KT, Médard E, Bani P, Devidal J-L, Tari D (2019) Fast ascent rate during the 2017–2018 Plinian eruption of Ambae (Aoba) volcano: a petrological investigation. Contrib Mineral Petrol 174:90. https://doi.org/10.1007/s00410-019-1625-z

Moussallam Y, Médard E, Georgeais G, Rose-Koga EF, Koga KT, Pelletier B, Bani Ph, Shreve TL, Grandin TL, Boichu M, Tari D, Peters N (2021) How to turn off a lava lake? A petrological investigation of the 2018 intra-caldera and submarine eruptions of Ambrym volcano. Bull Volcanol 83:36, this issue. https://doi.org/10.1007/s00445-021-01455-2

MoussallamY, Oppenheimer C, Scaillet B, Buisman I, Kimball C, Dunbar N, Burgisser A, Schipper CI, Andújar J, Kyle P (2015) Megacrystals track magma convection between reservoir and surface. Earth Planet Sci Lett 413:1-12. http://dx.doi.org/10.1016/j.epsl.2014.12.022

Moussallam Y, Oppenheimer C, Scaillet B, Gaillard F, Kyle P, Peters N, Hartley M, Berloe K, Donovana A (2014) Tracking the changing oxidation state of Erebus magmas from mantle to surface driven by magma ascent and degassing. Earth Planet Sci Lett 393:200–209. http://dx.doi.org/10.1016/j.epsl.2014.02.055

Mueller S, Llewellin EW, Mader HM (2011) The effect of particle shape on suspension viscosity and implications for magmatic flows. Geophys Res Lett 38:L13316. https://doi.org/10.1029/2011GL047167

Nabyl A, Dorel J, Lardy M (1997) A comparative study of low-frequency seismic signals recorded at Stromboli volcano, Italy, and at Yasur volcano, Vanuatu. New Zeal J Geol and Geophysics 40:549-558

Nadeau PA, Werner C A,Waite G P, Carn, SA, Brewer, ID, Elias T, Sutton AJ, Kern C (2015) Using SO_2 camera imagery and seismicity to examine degassing and gas accumulation at Kilauea volcano, May 2010. J Volcanol Geotherm Res 300-70–80. https://doi.org/10.1016/j.jvolgeores.2019-03.014

Naismith AK, Watson IM, Escobar-Wolf R, Chigna G, Thomas G, Coppola G, Chun C. (2019) Eruption frequency patterns through time for the current (1999–2018) activity cycle at Volcán de Fuego derived from remote sensing data: Evidence for an accelerating cycle of explosive paroxysms and potential implications of eruptive activity. J Volcanol Geotherm Res 371:206-219. https://doi.org/10.1016/j.jvolgeores.2019.01.001

Németh K, Cronin SJ (2011) Drivers of explosivity and elevated hazard in basaltic fissure eruptions: The 1913 eruption of Ambrym Volcano, Vanuatu (SW-Pacific). J Volcanol Geotherm Res 201:194-209. https://doi.org/10.1016/j.jvolgeores.2010.12.007

Németh K, Cronin SJ (2008) Volcanic craters, pit craters and high-level magma-feeding systems of a mafic island-arc volcano: Ambrym. Geol Soc London Spec Pub 302:87-102. https://doi.org/10.1144/SP302.6

Oppenheimer C, Lomakina AS, Kyle PR, Kingsbury NG, Boichu M (2009) Pulsatory magma supply to a phonolite lava lake. Earth Planet Sci Lett 284:392-398. https://doi.org/10.1016/j.epsl.2009.04.043

Oppenheimer C. Moretti R, Kyle PR, Eschenbacher A, Lowenstern JB, Hervig RL, Dunbar, NW (2011) Mantle to surface degassing of alkalic magmas at Erebus volcano, Antarctica. Earth Planet Sci Lett 306:261-271. https://doi.org/10.1016/j.epsl.2011.04.005

Pansino S, Calder E, Menand T (2019) Experimental analysis of bubble-driven magma motion in the conduit, for persistently active, open vent volcanoes. Bull Volcanol 81:12. https://doi.org/10.1007/s00445-019-1339-0

Parat F, Streck MJ, Holtz F, Almeev R (2014) Experimental study into the petrogenesis of crystal-rich basaltic to andesitic magmas at Arenal volcano. Contrib Mineral Petrol 168(2):1040. https://doi.org/10.1007/s00410-14-1040-4

Pardini F, Queiβer M, Naismith A, Watson IM, Clarisse L, Burton MR (2019) Initial constraints on triggering mechanisms of the eruption of Fuego volcano (Guatemala) from 3 June 2018 using IASI satellite data. J Volcanol Geotherm Res 376:59-61 https://doi.org/10.1016/j.jvolgeores.2014.12.005

Patanè D, Barberi G, De Gori P, Cocina O, Zuccarello L, Garcia-Yeguas A, Castellano M, D'Alessandro A, Sgroi T (2017) The shallow magma chamber of Stromboli Volcano (Italy), Geophys Res Lett 44 : 6589–6596. https://doi.org/10.1002/2017GL073008

Patrick M, Anderson K, Poland M, Orr T, Swanson D (2015) Lava lake level as a gauge of magma reservoir pressure and eruptive hazard. Geology 43(9):831–834

Patrick M, Johanson I, Shea T, Waite T (2020) The historic events at Kīlauea Volcano in 2018: summit collapse, rift zone eruption, and Mw 6.9 earthquake: preface to the special issue. Bull Volcanol 82:46. https://doi.org/10.1007/s00445-020-01377-5.

Patrick M, Orra T, Anderson K, Swanson D (2019). Eruptions in sync: Improved constraints on Kilauea Volcano's hydraulic connection. Earth Planet Sci Lett 507:50–61 https://doi.org/10.1016/j.epsl.2018.11.030

Patrick MR, Harris AJL, Ripepe M, Dehn J, Rothery DA, Calvari S (2007) Strombolian explosive styles and source conditions: insights from thermal (FLIR) video. Bull Volcanol 69:769-784

Peck DL, Hamilton MS, Shaw HR (1977) Numerical analysis of lava lake cooling models: part II, application to Alae lava lake, Hawaii. Am J Sci 277:415-437

Pering TD, Ilanko T, Wilkes TC, England RA, Silcock SR, Stanger LR, Willmott JR, Bryant RG, McGonigle AJS (2019) A Rapidly Convecting Lava Lake at Masaya Volcano, Nicaragua. Front Earth Sci 6:241. https://doi.org/10.3389/feart.2018.00241

Perring TD, Ilanko T, EJ Liu (2019) Periodicity in Volcanic Gas Plumes: A Review and Analysis. Geosciences 9:394. https://doi.org/10.3390/geosciences9090394

Pering TD, Liu EJ, Wood K, Wilkes TC, Aiuppa A, Tamburello G, Bitetto M, Richardson T, McGonigle, AJS (2020) Combined ground and aerial measurements resolve vent-specific gas fluxes from a multi-vent volcano. Nature Communications 11, 3039

Peters N, Oppenheimer C, Killingsworth DR, Frechette J, Kyle P (2014a) Correlation of cycles in Lava Lake motion and degassing at Erebus Volcano, Antarctica. Geochem Geophys Geosyst, 15, https://doi.org/10.1002/2014GC005399.

Peters N, Oppenheimer C, Kyle P, Kingsbury N (2014b) Decadal persistence of cycles in lava lake motion at Erebus volcano, Antarctica. Earth Planet. Sci. 395, 1-12

Peters NJ, Oppenheimer, C, Brennan P, Lok LB, Ash M, Kyle P (2018) Radar altimetry as a robust tool for monitoring the active lava lake at Erebus volcano, Antarctica. Geophys Res Lett 45:8897-8904. https://doi.org/10.1029/2018GL079177

Pichavant M, MacDonald R (2007) Crystallization of primitive basaltic magma at crustal pressures and genesis of the calk-alkaline igneous suite: experimental evidence from Saint Vincent, Lesser Antilles arc. Contr Mineral Petrol 154:535.558. https://doi.org/10.1029/2018GL079177

Pichavant M, Di Carlo I, Pompilio M, Le Gall N (2022) Timescales and mechanisms of paroxysm initiation at Stromboli volcano, Aeolian. Bull Volc 83:36. https://doi.org/10.1007/s00445-022-01545-9 this issue

Pioli L, Bonadonna C, Azzopardi BJ, Phillips JC, Ripepe M (2012) Experimental constraints on the outgassing dynamics of basaltic magmas. J Geophys Res 117(B03204):1-17. https://doi.org/10.1029/2011JB008392

Poland MP, Carbone D (2018) Continuous gravity and tilt reveal anomalous pressure and density changes associated with gas pistoning within the summit lava lake of Kilauea volcano, Hawai'i. Geophys Res Lett 45:2319–2327. https://doi.org/10.1002/ 017GL076936

Pouclet A, Bram K (2021) Nyiragongo and Nyamuragira: a review of volcanic activity in the Kivu rift, western branch of the East African Rift System. Bull Volcanol 83:10

Radebaugh J, Lopes RM, Howell RD, Lorenz RD, Turtle EP (2016) Eruptive behavior of the Marum/Mbwelesu lava lake, Vanuatu and comparisons with lava lakes on Earth and Io. J Volcanol Geotherm Res, Special issue on Understanding volcanoes in the Vanuatu arc 322:105-118

Ramsey MS, Harris AJL (2013) Volcanology 2020: How will thermal remote sensing of volcanic surface activity evolve over the next decade? J Volcanol Geotherm Res 249: 217–233

Rasmussen DJ, Plank TA, Roman DC, Power JA, Bodnar RJ, Hauri EH (2018) When does eruption run-up begin? Multidisciplinary insight from the 1999 eruption of Shishaldin volcano. Earth Planet Sci Lett 486:1-14

Richardson JP, Waite GP, Palma JL (2014) Varying seismic-acoustic properties of the fluctuating lava lake at Villarrica volcano, Chile. J Geophys Res Solid Earth 119:5560–5573. https://doi.org/10.1002/ 2014JB011002

Ripepe M, Rossi M, Saccorotti G (1993) Image processing of the explosive activity at Stromboli Volcano. J Volcanol Geotherm Res 54:335-351

Ripepe M, Ciliberto S, Schiava MD (2001) Time constraints for modeling source dynamics of volcanic eruptions at Stromboli. J Geophys Res 106:8713-8727

Ripepe M, Marchetti E, Ulivieri G, Harris A, Dehn J, Burton M, Caltabiano T, Salerno G (2005) Effusive to explosive transition during the 2003 eruption of Stromboli volcano. Geol 33(5):341-344

Ripepe M, Del Donne D, Harris A, Marchetti E, Ulivieri G (2008) Dynamics of Strombolian Activity in The Stromboli Volcano: An Integrated Study of the 2002-2003 Eruption. Geophys Monogr Ser, 182:39-48, editted by Calvari et al. AGU, Washington DC

Ripepe M, Marchetti E (2002) Array tracking of infrasonic sources at Stromboli volcano. Geophys Res Lett 29: 22, 2076, https://doi.org/10.1029/2002GL015452

Roberge J, Delgado Granados H, Wallace P (2009) Mafic magma recharge supplies high CO_2 and SO_2 gas fluxes from Popocatépetl volcano, México. Geol Soc Am 37:107-110. https://doi.org10.1130/G25242A.1

Rodríguez L, Watson IM, Rose WI, Branan YK, Bluth GJS, Chigna G, Mattías O, Escobar D, Carn S, Fischer TP (2004) SO_2 emissions to the atmosphere from active volcanoes in Guatemala and El Salvador, 1999-2002. J Volcanol Geotherm Res 138:325–344. https://doi.org/10.1016/j.jvolgeores.2004.07.008

Roggensack K (2001) Unraveling the 1974 eruption of Fuego volcano (Guatemala) with small crystals and their young melt inclusions. Geol 29(10):911–914. https://doi.org/10.1130/0091

Rose WI (1972) Pattern and mechanism of volcanic activity at the Santiaguito volcanic dome, Guatemala. Bull Volcanol 36:73-94

Rose Jr, WI (1972) Notes on the 1902 eruption of Santa Maria volcano, Guatemala. Bull Volcanol 36:29-45

Rose Jr WI, Anderson Jr AT, Woodruff LG, Bonis SB (1978) The October 1974 basaltic tephra from Fuego volcano: description and history of the magma body. J Volcanol Geotherm Res 4(1-2):3–53. https://doi.org/10.1016/0377-0273(78)90027-6

Rose WI (1987) Santa Maria, Guatemala: Bimodal soda-rich calc-alkalic stratovolcano. J Volcanol Geotherm Res 33: 109-129

Rose WI (1987) Volcanic activity at Santiaguito Volcano 1976-1984. Geol Soc Am Spec Pap 212:17-27

Rose Jr WI, Self S, Murrow PJ, Bonadonna C, Durant AJ, Ernst GGJ (2008) Nature and significance of small volume fall deposits at composite volcanoes: Insights from the October 14, 1974 Fuego eruption, Guatemala. Bull Volcanol 70(9):1043–1067. https://doi.org/10.1007/s00445-007-0187-5

Rose IW, Palma JL, Delgado Granados H, Varley N (2013a) Open-vent volcanisms and related hazards: Overview. In Rose WI, Palma JL, Delgado Granados H, Varley N (Eds) Understanding open-vent volcanism and related hazards: Spec Paper 498:vi-xiii. https://doi.org/10.1130/2013.2498 (00)

Rose WI, Palma JL, Escobar Wolf R, Matías-Gomez, RO (2013b) A 50 yr eruption of a basaltic composite cone: Pacaya, Guatemala. In Rose WI, Palma JL, Delgado Granados H, Varley N (Eds) Understanding open-vent volcanism and related hazards: Spec Paper 498: 1–21 Geol Soc Amer. https://doi.org/10.1130/2013.2498(01)

Rosi M, Pistolesi M, Bertagnini A, Landi P, Pompillio M, Di Roberto A (2013) Stromboli volcano, Aeolian Islands (Italy): present eruptive activity and hazards. Geol Soc London, Mem 37:473-490. https://doi.org/10.1144/M37.14

Rout SS, Wörmer G (2020) Constraints on the pre-eruptive magmatic history of the Quaternary Laacher See volcano (Germany). Contrib Mineral Petrol 175:74. https://doi.org/10.1007/s00410-020-01710-3

Ryder CH, Gill JB, Tepley F III, Ramos F, Reagan M (2006) Closed to open-system differentiation at Arenal volcano (1968–2003). J Volcanol Geoth Res 157:75–93

Sahetapy-Engel S, Harris AJL, Marchetti E (2008) Thermal, seismic and infrasound observations of persistent explosive activity and conduit dynamics at Santiaguito lava dome, Guatemala. J Volcanol Geotherm Res 173:1-14. https://doi.org/10.1016/j.jvolgeores.2007.11.026

Sahetapy-Engel ST, Harris AJL (2009a) Thermal structure and heat loss at the summit crater of an active lava dome. Bull Volcanol 71:15–28. http:// dx.doi.org/10.1007/s00445-008-0204-3

Sahetapy-Engel ST, Harris AJL (2009b) Thermal-image-derived dynamics of vertical ash plumes at Santiaguito volcano, Guatemala. Bull Volcanol 71:827–830. http://dx.doi.org/10.1007/s00445-009-0284-8

Sánchez C, Álvarez B, Melo F, Vidal V (2014) Experimental modeling of infrasound emission from slug bursting on volcanoes. Geophys Res Lett 41:6705–6711. https://doi.org/10.1002/2014GL061068

Schaaf P, Stimac J, Siebe C, Macías JL (2005) Geochemical evidence for mantle origin and crustal processes in volcanic rocks from Popocatépetl and surrounding monogenetic volcanoes, Central Mexico. J Petrol 46:1243–1282. https://doi.org/10.1093/petrology/egi015

Scharff L, Hort M, Harris AJ, Ripepe M, Lees J, Seyfried R (2008), Eruption dynamics of the SW crater of Stromboli volcano, Italy. J Volcanol Geotherm Res 176:565–570. https://doi.org/10.1016/j.jvolgeores.2008.05.008

Scharff L, Ziemen F, Hort M, Gerst A, Johnson JB (2012) A detailed view into the eruption clouds of Santiaguito volcano, Guatemala, using Doppler radar. J Geophy. Res 117:B04201. https://doi.org/10.1029/2011JB008542

Sawyer GM, Oppenheimer C, Tsanev VI, Yirgu G (2008). Magmatic degassing at Erta ’Ale volcano, Ethiopia. J Volcanol Geotherm Res 178:837–846

Sawyer GM, Salerno G, Le Blond JS, Martin RS, Spampinato L, Roberts TJ, Mather TA, Witt MLI, Tsanev VI, Oppenheimer C (2011) Gas and aerosol emissions from Villarrica volcano, Chile. J Volcanol Geotherm Res 203:62–75. http://dx.doi.org/10.1016/j.jvolgeores.2011.04.003

Scott JAJ, Mather TA, Pyle DM, Rose WI, Chigna G (2012) The magmatic plumbing system beneath Santiaguito volcano, Guatemala. J Volcanol Geotherm Res 237-238:54–68. http://dx.doi.org/10.1016/j.jvolgeores.2012.05.014

Scott JAJ, Pyle DM, Mather TA, Rose WI (2013) Geochemistry and evolution of the Santiaguito volcanic dome complex, Guatemala. J Volcanol Geotherm Res 252:92-107. http://dx.doi.org/10.1016/j.jvolgeores.2012.11.011

Shinohara H (2008) Excess degassing from volcanoes and its role on eruptive and intrusive activity. Rev Geophys 46:RG4005. http://dx.doi.org/10.1029/2007RG000244

Shinohara H (2013) Volatile flux from subduction zone volcanoes: insights from a detailed evaluation of the fluxes from volcanoes in Japan. J Volcanol Geotherm Res 268:46–63. https://doi.org/10.1016/j.jvolgeores.2013.10.007

Shreve T, Grandin R, Boichu M, Garaebiti E, Moussallam E, Ballu V., Delgado F, Leclerc F, Vallée M, Henriot M, Cevuard S, Tari D, Lebellegard P, Pelletier B (2019) From prodigious volcanic degassing to caldera subsidence and quiescence at Ambrym (Vanuatu): the influence of regional tectonics. Sci Rep 9:18868. https://doi.org/10.1038/s41598-019-55141-7

Sims KWW, Aster RC, Gaetani G, Blichert-Toft J, Phillips EH, Wallace PJ, Mattioli GS, Rasmussen D, Boyd ES, Mount Erebus (2021) Eds Smellie JL, Panter KS, Geyer, A Volcanism in Antartica: 200 millions years of subduction, Rifting and Continental break-up Geological Society, London, Memoirs, 55, https://doi.org/10.1144/M55-2019-8

Singer BS, Smith KE, Jicha BR, Beard BL, Johnson CM., Rogers NW (2011) Tracking open-system differentiation during growth of Santa Maria Volcano, Guatemala. J Petrol 52:2335–2363

Spampinato L, Ganci G, Hernandez PA, Calvo D, Tedesco D, Pérez NM, Calvari S, Del Negro C, Yalire MM (2013) Thermal insights into the dynamics of Nyiragongo lava lake from ground and satellite measurements. J Geophys Res Solid Earth 118:5771-5784. https://doi.org/10.1002/2013JB010520

Spampinato L, Oppenheimer C, Cannata A, Montalto P, Salerno GG, Calvari S (2012) On the time-scale of thermal cycles associated with open-vent degassing. Bull Volcanol 74:1281-1292

Spampinato L, Oppenheimer C, Calvari S, Cannata A, Montalto P (2008) Lava lake surface characterization by thermal imaging: Erta 'Ale volcano (Ethiopia). Geochem Geophys Geosyst 9(12):Q12008. doi:10.1029/2008GC00216

Spina L, Taddeucci J, Cannata A, Gresta S, Lodato L, Privitera E, Scarlato P, Gaeta M, Gaudin D, Palladino DM (2016) Explosive volcanic activity at Mt. Yasur: A characterization of the acoustic events (9-12th July 2011). J Volcanol Geotherm Res, Special issue on Understanding volcanoes in the Vanuatu arc 322:175-183

Stevenson DS, Blake S (1998) Modelling the dynamics and thermodynamics of volcanic degassing. Bull Volcanol 60:307-317

Stix J (2007) Stability and instability of quiescently active volcanoes: The case of Masaya, Nicaragua. Geol 35(6):535–538. https://doi.org/10.1130/G23198A

Streck MJ, Dungan MA, Malavassi E, Reagan M, Bussy F (2002) The role of basalt replenishment in the generation of basaltic andesites of the ongoing activity at Arenal volcano, Costa Rica: evidence from clinopyroxene and spinel. Bull Volcanol 64:316–327

Suckale J, Qin, Z, Picchi D, Keller T, Battiato I (2018) Bistability of buoyancy-driven exchange flows in vertical tubes. J Fluid Mec. 850:525-550

Taddeucci J, Scarlato P, Capponi A, Del Bello E, Cimarelli C, D. Palladino M, Kueppers U (2012a) High-speed imaging of Strombolian explosions: The ejection velocity of pyroclasts. Geophys Res Lett 39:L02301. https://doi.org/10.1029/2011GL050404

Taddeucci, J, Alatorre-Ibargengoitia MA, Moroni M, Tornetta L, Capponi A, Scarlato P, Dingwell DB, De Rita D (2012b) Physical parameterization of Strombolian eruptions via experimentally-validated modeling of high-speed observations. Geophys Res Lett 39:L16306. https://doi.org/10.1029/2012GL052772

Taddeucci J, Sesterhenn J, Scarlato P, Stampka K, Del Bello E, Pena Fernandez JJ, Gaudin D (2014) Highspeed imaging, acoustic features, and aeroacoustic computations of jet noise from Strombolian (and Vulcanian) explosions. Geophys Res Lett 41:3096–3102. https://doi.org/10.1002/2014GL059925

Taddeucci, J, Pena Fernandez JJ, Cigala V, Kueppers U, Scarlato P, Del Bello E, Ricci T, Sesterhenn J, Panunzi S (2021) Volcanic vortex rings: Axial dynamics, acoustic features, and their link to vent diameter and supersonic jet flow. Geophys Res Lett, 48:e2021GL092899. https://doi.org/10.1029/2021GL092899

Taddeucci J, Edmonds M, Houghton BH, James MR, Vergniolle S (2015) Hawaiian and Strombolian Eruptions - including Fire Fountaining. "Encyclopedia of Volcanoes", 2nd eddition, ed. Sigurdsson H, Houghton B, Rymer H, Stix J, McNutt S, Academic press, 27:485-503

Tamburello G, Aiuppa A, Kantzas EP, McGonigle AJS, Ripepe M (2012) Passive vs. active degassing modes at an open-vent volcano (Stromboli, Italy). Earth Planet Sci Lett 249-360:106–116

Taquet N, Stremme W, Grutter M, Baylón J, Bezanilla A, Schiavo B, Rivera C, Campion R, Boulesteix T, Nieto-Torres A, Espinasa-Pereña R, Blumenstock T, Hase F (2019) Variability in the gas composition of the Popocatépetl volcanic plume. Front Earth Sci 7:114. https://doi.org/10.3389/feart.2019.00114

Thivet S, Harris AJL, Gurioli L, Bani P, Bernie T, Bombrun M, Marchetti A (2021) Multi-parametric field experiments links explosive activity and persistent degassing at Stromboli. Frontiers Earth Sci 9:669661. https://doi.org/10.3389/feart. 2021. 669661

Turcotte DL, Ockendon H, Ockendon JR, Cowley SJ (1990) A mathematical model of vulcanian eruptions. Geophys J Int 103:211–217

Valade S, Ripepe M, Giuffrida G, Karume K, Tedesco D (2018) Dynamics of Mount Nyiragongo lava lake inferred from thermal imaging and infrasound array. Earth Planet Sci Lett 500:192–204.

Vergniolle S, Jaupart C (1986) Separated two-phase flow and basaltic eruptions. J Geophys Res 91(B12):12842-12860

Vergniolle S, Brandeis G (1994) Origin of the sound generated by Strombolian explosion. Geophys Res Lett 21:1959-1962

Vergniolle S, Brandeis G (1996) Strombolian explosion: 1. A large bubble breaking at the surface of a lava column as a source of sound. J Geophys Res 101:20,433-20,447

Vergniolle S, Caplan-Auerbach J (2004) Acoustic measurements of the 1999 eruption of Shishaldin volcano, Alaska: 2) Precursor to the Subplinian activity. J Volcanol Geothermal Res 137:135-151

Vergniolle S, Caplan-Auerbach J (2006) Basaltic thermals and Subplinian plumes: Constraints from acoustic measurements at Shishaldin volcano, Alaska. Bull Volcanol 68(7-8):611-630

Vergniolle S, Gaudemer Y (2015) From reservoirs and conduits to the surface: a review on the role of bubbles in driving basaltic eruptions, Carey RJ, Cayol V, Poland MP, Weis D (eds.), Am Geophysical Union Monograph: " Hawaiian Volcanism: From Source to Surface" 208(14): 289-322. https://doi.org/10.1002/9781118872079.ch14, 2015.

Vergniolle S, Bouche E (2016) Gas-driven lava lake fluctuations at Erta'Ale volcano (Ethiopia) revealed by MODIS measurements. Bull Volcanol 78:60 https://doi.org/10.1007/s00445-016-1047-y

Wade JA, Plank T, Melson WG, Soto GJ, Hauri EH (2006) The volatile content of magmas from Arenal volcano. J Volcanol Geotherm Res 157:94–120. https://doi.org/.1016/j.jvolgeores.2006.03.045

Wallace PJ, Edmonds M (2011) The sulphur budget in magmas. Evidence from melt inclusions, submarine glasses and volcanic gas emissions. Rev Mineral Geochem 73:215-246. https://doi.org/ 10.2138/rmg.2011.73.8

Wallace PA, Lamb OD, DeAngelis S, Kendrick JE, Hornby AJ, Díaz-Moreno A, González PJ, vonAulock FW, Lamur A, Utley JEP, Rietbrock A, Chigna G, Lavallée Y (2020) Integrated constraints on explosive eruption intensification at Santiaguito dome complex, Guatemala. Earth Planet Sci Lett 536:116139. https://doi.org/10.1016/j.epsl.2020.116139

Williams-Jones G, Rymer H (2015) Hazards of volcanic gases. In Sigurdsson H, Houghton B, Rymer H, Stix J, McNutt S (eds). The Encyclopedia of Volcanoes pp 985-992.

Witsil AJC, Johnson JB (2018) Infrasound explosion and coda signal investigated with joint analysis of video at Mount Erebus, Antarctica. J Volcanol Geotherm Res 357:306-320

Witt MI, Mather TA, Pyle DM, Aiuppa A, Bagnato E, Tsanev VI (2008) Mercury and halogen emissions from Masaya and Telica volcanoes, Nicaragua. J Geophys Res 113(B6). https://doi.org/10.1029/2007JB005401

Witter JB, Kress VC, Delmelle P, Stix J (2004) Volatile degassing, petrology, and magma dynamics of the Villarrica Lava Lake, Southern Chile. J Volcanol Geotherm Res 134:303-337. https://doi.org/10.1016/j.jvolgeores.2004.03.002

Witter JB, Kress VC, Newhall CG (2005) Volcan Popocatépetl, Mexico. Petrology, magma mixing, and immediate sources of volatiles for the 1994 present eruption. J Petrol 46:2337–2366. https://doi.org/1010.1093/petrology/egi058

Woitischek J, Woods AW, Edmonds M, Oppenheimer C, Aiuppa A, Pering TD, Ilanko T, D'Aleo R, Garaebiti E (2020) Strombolian eruptions and dynamics of magma degassing at Yasur Volcano (Vanuatu). J Volcanol Geotherm Res 398:106869. https://doi.org/10.1016/j.jvolgeores.2020.106869

Woods AW (1995) A model of vulcanian explosions. Nuclear Engineering and Design, 155:345–357

Worster MG, Huppert HE, Sparks RSJ (1993) The crystallization of lava lakes. J Geophys Res 98(B9):15891-15901

Woulff G and McGetchin TR (1976) Acoustic noise from volcanoes: Theory and experiments. Geophys J Roy Astron Soc 45:601-616

Wright, R (2016) MODVOLC: 14 years of autonomous observations of effusive volcanism from space. In Harris AJL, De Groeve T, Garel F, Carn SA (eds) 2016. Detecting, Modelling and Responding to Effusive Eruptions. Geological Society, London, Special Publications, 426:23–53

Yamamoto H, Watson IM, Phillips JC, Bluth GJ (2008) Rise dynamics and relative ash distribution in vulcanian eruption plumes at Santiaguito Volcano, Guatemala, revealed using an ultraviolet imaging camera. Geophys Res Lett, 35:8

Zurek J, Moune S, Williams-Jones G, Vigouroux N, Gauthier P-J (2019) Melt inclusion evidence for long term steady-state volcanism at Las Sierras-Masaya volcano, Nicaragua. J Volcanol Geotherm Res 378:16-28.https://doi.org/10.1016/j.jvolgeores.2019.04.007

Figure captions

Fig. 1 SiO_2 distribution in magmas of Erta 'Ale (Field et al. 2012); Masaya (Zureck et al. 2019); Fuego (Berlo et al. 2012); Nyiragongo (Minissale et al. 2019; Demant and Lubala, 1994); Nyamuragira (Head et al. 2011); Stromboli (Landi et al. 2006, 2009; Bertagnini et al. 2008; Pompilio et al. 2011; Métrich et al. 2010, 2021); Ambrym (Allard et al. 2016a, b) ; Pacaya (Cameron et al. 2002) ; Yasur (Métrich et al. 2011); Erebus (Kelly et al. 2008); Arenal (Bolge et al. 2006); Santiaguito (Scott et al. 2013); Popocatépetl (Schaaf et al. 2005).

Fig. 2 Plumbing systems and associated mechanisms at: a) Kilauea (slightly adapted from Ferguson et al. 2016); b) Nyiragongo (Pouclet and Bram, 2020); c) Stromboli during the small-scale paroxysms (slightly adapted from Métrich et al. 2021); d) from seismic tomographic inversion from combining artificial and natural seismic sources, showing the magma pathway (red arrows) and the high velocity zone associated to the crystallised magma body (slightly adapted from Patanè et al. 2017). SdF, Stcc and iso, HVB stand for Sciara del Fuoco, Strombolicchio, isosurface of constant seismic velocity propagation (iso6 is for 6 km/s) and high-velocity body.

Fig. 3 Potential bubble geometries for rising bubbles (a) and stationary bubbles (b): left: small; middle: relatively large and defined as spherical cap bubble; right: very large and called Taylor bubble; b) flat bubble, i.e. thin and very long, resulting from a local coalescence within a foam accumulated below the crust at the top of a lava lake and defined in Bouche et al. 2010.

Fig. 4 Lava lake of Kilauea at: a) Puu O'o on March 1988, showing a broken bubble of a few meters in diameter (photo by S. Vergniolle); b) summit on 29 July 2016 (courtesy of M. Patrick); c) summit on 6 May 2018, as the lake drained away during the 2018 lower East Rift Zone eruption, with a crater of diameter of 150 m (courtesy of M. Patrick). Note the difference in the lava lake level between 2b and 2c, analysed by Patrick et al, 2015.

Fig. 5 Lava lake of Nyiragongo with a diameter of 250-260 m along the east-west axis and 200 m along the north-south axis (courtesy of B. Smets): a) Panoramic view of the lava lake on 12 September 2011 displaying a hot central zone and a partly solidified annulus. b) Many incandescent cracks can be seen in central area on 12 September 2011; c) overflows of the lava lake with the former lava lake appearing as an annular incandescent ring, on 12 September 2011; d) bubble bursting at the surface of the lava lake, in 2016.

Fig. 6 Top of exposed magma column of Erebus (courtesy of C. Oppenheimer): a) with a diameter of 60 m, 7 December 2003 at 11h15 UTC; b) low-level lava lake, 30-40 m in diameter, 3 December 2012 at 9h54 UTC; c) fresh bombs can be seen on the side of the crater, 60 m in diameter, 15 December 2004 at 23h57 UTC; d) weak degassing (blue cloud), 17 December 2010 at 10:44:05.

Fig. 7 Lava lake of Erta 'Ale: a) 29-30 January 2003 (courtesy of J-M Bardintzeff), the diameter is nearly 90 m; b) 22 March, 2003 (photo taken by T. Staudacher and slightly adapted from Vergniolle and Bouche, 2016); the diameter is 30 m; c) December 2004, the lava lake is entirely encrusted (diameter > 100 m; courtesy of J-M Bardintzeff); d) thermal image on 26 March 2003 (taken by T. Staudacher) with a lava lake of diameter equal 30 m, and with insert of visible image of a spherical cap bubble in March 2001 (adapted from Bouche et al. 2010 photo 4d).

Fig. 8 Lava lakes of Ambrym: a) Benbow crater (courtesy of J-M Bardintzeff), with diameters of 2 km for the caldera, 800 m for the largest crater in front, 200-300 m for the two small craters; b) Marum crater, 80 m in diameter, 13 August 2013 at 14h01 (courtesy of T. Boyer); c) Marum, bubble diameter of 8-10 m, photo taken at 80 m distance, October 2007 (courtesy of P. Allard); d) Marum, bubble bursting on 22 June 2015 at 12h34 (courtesy of T. Boyer); e) Marum, diameter of 90 m, depth of 350m, 14 November 2016 at 11h20, the lava lake had a partial thin crust cover, with incandescent cracks (courtesy T. Boyer); f) lava flow on 9 March 2015, the cone in the back is Niri Maben Mbwelesu (courtesy T. Boyer).

Fig. 9 Lava lake at Masaya, a) 16 January 2009, degassing from hidden thermally radiating lava lake (courtesy of P. Delmelle); b) in 2016 dimensions of 40x30 m, depth: 250 m (courtesy of J-M Bardintzeff); c) 18 February 2017 (courtesy of P. Delmelle) approximatively 15 m of diameter.

Fig. 10 Sketch for the variations of the lava lake level at Erta 'Ale, explained to result from the variations in the thickness of a foam accumulated at the top of the magma reservoir (slightly adapted from Vergniolle and Bouche, 2016): a) lava lake is at a high level when the foam is growing in the reservoir due to a non-zero underlying gas flux, as in 9-13 Dec 2002; b) low level lava lake, when the underlying gas flux in the reservoir had stopped leading to the foam thinning due to its spreading in the conduit, as for the period December 2002-May 2003; c) changes of the lava lake volume, as deduced from MODIS records (diamonds) and compared with a model of foam thickness, used independently with two different boundary conditions, a non-zero underlying gas flux (rise of lava lake) and a zero underlying gas flux (descent of the lava lake). The best fit between the MODIS records and the numerical solving gives two constrains, on the underlying gas flux and the area of the magma reservoir (Vergniolle and Bouche, 2016). Note that μ_l, ρ_l, Q_{in} and Q_{out} stand for magma viscosity, magma density, underlying gas flux below the foam and the gas flux at the surface. The foam with a gas volume fraction, ε, □□□□□ towards the conduit at a velocity □□□□□□□□ and has a thickness h(r,t), which varies with the radial coordinate, r, within the radius of the magma reservoir, R_c, and the time t. t_{rise} and t_{fall} are the times at which the level of the lava lake rises and ΔV_{NTI} is the relative volume of the lava lake in respect to that of March 2003 (see details in Vergniolle and Bouche, 2016).

Fig. 11 Models of degassing in the conduit, initially proposed for Erta 'Ale (Bouche et al. 2010) and applied to: a) Erta 'Ale with an updated value of the magma viscosity; b-c) Ambrym at two different periods marked by different bubble diameters at the surface. The degassing at Erta Ale is driven by the rise of large bubbles able to produce a bubbly wake, as deep as 1 km and up to the surface, while this type of degassing only exist from 500-1000m to the surface at Nyiragongo and at shallow depths at Villarica. The degassing at Ambrym is relatively similar to that of Erta Ale, when the bubbles are large, >8.5 m (see text for details). The drastic change in magma viscosity with the loss of dissolved water and the calculation of the gas volume fraction by assuming stagnant small bubbles and a fully degassing magma from gas exsolution had led us to use the viscosity of the undegassed magma below 500 m and that of the fully degassed magma above (see text and table 3 for details). Note that U_b and U_w are the vertical velocities of the driving large bubble and its detached bubbly wake (of length L_w), respectively, while α_l and α_w are the gas volume fractions within the lava lake and the wake, respectively.

Fig. 12 Stromboli, a) a typical strombolian explosion in 1979, approximately of 150 m in height (courtesy of J-M Bardintzeff); b) gas-rich explosion October 2005, height of ejecta between 3 and 5 m (photo taken by N. Métrich), 20 m in height (T Ricci); c) start of an ash-rich explosion at vent N1, 29 September 2019 at 10h55 local time, approximately 30 m in height, (courtesy of T. Ricci); d) southwestern vent in 1970, showing the top of the nearby magma column, an exceptional photo due to danger, as well as on its information on Stromboli's eruptive pattern 40 years ago (courtesy of G. Sartoris), with an opening potentially of 1 m (order of magnitude) ; e) lava pond due to bubble rise at vent N2, 16 November 2008 at 15hr46, length of major axis of the red ellipse between 3 and 4 m, (courtesy of T. Ricci); f) a few seconds later at vent N2, 16 November 2008, 15hr46 (scale identical to e) (courtesy of T. Ricci).

Fig. 13 a) an ash-rich explosion at Yasur, reaching a maximum height of 100m with ejecta falling back in crater in a radius of 150m from the emission point, on 1 August 2008 at 17h18 (local hour) (courtesy of A. Finizola); b-d) Arenal's edifice (courtesy of O. Aragon) with b) a typical vulcanian explosion, leading to a small eruptive column of 400 m in height, in 1990, c) a typical strombolian explosion with lava flows, in 1995 at 20h20, the red part with ballistic blocks is approximately 500-600 m; d) close-up of a typical strombolian explosion with lava flows, in 1989 at 20h15, between 100 and 200 m, showing the two different vents existing in the C crater.

Fig. 14 a-b) Popocatépetl with a crater of 300 m in diameter (courtesy of R. Campion) with a) lava dome at a high level, showing the passive degassing on an annular ring at the origin of the large SO_2 flux, on 28 February 2019 and b) lava dome at a low level, on 18 February 2020, the rise of the lava dome remaining puzzling for this dacitic magma composition, leading to vulcanian explosions, hence initiated below a sealed vent; c) small ash-and-gas explosion at Santiaguito, reaching a height of 500-1000 m, in 1978 (courtesy of J-M Bardintzeff).

Fig. 15 Bi-directional flow models for open-vent volcanoes, such as Stromboli, Yasur, Erebus and lava lakes, (see text for details), a) developed for explaining the excess degassing (slightly adapted from Stevenson and Blake, 1998); b) assuming that the velocity of the degassing magma, v_s, is maximum and adding the degassing and ignore the crystallisation path at Stromboli (slightly adapted from Burton et al. 2007b). Note that v_d is the velocity of the descending fluid of viscosity η and density ρ, while φ is gas volume fraction in the ascending fluid and r_s the radius of the ascending fluid; c) core-annular flow including lateral gradients in magma viscosity and density and solving for inclined and vertical conduit and combined with petrologic data on magmatic volatile content at Villarica (slightly adapted from Palma et al. 2011). Note that ρ and μ stand for magma density and viscosity for the ascending fluid (subscript c) and the descending fluid (subscript a). R is the conduit radius and r the radial coordinate; d) 3 regimes are possibly as a function of the viscosity ratio, although the core-annular flow is the most frequent (slightly adapted from Beckett et al. 2014). Note that the ascending fluid is marked in grey; e) convective velocity and height of the convective cells, estimated from the re-dissolution of the tiny bubbles within the downwards motion of the degassed magma (slightly adapted from Carey et al. 2013).

Table captions:

Table 1 Main features of open-vent volcanoes (geodynamic context, activity period, magma composition, temperature, crystal volume fraction, magma supply rate) and associated references for : a) persistent lava lakes (Nyiragongo, Erta Ale, Masaya, Villarica, Kilauea, Ambrym) ; b) our selection of open-vent volcanoes without a lava lake (Stromboli, Yasur, Erebus, Popocatépetl, Arenal, Pacaya, Fuego, Santiaguito).

Table 2 Dissolved sulphur amounts in magmas (wt%) and SO2 fluxes for open-vent volcanic systems a) hosting a lava-lake (Nyiragongo, Erta Ale, Masaya, Villarica, Kilauea, Ambrym); b) without a lava lake (Stromboli, Yasur, Erebus, Popocatépetl, Arenal, Pacaya, Fuego, Santiaguito).

Table 3 Parameters (silica content, temperature, dissolved water content, viscosity, bubble volume observed at the surface, Reynolds numbers) used for the calculation of the Reynolds number at lava lakes and at different depths (500 m, 100m, 0m), assuming undegassed magma below 500 m and fully degassed magma above (see text for details).

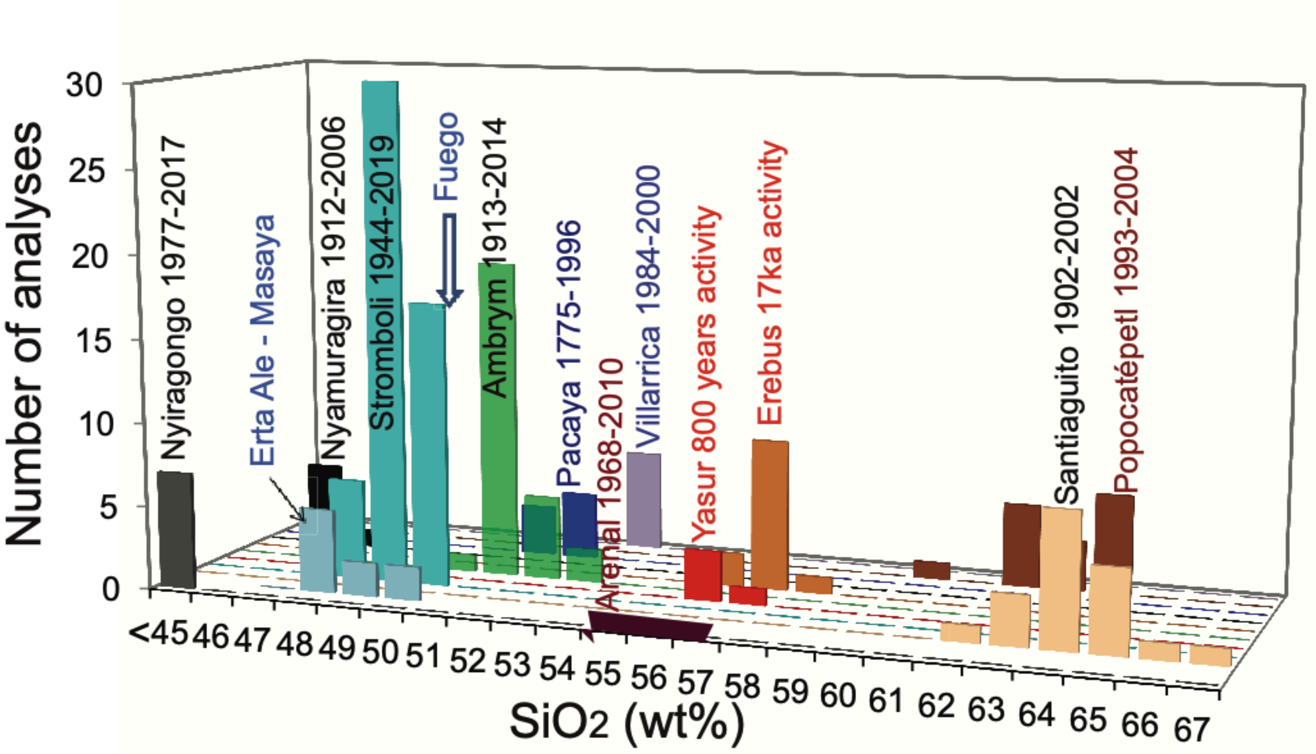

Number of analyses
30
25
20
15
10
5
0
Nyiragongo 1977-2017
Erta Ale - Masaya
Nyamuragira 1912-2006
Stromboli 1944-2019
Fuego
Ambrym 1913-2014
Pacaya 1775-1996
Arenal 1968-2010
Villarrica 1984-2000
Yasur 800 years activity
Erebus 17ka activity
Santiaguito 1902-2002
Popocatépetl 1993-2004
<45 46 47 48 49 50 51 52 53 54 55 56 57 58 59 60 61 62 63 64 65 66 67
SiO2 (wt%)

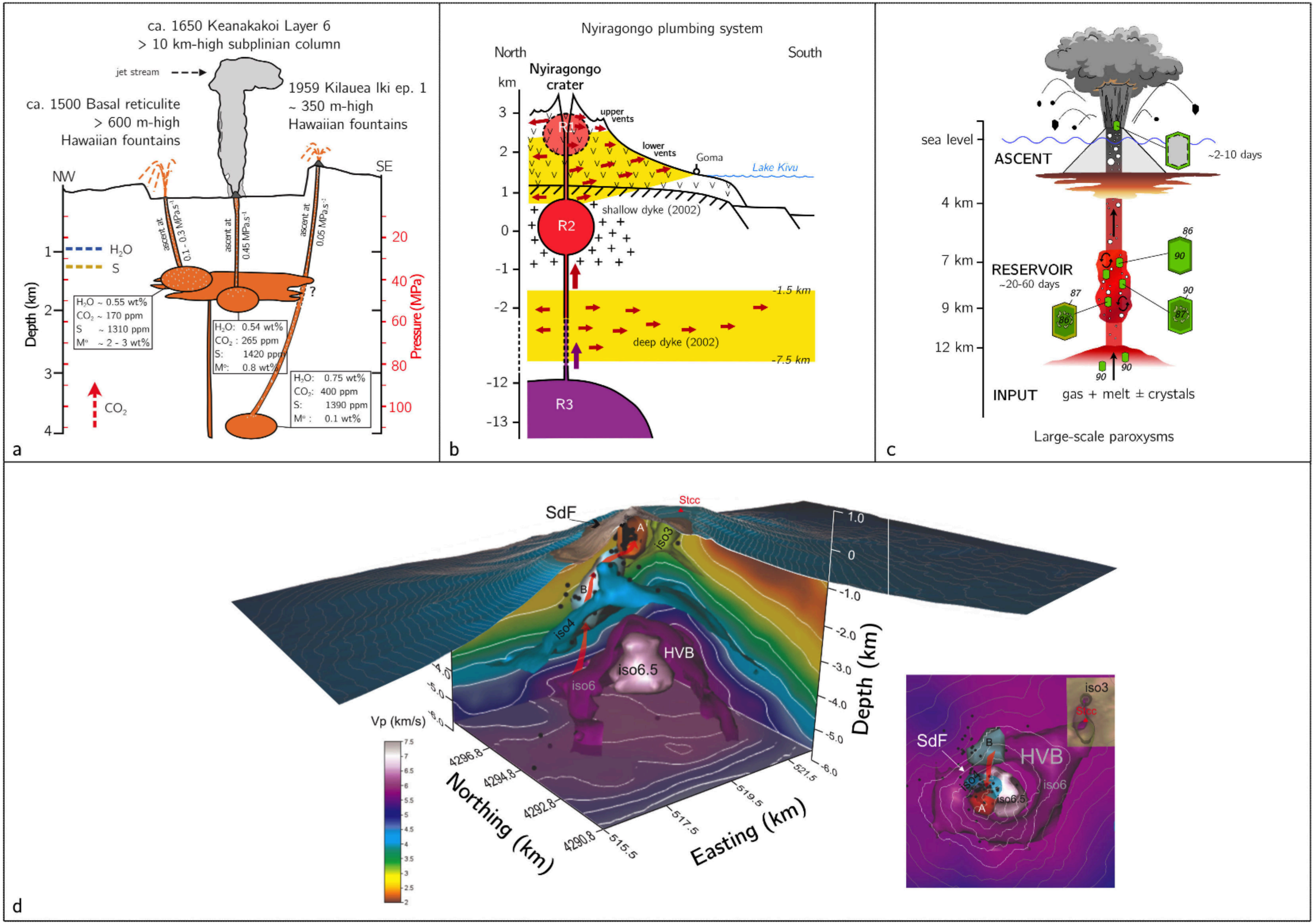

ca. 1650 Keanakakoi Layer 6
> 10 km-high subplinian column
jet stream
ca. 1500 Basal reticulite
> 600 m-high
Hawaiian fountains
1959 Kilauea Iki ep. 1
~ 350 m-high
Hawaiian fountains
NW
SE
Depth (km)
Pressure (MPa)
H_2O
S
ascent at 0.1 - 0.3 MPa.s⁻¹
ascent at 0.45 MPa.s⁻¹
ascent at 0.05 MPa.s⁻¹
H_2O ~ 0.55 wt%
CO_2 ~ 170 ppm
S ~ 1310 ppm
M° ~ 2 - 3 wt%
H_2O: 0.54 wt%
CO_2 : 265 ppm
S: 1420 ppm
M°: 0.8 wt%
H_2O: 0.75 wt%
CO_2: 400 ppm
S: 1390 ppm
M° : 0.1 wt%
CO_2
a
Nyiragongo plumbing system
North
South
km
Nyiragongo crater
upper vents
lower vents
Goma
Lake Kivu
R1
R2
R3
shallow dyke (2002)
deep dyke (2002)
-1.5 km
-7.5 km
b
sea level
ASCENT
~2-10 days
4 km
7 km
RESERVOIR
~20-60 days
9 km
12 km
INPUT
gas + melt ± crystals
Large-scale paroxysms
c
SdF
Stcc
A
B
iso3
iso4
iso6
iso6.5
HVB
Depth (km)
Vp (km/s)
Northing (km)
Easting (km)
d

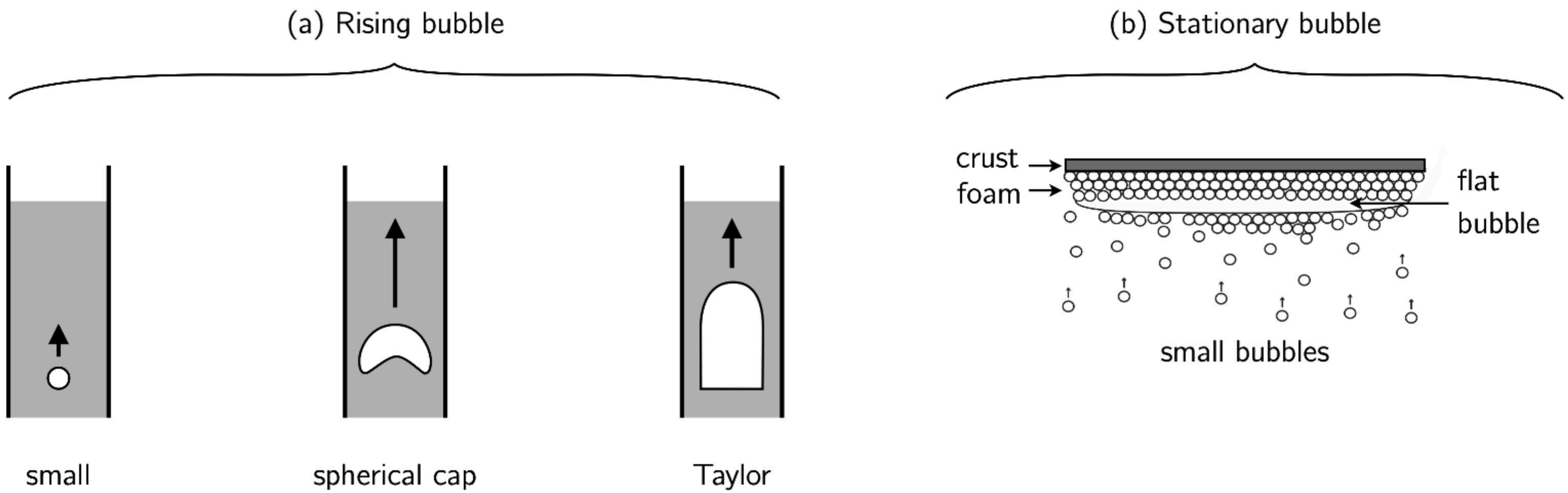
(a) Rising bubble
small
spherical cap
Taylor
(b) Stationary bubble
crust
foam
flat
bubble
small bubbles


a
b
c


a
b
c
d

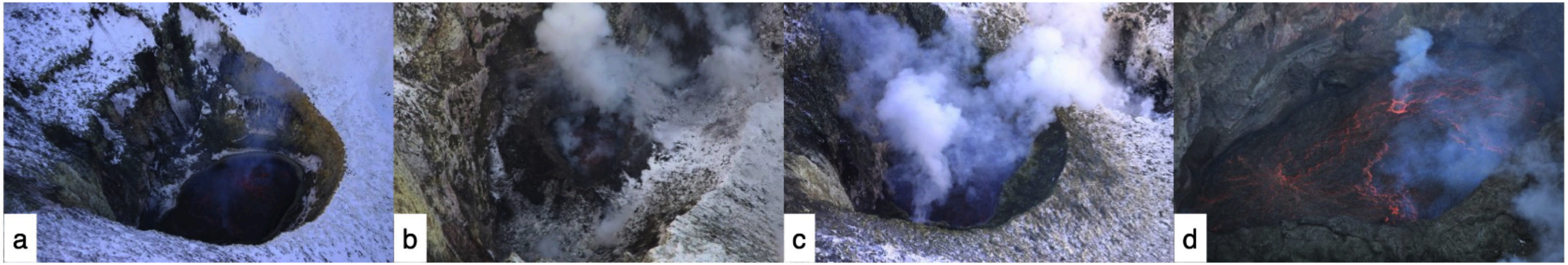
a
b
c
d

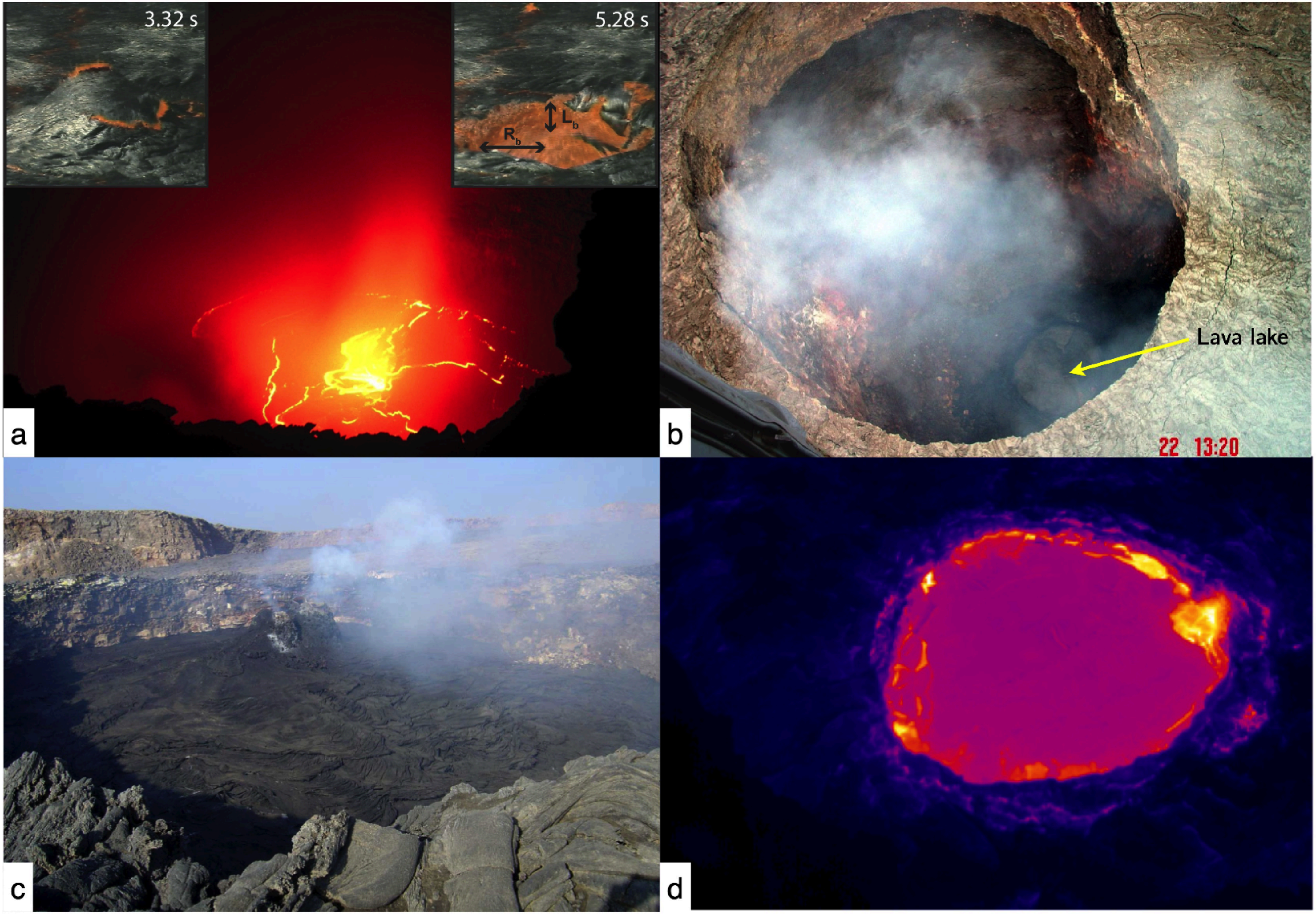

3.32 s
5.28 s
L_b
R_b
a
b
Lava lake
22 13:20
c
d

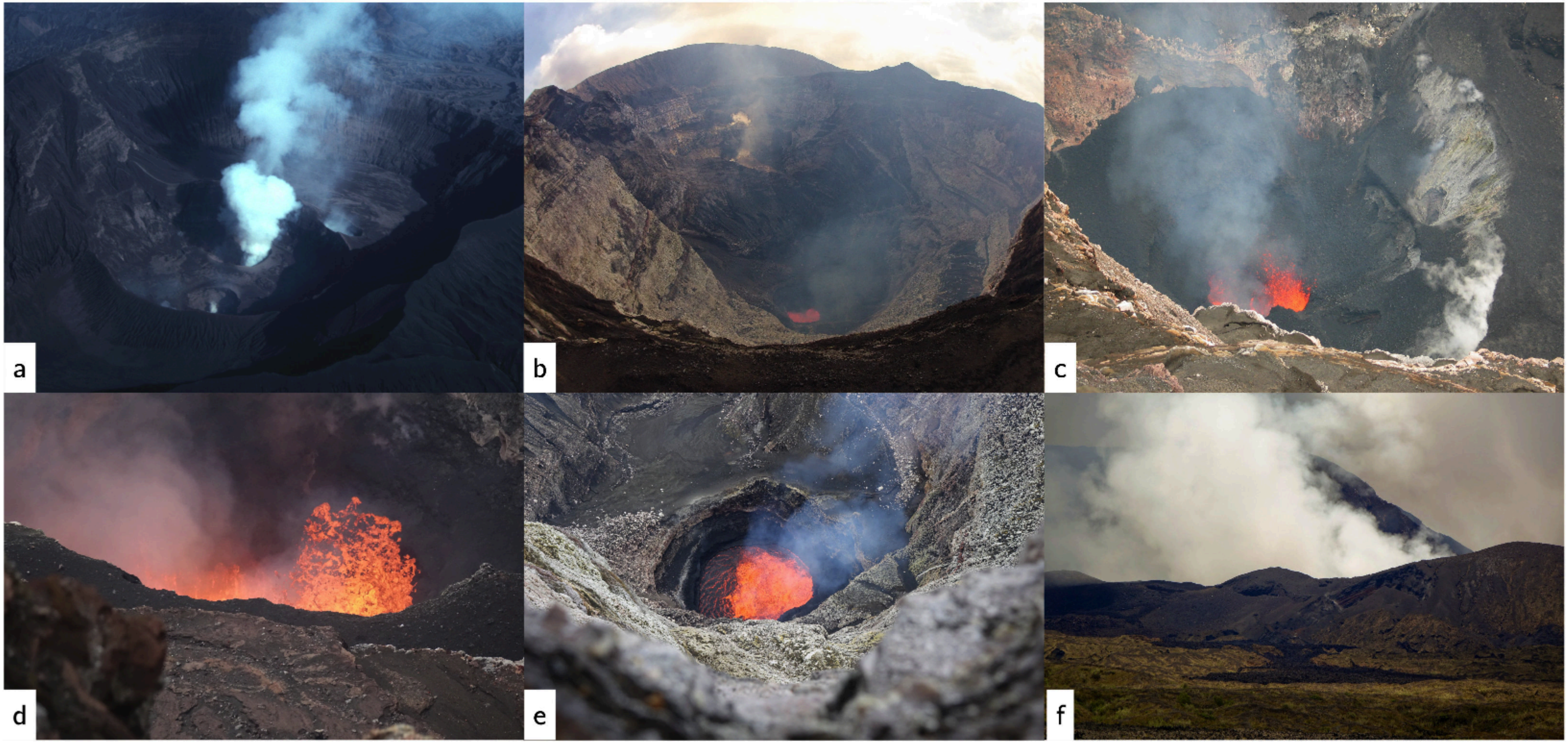
a
b
c
d
e
f


a
b
c

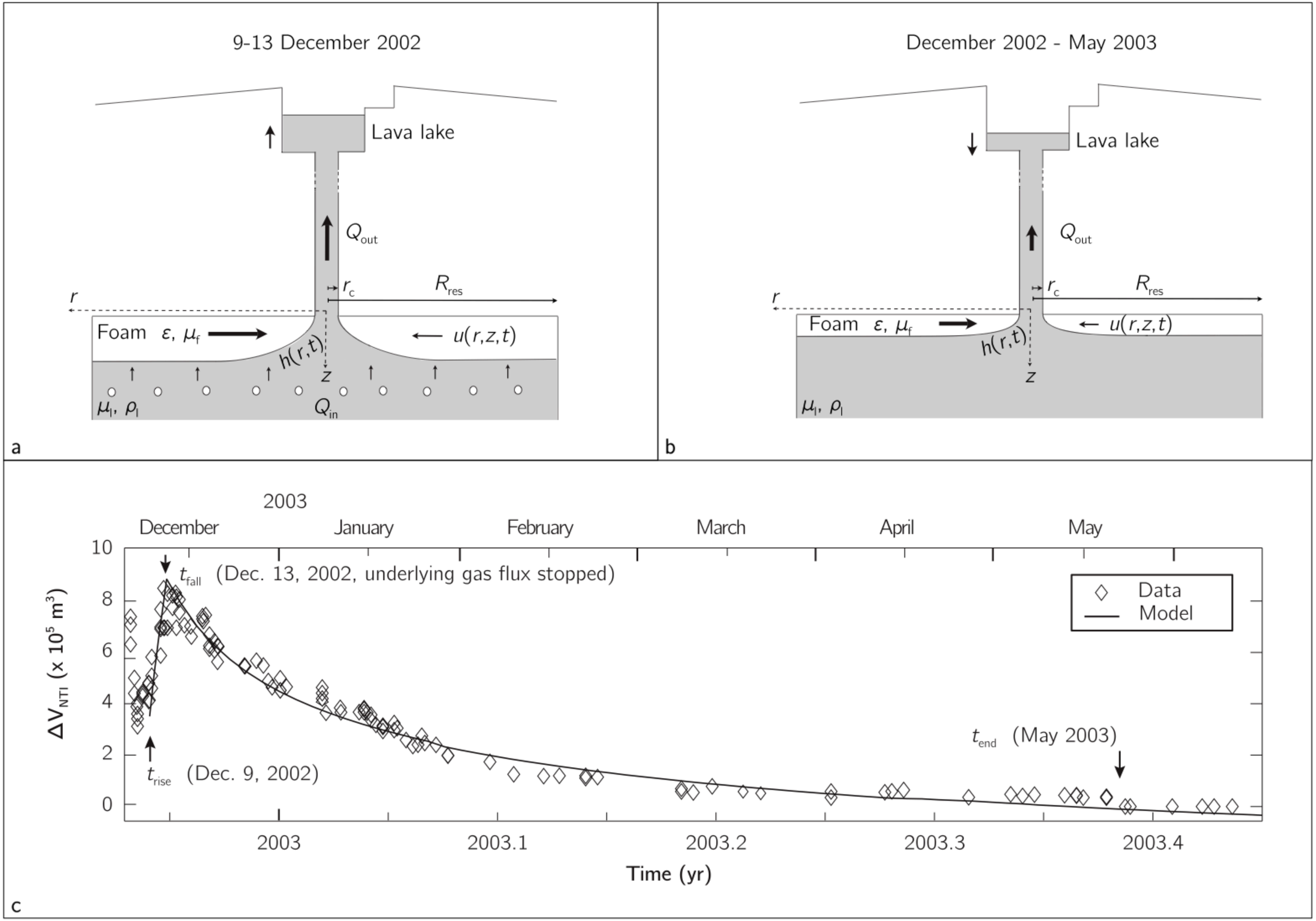

9-13 December 2002
Lava lake
Q_{out}
r
r_c
R_{res}
Foam ε, μ_f
$u(r,z,t)$
$h(r,t)$
z
μ_l, ρ_l
Q_{in}
a
December 2002 - May 2003
Lava lake
Q_{out}
r
r_c
R_{res}
Foam ε, μ_f
$u(r,z,t)$
$h(r,t)$
z
μ_l, ρ_l
b
2003
December
January
February
March
April
May
t_{fall} (Dec. 13, 2002, underlying gas flux stopped)
t_{rise} (Dec. 9, 2002)
t_{end} (May 2003)
Data
Model
ΔV_{NTI} (x 10^5 m^3)
Time (yr)
0
2
4
6
8
10
2003
2003.1
2003.2
2003.3
2003.4
c

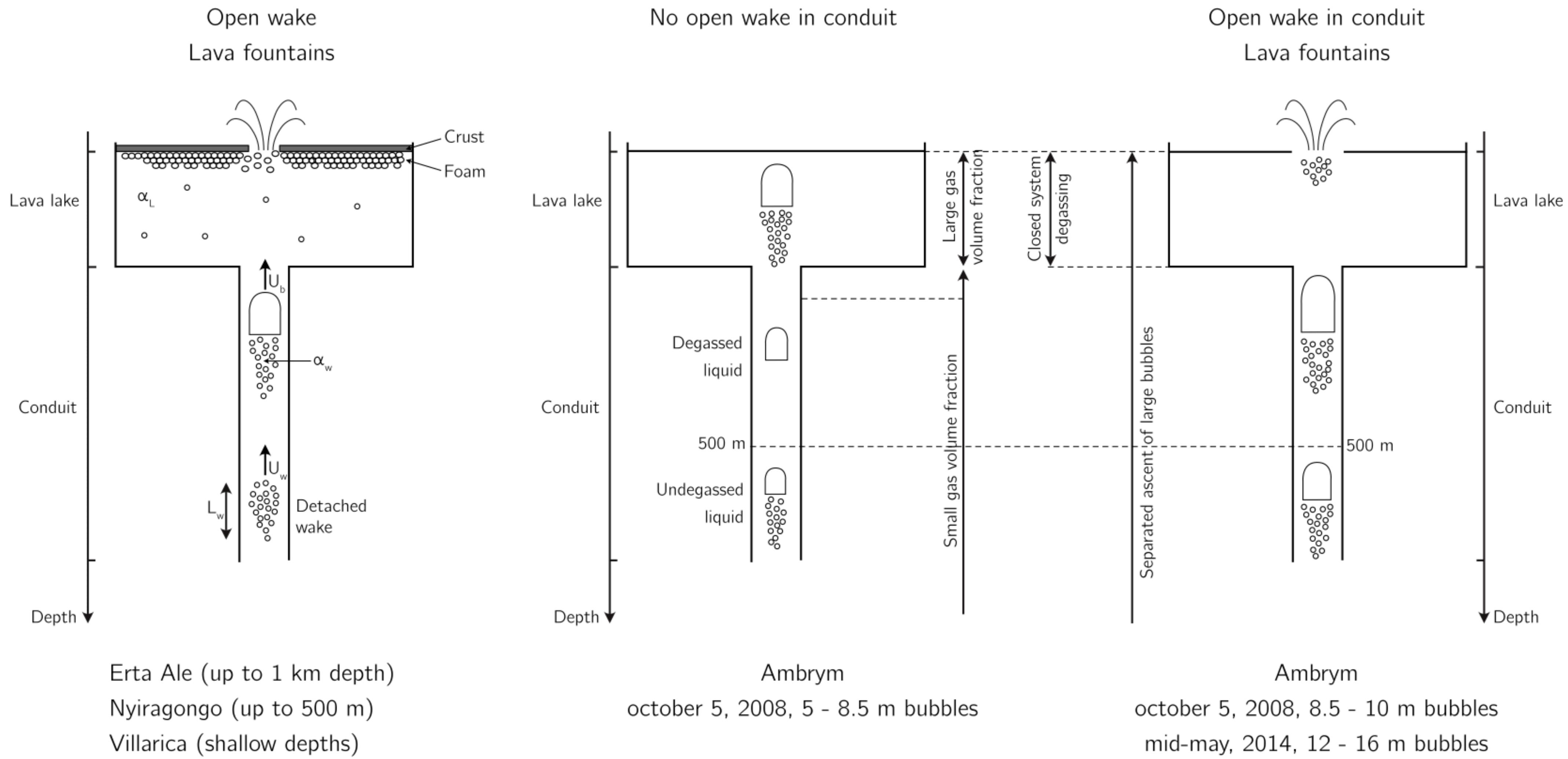

Open wake
Lava fountains
No open wake in conduit
Open wake in conduit
Lava fountains
Crust
Foam
Lava lake
α_L
U_b
α_w
Conduit
U_w
L_w
Detached wake
Depth
Lava lake
Degassed liquid
Conduit
500 m
Undegassed liquid
Depth
Large gas volume fraction
Closed system degassing
Small gas volume fraction
Separated ascent of large bubbles
500 m
Lava lake
Conduit
Depth
Erta Ale (up to 1 km depth)
Nyiragongo (up to 500 m)
Villarica (shallow depths)
Ambrym
october 5, 2008, 5 - 8.5 m bubbles
Ambrym
october 5, 2008, 8.5 - 10 m bubbles
mid-may, 2014, 12 - 16 m bubbles

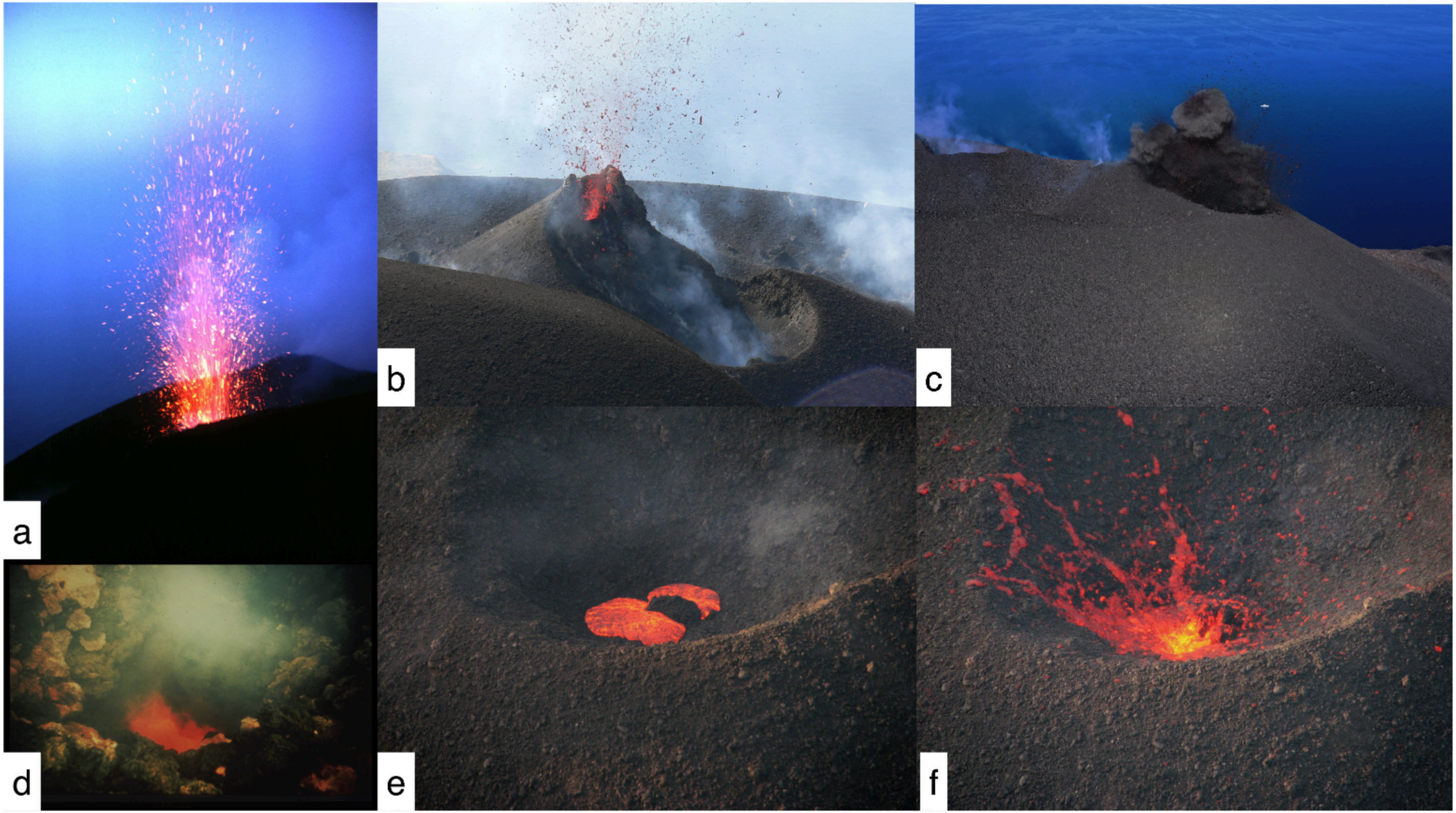
a
b
c
d
e
f

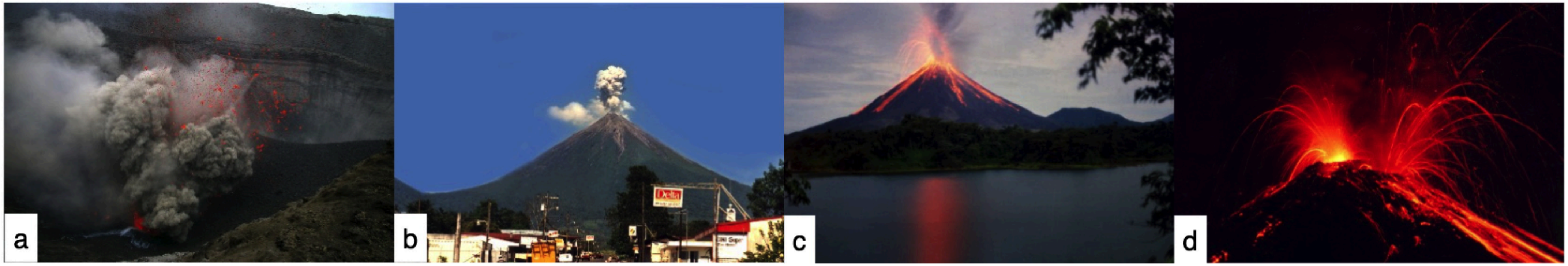
a
b
Delta
c
d

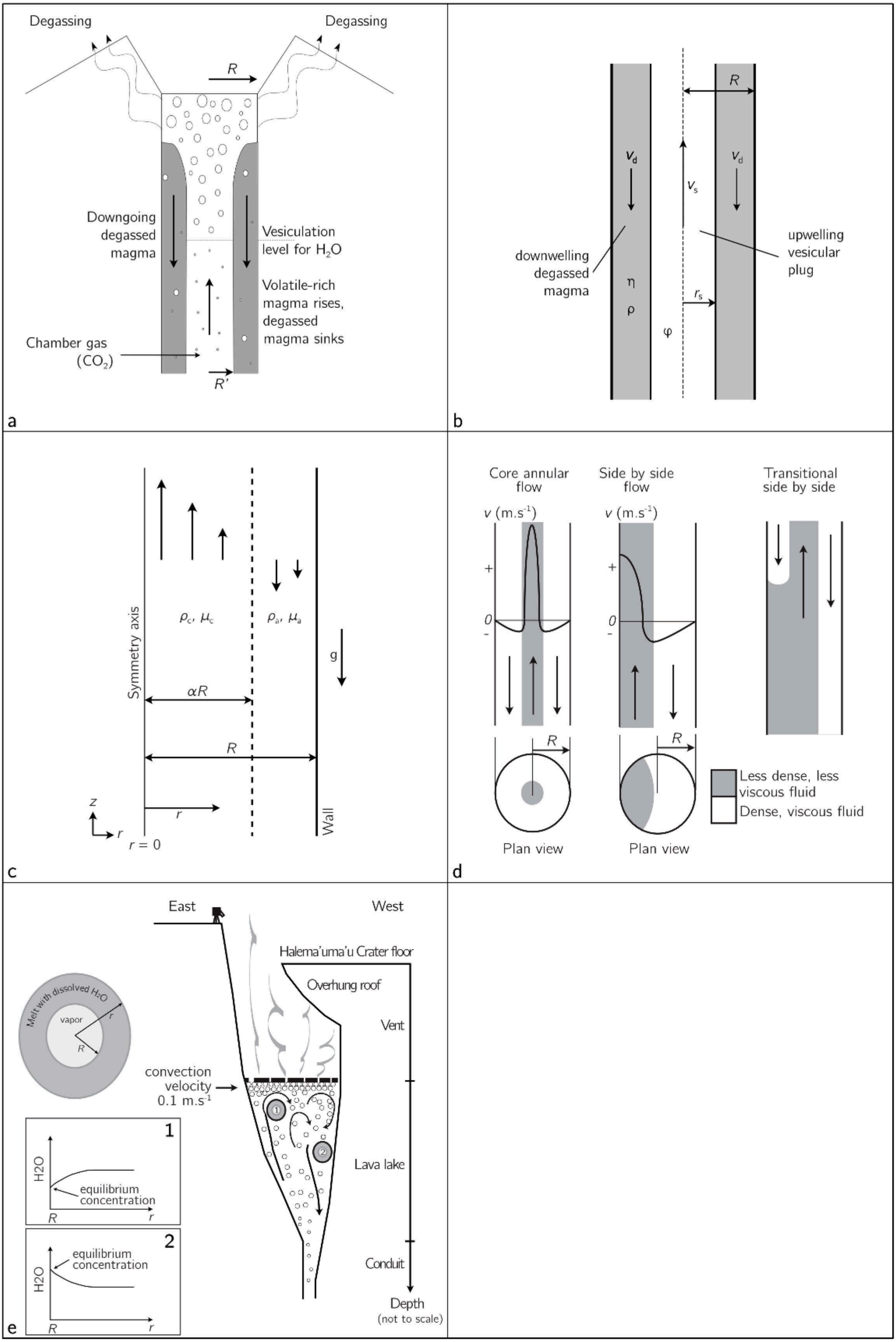

Degassing
Degassing
R
Downgoing degassed magma
Vesiculation level for H_2O
Volatile-rich magma rises, degassed magma sinks
Chamber gas (CO_2)
R'
a
R
v_d
v_d
v_s
upwelling vesicular plug
downwelling degassed magma
η
ρ
r_s
φ
b
Symmetry axis
ρ_c, μ_c
ρ_a, μ_a
g
αR
R
z
r
r
$r = 0$
Wall
c
Core annular flow
Side by side flow
Transitional side by side
v (m.s^{-1})
v (m.s^{-1})
+
0
-
+
0
-
R
R
Less dense, less viscous fluid
Dense, viscous fluid
Plan view
Plan view
d
East
West
Halema'uma'u Crater floor
Overhung roof
Vent
Lava lake
Conduit
Depth
(not to scale)
Melt with dissolved H_2O
vapor
r
R
convection velocity 0.1 m.s^{-1}
1
2
1
H2O
equilibrium concentration
R
r
2
equilibrium concentration
H2O
R
r
e

Supplementary material by Vergniolle and Metrich

"An interpretative view of open-vent volcanoes"

Figure caption:

Figure S1: **Fig S1 (a)** Viscosity (log Pa.s) as a function of inverse temperature (K^{-1}) for anhydrous and crystal- and bubble-free phonolite melts of Erebus (Le Losq et al., 2015); for phonolite from Vesuvius (GP79) the experimental data are from Giordano et al., (2009), for rhyolite and andesite melts from Neuville et al. (1993), and for a basalt melt from Villeneuve et al. (2008). Figure redrawn from Le Losq et al., (2015). (**b**) Viscosity (log Pa.s) as a function the temperature and the H_2O content of trachyandesitic melt of Yasur varying from 0 to 2.5 wt%, after Giordano et al., (2008). 52 wt% SiO_2 refers to Yasur present-day bulk rock and 56 wt% to the glassy matrix (Métrich et al., 2011). **(c)** Relative increase in magma viscosity as a function of the solid volume fraction, see text for details (slightly adapted from Mader et al., 2013). (d) Relative increase in magma viscosity as a function of the bubble shape, here quantified by the capillary number, see text for details, (slightly adapted from Mader et al., 2013).

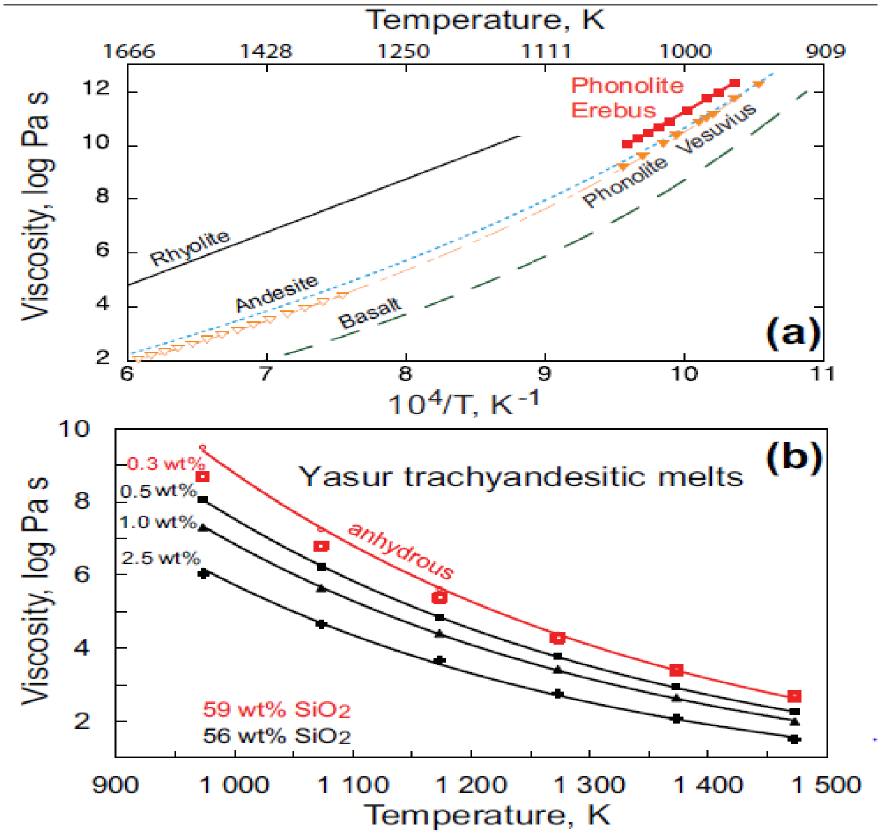

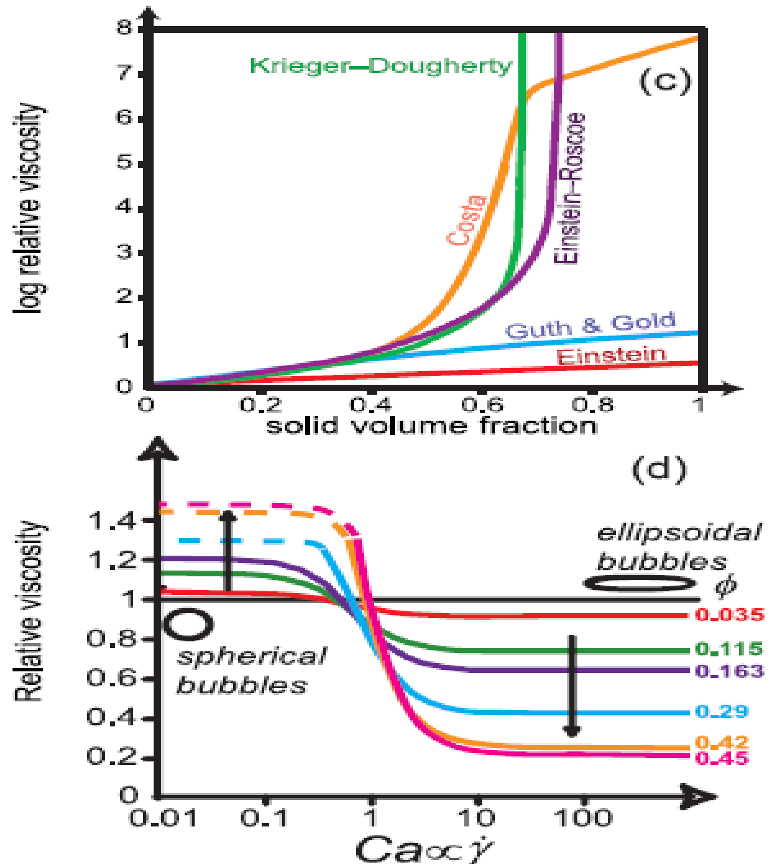

log relative viscosity
Krieger—Dougherty
(c)
Costa
Einstein–Roscoe
Guth & Gold
Einstein
solid volume fraction
0
0.2
0.4
0.6
0.8
1
2
3
4
5
6
7
8
(d)
Relative viscosity
1.4
1.2
1
0.8
0.6
0.4
0.2
0
ellipsoidal bubbles
ϕ
spherical bubbles
0.035
0.115
0.163
0.29
0.42
0.45
0.01
0.1
1
10
100
$Ca \propto \dot{\gamma}$